

**Physical and biochemical processes in
composting material**

Promotor: Dr. ir. P.A.C. Raats,
hoogleraar continuümmechanica

Co-promotor: Dr. I.A. van Haneghem,
universitair hoofddocent technische natuurkunde

J.T. van Ginkel

**Physical and biochemical processes in
composting material**

Proefschrift

ter verkrijging van de graad van
doctor in de landbouw- en milieuwetenschappen,
op gezag van de rector magnificus,
dr. C.M. Karssen,
in het openbaar te verdedigen
op dinsdag 10 september 1996
des namiddags te vier uur in de Aula
van de Landbouwwuniversiteit te Wageningen

ACKNOWLEDGEMENT

The study described in this thesis was carried out at the former Institute for Soil Fertility Research (IB-DLO), since November 1993 DLO Research Institute for Agrobiological and Soil Fertility (AB-DLO) in Haren, The Netherlands. The material costs of this research project were borne by The National Research Program on Reuse of Waste Materials (Nationaal Onderzoeksprogramma Hergebruik van Afvalstoffen, NOH), commissioned by the Dutch Organisation for Energy and Environment (Nederlandse Maatschappij voor Energie en Milieu, NOVEM). Project title: 'Simulation of composting, with emphasis on the heat balance and aeration', grant no. 24.21-500.10.

Nederlandse vertaling titel:

FYSISCHE EN BIOCHEMISCHE PROCESSEN IN COMPOSTEREND MATERIAAL

BIBLIOTHEEK
LANDBOUWUNIVERSITEIT
WAGeningen

CIP-DATA KONINKLIJKE BIBLIOTHEEK, DEN HAAG

Ginkel, Johannes Theodorus van

Physical and biochemical processes in composting material/

Johannes Theodorus van Ginkel

Thesis Landbouwwuniversiteit Wageningen. - With ref. - With summary in Dutch

ISBN 90-5485-562-2

STELLINGEN

1. Een samenhangende set data van fysische en biochemische eigenschappen van composterend materiaal is essentieel voor een betrouwbare voorspelling van het verloop van het composteringsproces.
(Dit proefschrift)
2. Het quotiënt van de hydrolysesnelheden van C- en N-verbindingen geeft een beter inzicht in het verloop van het composteringsproces dan de gewichtsverhouding van C en N in het uitgangsmateriaal.
(Dit proefschrift; Gottschall, 1984)
3. De invloed van dampdiffusie in vochtige poreuze media op de waarde van de warmtegeleidingscoëfficiënt gemeten volgens de niet-stationaire naaldmethode is nog onvoldoende experimenteel onderzocht.
(Dit proefschrift)
4. Geforceerde beluchting bij compostering leidt niet in alle gevallen tot een betere processturing.
(Dit proefschrift)
5. Het vochtgehalte is de belangrijkste fysische parameter van composterend materiaal.
(Dit proefschrift)
6. Het positieve effect van organische stof op de voor de plant beschikbare hoeveelheid water is alleen van toepassing op zandgronden.
(Baver, 1946)
7. Een algemeen geldend rijpheids criterium voor compost bestaat niet. Het onderzoek hiernaar zou zich moeten richten op de ontwikkeling van rijpheids criteria die gerelateerd zijn aan specifieke gebruiksdoelen van compost.
(Iannotti D.A., M.E. Grebus, B.L. Toth, L.V. Madden, and H.A.J. Holtink, 1994. Waste management. Oxygen respirometry to assess stability and maturity of composted municipal solid waste, J. Environ. Qual. 23: 1177-1183.)

8. Veel tips in populaire handleidingen over composteren anticiperen op een slecht verlopend proces.
(Maas A., en H. Perebooms, 1995. Zelfgemaakte compost, de beste voeding voor uw tuin. Ecologische Alternatieven 39. De Kleine Aarde.)
9. In tegenstelling tot wat vaak wordt beweerd, kunnen niet spore-vormende mesofiele bacteriën thermofiele omstandigheden in composterend materiaal overleven.
(Nakasaki K., M. Sasaki, M. Shoda, and H. Kubota, 1985. Characteristics of mesophilic bacteria isolated during thermophilic composting of sewage sludge. Appl. Environ. Microbiol. 49(1): 42-45.)
10. De opzet van het GFT-beleid door de rijksoverheid getuigt van slecht ondernemerschap.
11. Het streven in de biologische landbouw naar gesloten kringlopen op bedrijfsniveau gaat voorbij aan het feit dat boeren produkten verkopen.
(Anonymus, 1994. IFOAM Basic Standards for organic agriculture and food processing and guidelines for social rights and fair trade; decided by IFOAM General Assembly at Christchurch/New Zealand, December 15th.)
12. In de moderne samenleving eindigt de vrijheid van het spelende kind waar de vrijheid van de automobilist begint.

Stellingen behorend bij het proefschrift 'Physical and biochemical processes in composting material', geschreven door J.T. van Ginkel.

Wageningen, 10 september 1996.

ABSTRACT

Van Ginkel, J.T., 1996. Physical and biochemical processes in composting material. Ph.D. thesis, Agricultural University Wageningen, Wageningen, The Netherlands. 179 pp., 74 figs., 19 tables, 130 refs., English and Dutch summaries.

In the composting process temperature and oxygen concentrations are essential parameters. A main objective of this thesis is to formulate a mathematical model which can predict these parameters. In this model a number of important material properties must be used: composition in terms of volume fractions of solid, liquid and gaseous phases, air permeability, oxygen diffusion coefficient, thermal conductivity coefficient, O_2 -consumption, CO_2 -production and heat production. Another main objective of this thesis is the determination of these properties. A mixture of wheat straw and chicken manure was chosen as composting material. For the above mentioned material properties some overall conclusions can be drawn.

The volume fractions of the distinguished phases varied with position due to the compressibility of the composting material. An equation was deduced to predict the air-filled volume fraction as a function of the pile height.

The air permeability κ decreased with increasing air velocity. For raw material, κ decreased with the wetness at comparable air-filled volume fractions θ_g . The oxygen diffusion coefficient D_{O_2} was proportional to $\theta_g^{1.5}$. There was no effect of the age of the material on D_{O_2} . The thermal conductivity coefficient λ increased with the temperature. At constant temperature and for solid phase fractions less than 0.3, λ increased linearly with the liquid phase fraction.

The biochemical properties, such as the rates of heat production and oxygen consumption, were estimated from theoretical considerations and were determined experimentally in an isothermal calorimeter. The time course of the experimental production/consumption rates showed a characteristic pattern consisting of a peak activity during the first 4 to 5 days followed by a gradually decreasing pseudo-steady state.

Finally, experimental results of compost piles on a semi-practical scale were interpreted in terms of the identified processes and experimental values of material properties.

Additional keywords: subsidence, porosity, air permeability, diffusion, convection, thermal conductivity, oxygen consumption, heat production, carbon dioxide production, microbial activity, hydrolysis, simulation.

enkele hoofdstukken.

Met Jan Gerrits en Johan van Lier van het Proefstation voor de Champignoncultuur in Horst heb ik bijzonder plezierig samengewerkt. Jan, jouw praktische kennis van het composteringsproces was van grote waarde bij het opzetten van de eerste proeven. Johan, onze samenwerking bij de bestudering van het inklinkproces en de warmtegeleiding heb ik als bijzonder inspirerend ervaren.

Een speciaal woord van dank geldt voor Meint Veninga, die mijn steun en toeverlaat was bij vrijwel alle experimenten. Meint, dankzij jouw creativiteit bij het bouwen van meetopstellingen zijn de meeste experimenten gelukt. Je humor en je opgeruimde karakter droegen veel bij aan de prettige sfeer tijdens onze samenwerking.

Bij het echte composteringswerk kon ik bouwen op Okko Slim en zijn collega's van de Pot- en Vakproevendienst van het IB-DLO. Okko, jouw betrouwbaarheid bij het uitvoeren van de werkzaamheden gaven mij veel rust. De lekkende luchtpycnometer bezorgde je veel extra werk. Samen met de collega's van de werkplaats heb je hem uiteindelijk toch nog luchtdicht gekregen. Die lekkage deed mij bijna twijfelen aan de algemene gaswet.

Peter Zandt heeft veel moeite gedaan om een perfect datalogprogramma te maken voor het automatiseren van enkele meetopstellingen. Daarnaast gaat mijn dank uit naar Wim Chardon, Bram de Vos en zijn collega's van de afdeling Bodemfysica en de leden van de IB-discussiegroep 'Transportprocessen' voor de discussies en de hulp.

De collega's van de afdeling Bodembioogie gaven veel gezelligheid tijdens de koffiepauzes.

Tenslotte bedank ik Martijn voor haar solidariteit en haar ondersteuning na afloop van mijn baan bij het AB. Martijn, zonder jou had ik mijn werk nooit kunnen afmaken.

Jan

CONTENTS

1. Introduction to the composting process and compost use	1
1.1 Introduction	1
1.2 The waste problem	1
1.3 Use of composted and raw organic materials in agriculture and horticulture	2
1.3.1 Benefits	2
1.3.2 Hazards	4
1.4 Principles of the composting process	5
1.5 Models of the composting process	9
1.6 The aim of this study and the outline of this thesis	10
2. Mathematical modelling of the physical processes in a compost pile	13
2.1 Introduction	13
2.2 Composition of composting material, mass balances of the liquid and the solid phases and changes in the air-filled volume fraction	13
2.3 Dynamics of the gaseous phase	16
2.3.1 Mass balances	16
2.3.2 Convection and diffusion	19
2.4 Heat balance of the composting material	22
3. Bulk density and porosity distributions in a compost pile	25
3.1 Introduction	25
3.2 Bulk density, air-filled volume fraction and true density of dry matter	26
3.2.1 Bulk density and air-filled volume fraction as a function of position in a compost pile	26
3.2.2 Specific densities of dry and organic matter in compost	30
3.3 Materials and methods	32
3.4 Results	34
3.5 Discussion	40
3.6 Conclusions	43

CHAPTER 1. INTRODUCTION TO THE COMPOSTING PROCESS AND COMPOST USE

1.1 Introduction

Composting is one of the oldest bio-technological processes. It was already used by Chinese peasants 4000 years ago (Gottschall, 1984). During the process part of the organic matter is decomposed biologically. The final product can be used in agriculture as a soil amendment, in horticulture as a substrate for the production of mushrooms or ornamental plants, and in home gardens. Various advantages are attributed to compost, such as the improvement of soil structure, cation exchange capacity CEC, water holding capacity, and crop yields. The sanitation of organic waste is often mentioned as a major benefit of the process. Composting and compost use also have disadvantages. During the process emission of polluting substances may occur, such as H_2S , NH_3 , N_2O and CH_4 . In the absence of sufficient oxygen, organic acids are produced during the decomposition process. These acids inhibit plant growth.

In this chapter the advantages and disadvantages accompanying the process and the use of compost will be discussed. It also gives an introduction to the composting process and gives general information about physical, biological and chemical changes occurring in a compost pile.

1.2 The waste problem

In modern society huge amounts of organic waste are produced. Van Onna and Van der Veen (1990) give an overview of the annual production of organic waste in the Netherlands. Table 1.1 presents a summary of these data. Wastes originate from plant residues, manures, town waste and sludge cake from waste water treatment plants. They are often dumped in landfills where they cause environmental problems, such as leaching of minerals and heavy metals, and volatilization of foul smelling substances (Raveh and Avnimelech, 1979; Mesu, 1984). An alternative is to burn the waste in incinerators, but this method can cause air pollution. In many countries laws were passed to minimize these environmental problems. The investments needed to meet these regulatory demands generally increase disposal costs.

1987). Although the biological mechanisms involved in the suppressive properties are not well understood, application of compost in plant protection occurs on a small scale in U.S. horticulture, especially for ornamental plants (Logsdon, 1990).

1.3.2 Hazards

Dispersion of plant and human pathogens and viable plant seeds can be a problem associated with compost use. However, if operated under proper conditions, the composting process will destroy the viability of most seeds and pathogens. Although inhibitors and antagonists might play a role, thermal death is considered to be the most important cause of eradication of seeds and pathogens. With respect to thermal death it has to be emphasized that the temperature declines going from the hot interior to ambient values at the surface of the pile. This means that thermal zones will exist which are conducive to certain pathogens. Properly turning the pile inside out will ensure that the material originally located in the outer zone is also exposed to lethal temperatures. However, this turning or mixing can lead to recontamination (Cooper and Golueke, 1977).

A temperature of 65 °C for at least 30 minutes is considered as a critical threshold for plant pathogens (Bollen, 1969; Lopez-Real and Foster, 1985; Bollen et al., 1989).

Seeds are most susceptible to thermal death during germination (Rubin and Benjamin, 1984). Dry seeds can tolerate much higher temperatures than moist seeds. This is fortunate because moist conditions commonly prevail in a compost pile. Temperatures between 60 and 75 °C are sufficient to kill all common weed seeds (Lavake and Wiese, 1977; Griffis and Mote, 1978).

Human pathogens are also inactivated at high temperatures (Burge, 1983). The heat resistance of human pathogens increases markedly under dry conditions (Cooper and Golueke, 1977). Therefore, wet conditions must prevail in the compost pile. Standards have been proposed by the Environmental Protection Agency (EPA) of the USA to judge pathogen kill. The EPA recommends a five days period at 55 °C (U.S. EPA, 1981), whereas De Bertoldi et al. (1988) suggest that a three days period at 65 °C and moist conditions are required.

Temperatures above 65 °C at the onset of the composting process reduce the decomposition rate causing a less stabilized product which is rich in nutrients and, therefore, a habitat for regrowth of pathogens such as Salmonella (Lopez-Real, 1990). The "hotter the better" concept is therefore only valid for temperatures below 65 °C.

Another problem to be mentioned is that compost may contain phytotoxic substances which inhibit plant growth. Acetic acid formed during composting is the main organic acid responsible for the phytotoxic effect (Lynch, 1977; De Vleeschauwer et al., 1981). In a forced aeration system the disappearance of phytotoxins was three times faster than in a pile with turning only (Zucconi et al., 1981).

It can be concluded that good oxygenation and a temperature of 65 °C for at least 3 consecutive days are prerequisites to obtain compost of good quality.

1.4 Principles of the composting process

Gray et al. (1971) defined composting as the partial decomposition of heterogeneous organic matter by a mixed microbial population in a moist, warm, and aerobic environment. Processes taking place during composting are very similar to those occurring when organic materials like plant residues and animal manures are added to the soil surface. In these organic materials a dense population of various micro-organisms (bacteria, fungi) is found (Alexander, 1977). The micro-organisms use organic matter, minerals, and water for their metabolic activity. Each microbial species has an optimum temperature at which growth and multiplication rates are at a maximum level. Microbial processes take place in the top soil at prevailing humidity, aeration status, and temperature. Often the temperature is too low to allow decomposition at the maximum rate. The rate can be increased by gathering organic material into a pile in which the temperature will rise due to the enhanced microbial heat production resulting from higher organic matter densities and because of the relatively slow heat transfer to the environment.

The composting process passes through three characteristic stages distinguished by temperature as shown in figure 1.1 (Gray et al., 1971). The process starts spontaneously at ambient temperature by mesophilic microbes with an optimum temperature for activity of about 30 °C (Alexander, 1977). The temperature will rise from ambient to about 45 °C as a result of heat production by these organisms. This level is lethal to mesophilic organisms, but it is suitable for thermophilic microbes and they will speed up the decomposition process. In the thermophilic stage the temperature may increase up to 70 or 75 °C. As this temperature range is lethal to many microbes, the process slows down and the temperature stabilizes at this level or a little below. The thermophilic stage proceeds until all easily degradable organic matter is decomposed. Then, the process slows down further and the maturing stage begins at about 30 °C.

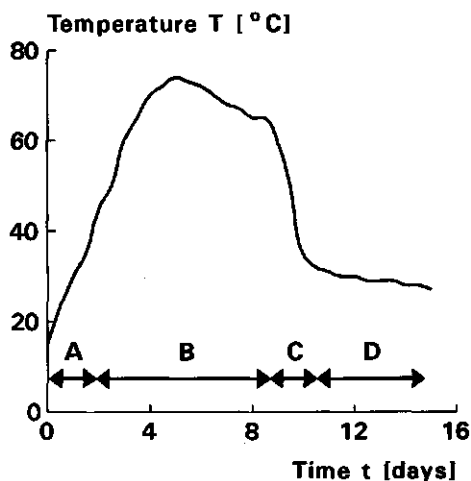


Figure 1.1 Temperature- time pattern indicating the phases of microbial activity. A- mesophilic, B- thermophilic, C- cooling, D- maturing (Gray et al., 1971).

Table 1.2 Composition of organic matter (Gray et al., 1971).

fraction	percentage in dry matter	
	plants	manures
hot/cold water solubles: sugar, starches, amino acids, aliphatic acids, urea and ammonium salts	5-30	2-20
ether/alcohol solubles: fats, oils, waxes and rasins	5-15	1- 3
proteins	5-40	5-30
hemicelluloses	10-30	15-25
cellulose	15-60	15-30
lignin	5-30	10-25
minerals (ash)	1-13	5-20

Organic matter serves as a feeding substrate for microbes. This substrate may arise from a variety of organic materials such as fresh plant materials, manures and the organic fractions of MSW and sludge. These materials can be considered as mixtures of sugars, hemicellulose, cellulose, lignin, fats, proteins and minerals. A rough estimate of the chemical composition is given in table 1.2. The composition of plant materials depends mainly on the plant species and age. Young succulent plants contain a lot of water-soluble matter and only small amounts of lignin, whereas older plants contain relatively large amounts of lignin. The composition of animal manures is determined by the type of animal and its feeding.

Micro-organisms utilize substrates for the production of new cell material (anabolism) and for the production of energy (catabolism). In catabolic processes energy is obtained by degradation of complex, energy rich compounds into simpler compounds with lower energy contents. Catabolic processes occurring in presence of oxygen are called aerobic, whereas processes taking place without oxygen are called anaerobic. Aerobic degradation yields more energy than anaerobic degradation. Anaerobic processes can give rise to the production of foul smelling substances, such as H_2S and butyric acid. Pathways of degradation processes will be discussed in more detail in chapter 5.

De Bertoldi et al. (1982) studied the effect of turning, sub atmospheric (suction) and super atmospheric (blowing) pressure aeration on moisture removal. The largest decrease in water content was obtained with blowing and temperature feedback control. With blowing the gravimetric water content decreased from 67 to 29%. With suction and with turning the final water contents were 45 and 43% respectively. Lopez-Real (1990) examined the material losses of a seaweed/straw mixture after 28 days of composting in a forced aeration system with turning. He found a total weight reduction of 50%, a volume reduction of 77% and a bulk density increase from 310 to 670 $kg\ m^{-3}$, indicating that subsidence occurred.

Miller et al. (1989) studied the spatial and temporal distributions of temperature and O_2 in compost piles for the production of mushroom substrate. Figure 1.2 shows characteristic patterns of temperature and oxygen concentrations in a cross-sectional plane of a compost pile. These patterns pertained to a static pile without forced aeration. Microbial heating started at the outer zones and upper corners of the pile. In the pile core the temperature rise was delayed because oxygen depletion occurred after 7 hours. Subsequently, the temperature in the outer zones reached levels which inhibited microbial activity. Then, oxygen consumption was reduced and oxygen was transferred to deeper layers in the pile. This promoted a temperature rise in the pile core.

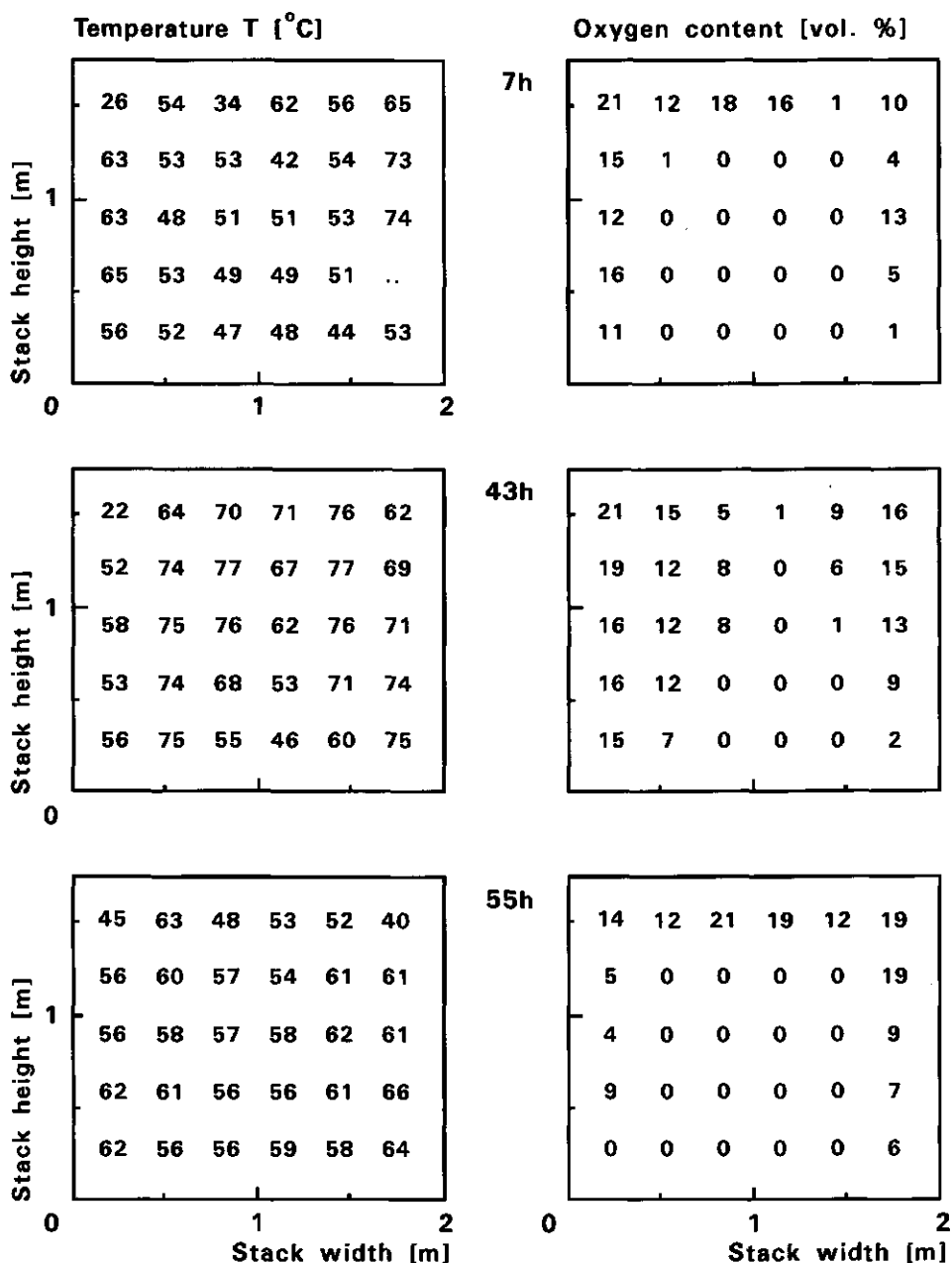


Figure 1.2 Distributions of the temperature and the oxygen concentration in a compost pile at 7, 43 and 55 hours after the start of the process. Turning of the pile occurred at 51 h (Miller et al., 1989).

At 51 hours the pile was turned and mixed. After that time the phenomena described previously recurred more intensely, probably because the microbial community has already developed during the period before the turning event.

Going from the outer shell to the centre of the pile the oxygen content decreased, whereas the carbon dioxide content increased. A maximum CO_2 -content of 21 vol.% could be expected from the stoichiometry of the aerobic degradation reaction of glucose. However, the carbon dioxide content decreased to a value of 40 vol.%. This indicated that fermentation occurred.

1.5 Models of the composting process

In composting several goals have to be met. Often, these goals are conflicting, e.g. sanitation requires a higher temperature than a maximum degradation rate does. To improve the process management, simulation models can be of considerable value.

Haug (1993) presented a model which describes the composting of sewage sludge cake. The composting mass was schematically represented by a gas, liquid and solid phase. Organic matter degradation was considered as a first order reaction with respect to the substrate concentration. The rate constant in this equation was a function of temperature. Rate limitations due to suboptimal values of the air filled volume fraction, moisture content and oxygen concentration in the gas phase were taken into account. Haug used an integral approach to describe the processes. This means that the heat and mass balances were calculated with respect to the compost pile as a whole. Thus, his model cannot be used to calculate temperature or oxygen profiles in a cross section of a compost pile and this precludes a sound validation of the model.

Forced convection was used as a starting point in Haug's model. As a result of the integral approach, the flow pattern of the convective air stream was not computed by the model. Free convection was only studied theoretically using a pore tube model. The flow in a tube was assumed to be laminar and its friction losses were estimated by using the Hagen-Poiseuille law. Whether or not free convection can satisfy the oxygen requirements depends on the air filled porosity. It was stated that free convection may increase during the process due to an increase of air filled porosity caused by water loss (Haug, 1993). Free air space will probably not increase in a major part of the pile because subsidence will occur during the composting process.

Nakasaki et al. (1987a) published a comparable but simpler model also describing the composting of sewage sludge cake. Their integral approach was based on a heat and mass balance of a complete batch reactor. Forced aeration

A mixture of chicken manure and wheat straw is used as composting material for the experiments described in this thesis. Compared to other substrates, e.g. town waste, the straw/manure mixture is well defined. Since the mixture is also used in horticulture to prepare a substrate for the production of the edible mushroom *Agaricus Bisporus*, there exists a lot of practical experience and scientific knowledge on this material which can be used in this study.

CHAPTER 2. MATHEMATICAL MODELLING OF THE PHYSICAL PROCESSES IN A COMPOST PILE

2.1 Introduction

In this chapter a mathematical model is introduced, aimed at describing the temperature and gas concentration distributions in a compost pile. Temperature distributions are determined by the heat balance including expressions for the fluxes and the source/sink terms. The distributions of various constituents of the gaseous phase are similarly determined by the mass balances of these species. The heat and mass transfer fluxes depend on the physical properties of the composting material. In turn, these properties are strongly influenced by the physical composition of the material (section 2.2). The dynamics of the gaseous phase, including the transport processes involved in the mass balances of this phase, are described in section 2.3. The heat balance of the composting material is discussed in section 2.4.

2.2 Composition of composting material, mass balances of the liquid and the solid phases and changes in the air-filled volume fraction

The composting material can be characterized by volume fractions, densities and concentrations using the theory of mixtures (Raats, 1987). The material is considered as a porous medium consisting of a solid, a liquid and a gaseous phase. The volume fractions of these phases are θ_s , θ_l and θ_g , respectively. They are subject to the constraint:

$$\theta_s + \theta_l + \theta_g = 1. \quad (2.1)$$

The solid mass is obtained by drying the material. If this material is subsequently heated at 600 °C, organic substances will decompose and ash will remain. Thus, the volume fraction of the solid phase consists of organic material and ash:

$$\theta_s = \theta_o + \theta_a. \quad (2.2)$$

About 50% of the organic fraction will degrade during the composting process by microbial activity. The ash fraction contains various minerals such as silicates, phosphates and carbonates, and is considered to be non-reacting.

The true density γ_i [kg m⁻³] of phase i is equal to the mass of phase i divided by the volume occupied by phase i , whereas the bulk density ρ_i [kg m⁻³]

of phase i is equal to the mass of phase i divided by the volume occupied by all the phases. Thus,

$$\rho_i = \theta_i \gamma_i. \quad (2.3)$$

The total bulk density ρ of the composting material is the sum of all the partial bulk densities ρ_i :

$$\rho = \rho_s + \rho_l + \rho_g = \theta_s \gamma_s + \theta_l \gamma_l + \theta_g \gamma_g. \quad (2.4)$$

In general, the contribution of the gaseous phase to the total bulk density is negligible and therefore ρ is approximately equal to the sum of ρ_s and ρ_l :

$$\rho \approx \rho_s + \rho_l. \quad (2.5)$$

Two ratios are often used to characterize composting material. These are the gravimetric dry matter content d_s [-], defined by:

$$d_s = \frac{\rho_s}{\rho}, \quad (2.6)$$

and the wetness w [-], defined by:

$$w = \frac{\rho_l}{\rho_s}. \quad (2.7)$$

In chapter 3 the dry matter content d_s will be used to calculate the bulk density distribution. In chapter 4 the wetness turns out to be an important ratio to describe the air permeability.

Composting material is compressible and exhibits both elastic and plastic behaviour (Lopez-Real, 1990, Randle and Flegg, 1985). Due to the compressibility the bulk density is a function of the local pressure in the material and therefore depends on the vertical position in the pile. Lopez-Real (1990) demonstrated that the volume of compost reduces during the process not only as a result of dry matter and water losses, but also due to gradual mechanical deformation under constant pressure conditions. Therefore, bulk density and air filled porosity vary with position and time. This is discussed in chapter 3.

In a compost pile air flows from the bottom or side of the pile to the top, while the material itself deforms slowly and its mass changes as a result of biological degradation and condensation/evaporation. At the start of the computations the composting material is considered non-rigid and the deformation is regarded to be instantaneous. Then, the initial distributions of air-filled porosity, bulk density and dry matter content are calculated, accounting for the compressibility of the material. Next, during the dynamic simulations the material is considered rigid. This means that bulk density of the composting material and porosity may change due to degradation processes and transfer of water (as liquid and/or vapour), but that the total volume stays constant.

The gaseous phase is considered to consist of nitrogen (N_2), oxygen (O_2), carbon dioxide (CO_2) and water vapour (H_2O). The true density of the gaseous phase is then given by:

$$\gamma_g = \sum_j \gamma_{gj}, \quad (2.8)$$

where γ_{gj} is the density [$kg\ m^{-3}$] of constituent j in the gaseous phase, and j stands for N_2 , O_2 , CO_2 or H_2O . Oxygen and carbon dioxide are involved in the biological degradation process (chapter 1).

During the process part of the solid phase will decompose. The insoluble substrate is hydrolyzed by the action of extracellular enzymes produced by the microbial population. The products of hydrolysis will dissolve in the water. A detailed discussion of the degradation process and the mathematical equations describing this process will be given in chapter 5. The rate of hydrolysis can be expressed by a first order function of the organic matter density (Eastman and Ferguson, 1981). Then, the mass balance of the solid phase is given by:

$$\frac{\partial \rho_s}{\partial t} = \frac{\partial \rho_o}{\partial t} = - \zeta_c^* \rho_o \quad (2.9)$$

where ζ_c^* is the rate constant of hydrolysis [s^{-1}]. The subscript C refers to carbon and the asterisk is used to distinguish this constant from the rate constant of hydrolysis introduced in chapter 5 which is expressed in other units.

The bulk density of the liquid phase ρ_l can change due to flow of water and evaporation/condensation processes. Since composting material is considered

rigid during the process, there is no effect of subsidence. The local mass balance of the liquid phase is written as:

$$\frac{\partial p_l}{\partial t} = - \nabla \cdot (\gamma_l u) - r_{H_2O}, \quad (2.10)$$

where u is the filter velocity of the liquid phase [$m \ s^{-1}$] and r_{H_2O} the rate of evaporation [$kg \ m^{-3} \ s^{-1}$]. To determine the filter velocity u of the liquid phase, information is needed about the characteristics of water retention and hydraulic conductivity. Both parameters must be known for various bulk densities. Unfortunately, only very limited data on the water retention characteristic are available (Raviv et al., 1987; Miller, 1989), so that a quantitative description of water transport in composting material is not yet possible. Therefore it is assumed that there is no flow of liquid water unless the local dry matter content or the air-filled volume fraction decrease below certain minimum levels. These levels are determined by the smallest values ever measured in this study.

Changes in bulk densities of the liquid and the solid phases give rise to changes in the air-filled volume fraction. From the equations (2.1), (2.3), (2.9) and (2.10) it follows immediately that:

$$\frac{\partial \theta_a}{\partial t} = - \frac{1}{\gamma_o} \frac{\partial p_s}{\partial t} - \frac{1}{\gamma_l} \frac{\partial p_l}{\partial t}. \quad (2.11)$$

Thus, drying and decomposition of the solid phase increase the air-filled volume fraction.

2.3 Dynamics of the gaseous phase

2.3.1 Mass balances

In the model nitrogen, oxygen, carbon dioxide and water vapour are considered as the main constituents of the gaseous phase. It is assumed that these constituents behave as perfect gases. Since the emphasis of this study is on the calculation of the distributions of temperature and oxygen concentrations, nitrogen fixation and denitrification are not considered and thus the source term of nitrogen is zero. Rates of oxygen consumption and carbon dioxide production depend on the rate of hydrolysis and the dynamics of the microbial

population (chapter 5).

The densities of all constituents of the gaseous phase change with temperature according to the perfect gas law. The density of water vapour also changes with temperature because the saturated vapour pressure depends on temperature. Under conditions of natural convection, the vapour pressure is considered to be equal to the saturated vapour pressure at any time and position in the compost pile (chapter 6)

It is assumed that at least a part of the gaseous phase can be regarded as a continuous system of interconnected pores. Convection and diffusion of gases will occur in this pore system. For each constituent j of the gaseous phase the following mass balance equation holds (Bird et al., 1960):

$$\frac{\partial(\theta \gamma_{gi})}{\partial t} = - \nabla \cdot (\gamma_{gi} \mathbf{v}_i) + r_i, \quad (2.12)$$

where \mathbf{v}_i is the velocity of constituent j [m s^{-1}], and r_j the production rate of j [$\text{kg m}^{-3} \text{s}^{-1}$]. The velocity \mathbf{v}_i is the sum of the filter velocity of the gaseous phase and the diffusive velocity of constituent j :

$$\mathbf{v}_i = \mathbf{v} + \mathbf{v}_i^D. \quad (2.13)$$

The left hand side of equation (2.12) can be expanded to:

$$\frac{\partial(\theta \gamma_{gi})}{\partial t} = \theta \frac{\partial \gamma_{gi}}{\partial t} + \gamma_{gi} \frac{\partial \theta}{\partial t}. \quad (2.14)$$

Since the constituents of the gaseous phase are assumed to obey the perfect gas law the density γ_{gi} can be expressed as a function of P_j and T :

$$\gamma_{gi} = \frac{M_j P_j}{R T}, \quad (2.15)$$

where M_j [kg kmol^{-1}] is the molecular weight of constituent i , R [$\text{J kmol}^{-1} \text{K}^{-1}$] the gas constant, P_j [Pa] the partial pressure of constituent j and T the temperature [K]. The perfect gas law for each constituent implies the perfect gas law for the gaseous phase as a whole. Thus,

$$\gamma_g = \sum_i \gamma_{gi} = \sum_i \frac{M_i P_i}{R T} = \frac{\sum_i P_i M_i}{R} \frac{\sum_i P_i}{T} = \frac{M_g P}{R T}, \quad (2.16)$$

where P is the total pressure of the gaseous phase [Pa]. The average molecular mass of the gaseous phase M_g is the P_i -weighted mean of the molecular masses of the constituents of the gaseous phase. Substitution of (2.15) into (2.14), followed by substitution of that result together with (2.13) into (2.12), gives:

$$\frac{M_j}{RT} \left\{ \theta_g \left(\frac{\partial P_j}{\partial t} - \frac{P_j}{T} \frac{\partial T}{\partial t} \right) + \frac{\partial \theta_g}{\partial t} P_j \right\} = \nabla \cdot (\gamma_{gj} \mathbf{v} + \gamma_{gj} \mathbf{v}_j^D) + r_j. \quad (2.17)$$

Addition of (2.17) for all species yields the mass balance of the entire gas phase:

$$\begin{aligned} \frac{M_{N_2}}{RT} \left\{ \theta_g \left(\frac{\partial P_{N_2}}{\partial t} - \frac{P_{N_2}}{T} \frac{\partial T}{\partial t} \right) + \frac{\partial \theta_g}{\partial t} P_{N_2} \right\} &= - \nabla \cdot (\gamma_{gN_2} \mathbf{v} + \gamma_{gN_2} \mathbf{v}_{N_2}^D) \\ \frac{M_{O_2}}{RT} \left\{ \theta_g \left(\frac{\partial P_{O_2}}{\partial t} - \frac{P_{O_2}}{T} \frac{\partial T}{\partial t} \right) + \frac{\partial \theta_g}{\partial t} P_{O_2} \right\} &= - \nabla \cdot (\gamma_{gO_2} \mathbf{v} + \gamma_{gO_2} \mathbf{v}_{O_2}^D) + r_{O_2} \\ \frac{M_{CO_2}}{RT} \left\{ \theta_g \left(\frac{\partial P_{CO_2}}{\partial t} - \frac{P_{CO_2}}{T} \frac{\partial T}{\partial t} \right) + \frac{\partial \theta_g}{\partial t} P_{CO_2} \right\} &= - \nabla \cdot (\gamma_{gCO_2} \mathbf{v} + \gamma_{gCO_2} \mathbf{v}_{CO_2}^D) + r_{CO_2} \\ \frac{M_{H_2O}}{RT} \left\{ \theta_g \left(\frac{\partial P_{H_2O}}{\partial t} - \frac{P_{H_2O}}{T} \frac{\partial T}{\partial t} \right) + \frac{\partial \theta_g}{\partial t} P_{H_2O} \right\} &= - \nabla \cdot (\gamma_{gH_2O} \mathbf{v} + \gamma_{gH_2O} \mathbf{v}_{H_2O}^D) + r_{H_2O} \\ \hline \frac{M_g}{RT} \left\{ \theta_g \left(\frac{\partial P}{\partial t} - \frac{P}{T} \frac{\partial T}{\partial t} \right) + \frac{\partial \theta_g}{\partial t} P \right\} &= - \nabla \cdot \gamma_g \mathbf{v} + r_{O_2} + r_{CO_2} + r_{H_2O}. \quad (2.18) \end{aligned}$$

The diffusion velocities vanish in the summation of (2.18). This follows from equation (2.13) and the summation of $\gamma_{gi} \mathbf{v}_i^D$ over all gas species given by:

$$\sum_j (\gamma_{gj} \mathbf{v}_j^D) = \sum_j (\gamma_{gj} \mathbf{v}_j) - \sum_j (\gamma_{gj} \mathbf{v}) = \gamma_g \mathbf{v} - \gamma_g \mathbf{v} = 0. \quad (2.19)$$

The next subsection will focus on the processes affecting the mass balance of the gas phase.

2.3.2 Convection and diffusion

Two types of convection can be distinguished, natural (free) and forced convection. An air flow driven by buoyancy is called natural convection. Buoyancy is caused by density differences due to differences in temperature and/or composition. Forced convection is driven by pressure differences.

Fluid flow through porous media is described by Darcy's law:

$$\mathbf{v} = - \frac{\kappa}{\mu} (\nabla P - \gamma_g \mathbf{g}), \quad (2.20)$$

in which κ is the air permeability [m^2], μ the viscosity [N s m^{-2}], ∇P the pressure gradient [Pa m^{-1}], and \mathbf{g} the gravitational acceleration [m s^{-2}]. The air permeability depends on the size distribution, continuity and tortuosity of the air filled pore space. If forced aeration is used, it can be expected that the buoyancy term and the source terms are too small to affect the flow pattern significantly. If the buoyancy term is neglected, equation (2.20) reduces to:

$$\mathbf{v} = - \frac{\kappa}{\mu} \nabla P. \quad (2.21)$$

This equation will be used in chapter 4 to determine the air permeability of the composting material. For steady-state conditions equation (2.18) together with (2.21) becomes:

$$\nabla \cdot (\kappa \gamma_g \nabla P) = 0. \quad (2.22)$$

In chapter 7 equation (2.22) will be used to calculate air flow patterns for various forced aeration systems.

The diffusive velocities of various components in a multinary system are calculated by means of the Stefan-Maxwell equations (Bird et al., 1960; Hirschfelder et al., 1964):

$$\nabla \chi_j = \sum_{k=1}^n \frac{1}{c D_{jk}} (\chi_j N_k - \chi_k N_j), \quad (2.23)$$

where χ_j is the relative molar concentration of constituent j in the gaseous phase [-] defined as the molar concentration of j divided by the total molar concentration, N_j the molar flux of j [$\text{kmol m}^{-2} \text{s}^{-1}$], c the total molar concentration [kmol m^{-3}], and D_{jk} the binary diffusion coefficient [$\text{m}^2 \text{s}^{-1}$]. Equation (2.23) pertains to diffusion processes between n gas species in a system without walls. In a compost pile diffusion is restricted to the gaseous phase. The diffusing gas molecules collide with pore walls. In chapter 4 effective diffusion coefficients will be determined in which this wall effect is included. The magnitude of these effective diffusion coefficients will be smaller than the diffusion coefficients in a gas system without walls.

Since the molar flux N_j in equation (2.23) is equal to the product of the molar concentration c_j and the diffusive velocity v_j^D , (2.23) can be reformulated as:

$$\frac{1}{\chi_j} \nabla \chi_j = \sum_{k=1}^n \frac{1}{D_{jk}} \chi_k (v_k^D - v_j^D). \quad (2.24)$$

Equation (2.24) is expressed in molar concentrations, whereas the mass balance (2.18) is written in terms of densities. Therefore, equation (2.24) must also be expressed in densities. To achieve this, χ_j and $\nabla \chi_j$ are rewritten by means of the perfect gas law. Then, it follows that:

$$\chi_j = \frac{\frac{\gamma_{gj}}{M_j}}{\sum_{k=1}^n \frac{\gamma_{gk}}{M_k}}, \quad (2.25)$$

and

$$\nabla \chi_j = \nabla \frac{\left(\frac{\gamma_{gj}}{M_j} \right)}{\left(\sum_{k=1}^n \frac{\gamma_{gk}}{M_k} \right)} = \frac{\frac{1}{M_j} \left(\sum_{k=1}^n \frac{\gamma_{gk}}{M_k} \right) \nabla \gamma_{gj} - \left(\frac{\gamma_{gj}}{M_j} \right) \left(\sum_{k=1}^n \frac{1}{M_k} \nabla \gamma_{gk} \right)}{\left(\sum_{k=1}^n \frac{\gamma_{gk}}{M_k} \right)^2} \quad (2.26)$$

Finally (2.24) becomes:

$$\frac{\frac{1}{\chi_j} \nabla \gamma_{gj} \left(\sum_{k=1}^n \frac{\gamma_{gk}}{M_k} \right) - \left(\sum_{k=1}^n \frac{1}{M_k} \nabla \gamma_{gk} \right)}{\left(\sum_{k=1}^n \frac{\gamma_{gk}}{M_k} \right)^2} = \sum_{k=1}^n \frac{1}{D_{jk}} \frac{\left(\frac{\gamma_{gk}}{M_k} \right)}{\left(\sum_{p=1}^n \frac{\gamma_{gp}}{M_p} \right)} (\mathbf{v}_k^D - \mathbf{v}_j^D). \quad (2.27)$$

Expression (2.27) gives a set of n equations with n unknown velocities. This set can be solved with standard routines (Press et al., 1987).

The Chapman-Enskog theory is used to obtain an expression for the binary diffusion coefficient as a function of temperature. In this theory atoms and molecules are regarded as rigid spheres with a characteristic diameter σ (the collision diameter) (Hirschfelder et al., 1964):

$$D_{jk} = \frac{3}{8} \left(\frac{k^3 N_A}{\pi} \right)^{\frac{1}{2}} \frac{\left\{ T^3 (M_j + M_k) / (2 M_j M_k) \right\}^{\frac{1}{2}}}{P \sigma_{jk} \Omega_{jk}}, \quad (2.28)$$

where k is the Boltzmann constant [J K^{-1}], which is equal to 1.381×10^{-23} , N_A Avogadro's number [mol^{-1}] equal to 6.023×10^{23} , σ_{jk} the Lennard-Jones potential parameter or the collision diameter for unlike molecules of species j and k [m]. The collision diameter for unlike molecules is given by:

$$\sigma_{jk} = 0.5 (\sigma_{ji} + \sigma_{kk}), \quad (2.29)$$

where σ_{jj} and σ_{kk} are the collision diameters for like molecules j and k , respectively. The dimensionless collision integral Ω_{jk} is based on the Lennard-Jones intermolecular potential field and is a function of the dimensionless temperature defined by:

$$T^* = T k/E_{jk} \quad (2.30)$$

The Lennard-Jones potential parameter E_{jk} is the maximum energy of attraction between unlike molecules j and k [J]. This parameter is given by:

$$E_{jk} = \sqrt{E_{jj} \cdot E_{kk}}, \quad (2.31)$$

where E_{jj} and E_{kk} are the Lennard-Jones potential parameters for like molecules j and k , respectively. Values of σ_{jj} and E_{jj}/k are given by Mason and Monchick (1962) and Monchick and Mason (1961). Hirschfelder et al. (1964) and Bird et al. (1960) give data of the collision integral Ω_{jk} .

2.4 Heat balance of the composting material

In composting material liquid water may flow relative to the solid phase due to differences in water potential. In the model it is assumed that the flow rate is so small, that thermal equilibrium exists between the solid and the liquid phase. Under the condition of natural convection, the same assumption is made with respect to the flow rate of the gaseous phase. Thus, from a thermal point of view, the three phases are treated as one single phase.

If the radiative heat transfer in the compost pile is omitted, the sensible heat balance of the compost phase is given by:

$$\rho C \frac{\partial T}{\partial t} = - \nabla \cdot [\gamma_l C_l u T + \gamma_g C_{gp} v T - \lambda \nabla T] - H r_{H_2O} + Q, \quad (2.32)$$

where C and C_l are the specific heat capacities [$J \text{ kg}^{-1} \text{ K}^{-1}$] of composting material and water, respectively, C_{gp} is the specific heat capacity of air at constant pressure, λ the coefficient of thermal conductivity [$W \text{ m}^{-1} \text{ K}^{-1}$], H the heat of evaporation [$J \text{ kg}^{-1}$], and Q the microbial heat production rate [$W \text{ m}^{-3}$]. Since the flow rates of water and gas are assumed to be very small, the effect of hydrodynamic dispersion on λ is regarded negligible.

Energy is needed to evaporate water. If water evaporates at one place and

condenses at another place, heat transfer occurs. This type of heat transfer is called latent heat transfer. It is determined by the rate of evaporation r_{H_2O} multiplied by the heat of evaporation H . The rate of evaporation follows from equation (2.17) and the assumption that the vapour pressure is equal to the saturated vapour pressure:

$$r_{H_2O} = \frac{M_{H_2O}}{RT} \left\{ \theta_g \left[\frac{\partial P_{sat}}{\partial t} - \frac{P_{sat}}{T} \frac{\partial T}{\partial t} \right] + \frac{\partial \theta_g}{\partial t} P_{sat} \right\} + \nabla \cdot (\gamma_{gH_2O} \mathbf{v}_{H_2O}), \quad (2.33)$$

where P_{sat} is the saturated vapour pressure [Pa]. Equation (2.33) states that r_{H_2O} is the matching factor between changes in saturated vapour pressure, due to changes in temperature and air-filled volume fraction, and the net vapour transport.

If the velocities \mathbf{v} of the gaseous phase and the liquid phase are reduced to zero, equation (2.32) reduces:

$$\rho C \frac{\partial T}{\partial t} = \lambda \nabla^2 T + Q. \quad (2.34)$$

This equation is used in chapter 4 to determine the thermal conductivity coefficient of the composting material.

CHAPTER 3. BULK DENSITY AND POROSITY DISTRIBUTIONS IN A COMPOST PILE

3.1. Introduction

Transport of heat and mass in a compost pile is significantly affected by the geometry and size distribution of the pore space and the composition of the composting material. Therefore it is at least necessary to have information about the spatial distribution of porosity. Porosity can be calculated from dry matter content, true density of dry matter and total bulk density. Dry matter content and true density of dry matter are experimentally determined. Hence, the bulk density remains to be determined before porosity can be calculated. To describe the bulk density distribution, distinction is made between time dependent and time independent phenomena. The time independent phenomenon results from the compressibility of composting material (Randle and Flegg, 1985). Due to this property the bulk density is a function of the local pressure and therefore depends on the position in the pile. Compressibility is defined as the reciprocal of materials resistance against mechanical deformation, or more precisely, as the ratio between deformation and stress. The time dependent phenomenon is illustrated by the results of Lopez-Real (1990) (chapter 1). Subsidence is defined as the increase of mechanical deformation with time under constant pressure conditions. When a compost pile is built, the initial bulk density distribution is only determined by the compressibility of the composting material. However, during the process bulk density and porosity are also influenced by the combined effects of subsidence, loss of organic matter due to biological degradation processes and changing of water contents due to transport processes.

This chapter mainly deals with the description of the initial distribution of bulk density and porosity at the moment the pile is built or rebuilt. For composting material, no detailed discussion of the relation between bulk density and position was found in the literature. In section 3.2 this relation is deduced from theoretical and empirical considerations. This section also gives formulae to calculate the true densities of dry matter and organic matter. The true density of dry matter is used in the computation of porosity distributions in sections 3.4 and 3.5. In section 3.3 the design of experiments is described. The results are presented in section 3.4. A discussion of the results is given in sections 3.5. Unless otherwise stated, the errors of experimentally determined quantities given in this and the following chapters are expressed as standard error on the mean (Squires, 1976; Lyons, 1991).

3.2 Bulk density, air-filled volume fraction and true density of dry matter

3.2.1 Bulk density and air-filled volume fraction as a function of position in a compost pile

The force balance of a thin layer of composting material, somewhere in the pile, is used to derive the relation between bulk density and height in a compost pile (see figure 3.1).

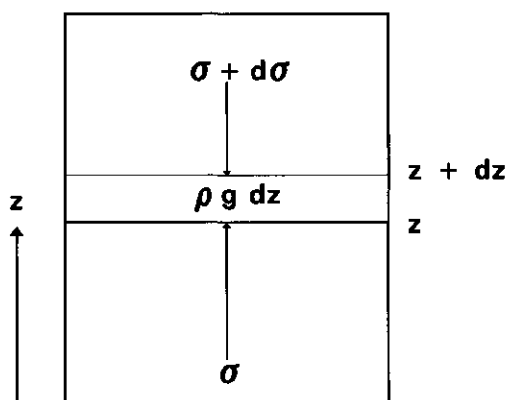


Figure 3.1 Force balance of a thin layer of composting material.

This force balance is written as:

$$d\sigma = - \rho(z) g dz, \quad (3.1)$$

where σ is the stress [N m^{-2}] and $\rho(z)$ the total bulk density at z [kg m^{-3}]. In addition to (3.1), a relation between σ and ρ is needed. Bernstein (1912) investigated the baling process of rye straw. He developed a relation between stress and dry bulk density. This relation, expressed in symbols used in this thesis, is given by:

$$\sigma = E (\rho_s - \rho_{su}), \quad (3.2)$$

in which E [J kg^{-1}] is a measure of the resistance against deformation for the composting material and ρ_{su} the unloaded dry bulk density [kg m^{-3}], occurring at the top of the pile. This equation also holds for composting material as will be shown in section 3.4. If the compression occurs at constant dry matter content,

it follows immediately from (3.2) that:

$$\sigma = E d_s (\rho - \rho_u), \quad (3.3)$$

where ρ_u is the unloaded total bulk density [kg m^{-3}]. Differentiation of σ with respect to ρ gives:

$$d\sigma = E d_s d\rho. \quad (3.4)$$

Substitution of (3.1) into (3.4) and re-arranging leads to the differential equation:

$$\frac{1}{\rho} d\rho = - \frac{g}{E d_s} dz. \quad (3.5)$$

At the top of the pile ($z = Z$) the bulk density is equal to the unloaded bulk density. This implies the boundary condition:

$$\rho = \rho_u \text{ at } z = Z. \quad (3.6)$$

The gravimetric dry matter content d_s is assumed to be independent of height z in the pile. The solution of (3.5) with boundary condition (3.6) is:

$$\rho = \rho_u \exp\left(\frac{g(Z - z)}{E d_s}\right). \quad (3.7)$$

The assumption of a homogeneous gravimetric dry matter content can be compared with some experimentally determined distributions. The experiments are described in section 3.3 and the results are given in the figures 3.2a to 3.2c. Figures 3.2a and 3.2b show the dry matter distributions at the start and at day 7 of experiments 1 and 2, respectively. The respective initial dry matter contents of the experiments 1 and 2 were 0.20 and 0.21. Figure 3.2a shows that the dry matter content changed from 0.20 to an average value of 0.25 on day 7. The largest deviation from the average value at day 7 occurred at the top layer. Here, the dry matter content was 0.19. Figure 3.2b shows that the distribution of the dry matter did not change during the seven days period, except from the bottom layer.

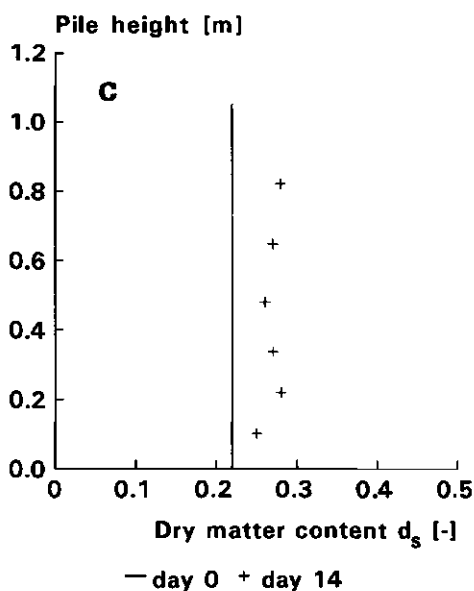
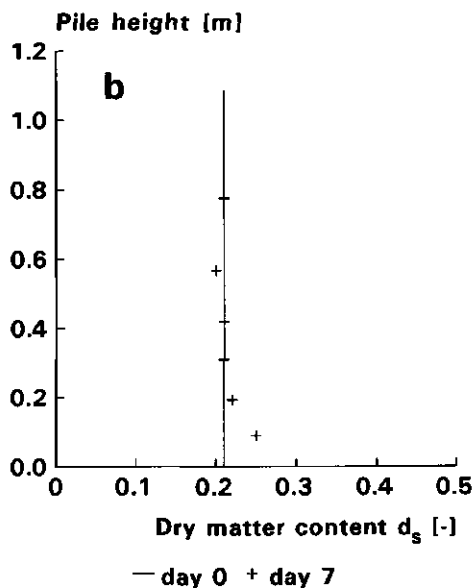
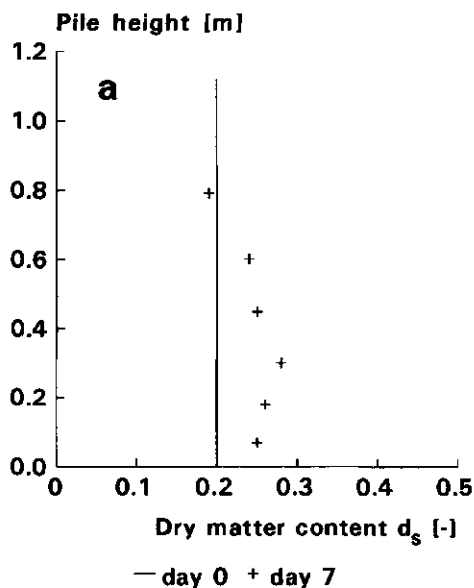


Figure 3.2 Distribution of the dry matter content d_s of experiments (a) 1, (b) 2 and (c) 3, respectively. The respective values of the initial dry matter content were 0.20, 0.21 and 0.22.

Figure 3.2c gives the dry matter distributions at day 0 and day 14 of experiment 3. The composting material used in this experiment had an initial dry matter content of 0.22. The dry matter distribution at day 14 is approximately parallel to the distribution at day 0. The assumption of a homogeneous dry matter distribution only pertains to the moment the pile has just been set up. After that moment redistribution of water can occur. Therefore it can be expected that the distributions at the end of day 0 will be more homogeneous than at days 7 and 14 shown in the figures 3.2a to 3.2c. From these figures it is concluded that, as a first approximation, the assumption of homogeneity is acceptable for compost piles at day 0 with a maximum height of 1.2 m and a dry matter content greater than 0.20.

To check the validity of the assumption in more detail it is necessary to analyze the behaviour of the liquid fraction. The assumption is valid as long as the liquid fraction is stationary relative to the matrix of dry organic matter. Information about the matric suction and the hydraulic conductivity of composting material is needed to describe the transport of water in a compost pile. As hardly any information about these transport parameters of composting material is found in the literature, it is impossible to determine if and to what extent transport of water will occur. However, it is certain that the discharge of water starts if the air filled volume fraction becomes zero as a result of compression. Then, the assumption of a homogeneous gravimetric dry matter content is no longer valid and (3.7) no longer holds. A second reason that (3.7) becomes invalid is the changing value of E if the air-filled volume fraction becomes zero and water seeps out. Further, it has to be emphasized that Z , and d_s are functions of time because water and dry matter are lost during the composting process.

The air filled volume fraction θ_g , calculated from the equations (2.1), (2.3) and (2.6), is given by:

$$\theta_g = 1 - \theta_s - \theta_l = 1 - \frac{\rho d_s}{\gamma_s} - \frac{\rho (1 - d_s)}{\gamma_l} \quad (3.8)$$

Substitution of (3.7) into (3.8) gives the relation between air filled volume fraction and height:

$$\theta_g = 1 - \left(\frac{d_s}{\gamma_s} + \frac{(1 - d_s)}{\gamma_l} \right) \rho_u \exp \left(\frac{g(Z - z)}{E d_s} \right) \quad (3.9)$$

Then γ_o is calculated using experimental values of γ_s , c_o and c_a . The true density γ_a can be obtained from the literature.

3.3. Materials and methods

In this section three identical experiments are presented. The experiments 1 and 2 are used to determine E. Experiment 3 is used to examine the validity of equation (3.3).

Composting experiments were carried out with a mixture of chicken manure and wheat straw. The mixture was prepared by chopping 300 kg of wheat straw to median stalk length of about 7.5 cm, wetting the straw during one week by spraying tap water on it and next adding 300 kg of chicken manure. The mixture was homogenized by passing it several times through a dung spreader. Finally, the mixture consisted of a straw matrix with embedded clods of chicken manure. These clods had a diameter of about 2 to 5 cm. The straw matrix consisted of stalks enveloped by a slurry of manure. For experiments 1, 2 and 3 the initial values of dry matter content were equal to 0.20, 0.21 and 0.22, respectively.

A rectangular container with dimensions $1.47 \times 1.47 \times 1.22 = 2.64 \text{ m}^3$ was made of plywood and provided with a grid floor. This container was filled with six layers of composting material with an initial weight of about 130 kg each, separated from each other by means of a rigid iron grid mounted in a wooden frame. The grids consisted of a wire netting with a mesh size of 9 mm, which was assumed to be large enough to ensure undisturbed transfer of heat, gases and liquids between the layers. Each grid weighed 15 kg. These grids were used as markers to measure the deformation of individual layers. A thin steel wire was fixed at each corner of the grids. These wires were guided over the brim of the container and were stretched by a small weight.

At filling the distances h_1 and h_2 were measured (see figure 3.3), in which h_1 is the distance between the grid on top of the most recently stacked layer and the brim of the container and h_2 the distance between the brim of the container and the end of each wire. When the filling process was completed the distances h_2 of each layer were measured. To follow the deformation of the layers during the process, the distances h_2 were measured at regular time intervals. The values h_1 and h_2 were used to calculate the distance between two contiguous grids. The volume of a layer was calculated by multiplying the area of a grid by the distance between the two contiguous grids. At filling the weight of each layer was determined and samples were taken of the raw mixture.

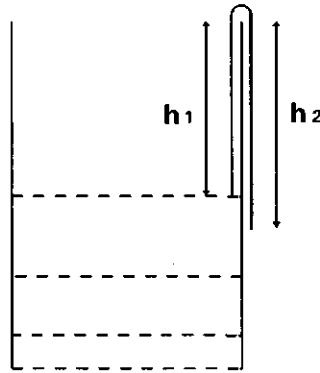


Figure 3.3 Heights measured when the pile was (re)built. Height h_1 is the distance between the most recently stacked grid and the brim of the container; h_2 is the distance between the brim and the end of the wire attached to the corner of the grid.

All three experimental runs lasted four weeks each. Usually a compost pile is turned at regular time intervals. In this study the time interval was one week. At the end of each period of seven days the compost pile was taken down and rebuilt layer by layer. Each layer of composting material was well mixed, weighed, sampled and kept separate from the other layers. When the pile was rebuilt, the individual layers were stacked in the same order as the week before. Samples were taken to determine the dry matter content. Each sample was weighed, dried at 105°C and weighed again. The unloaded total bulk density of a layer was defined as the total bulk density of that layer at the moment it was just stacked on the pile and loaded with one single grid. The stress exerted on a layer was calculated as the sum of weights of the layers, including the grids placed above the considered layer, plus half of its own weight.

The air-filled volume fraction was measured by means of an air pycnometer as described by Day (1964). It uses the principle of Boyle's law. The air-filled volume fraction of a sample is calculated from the resulting pressure when a gas at a measured volume and pressure expands into a larger volume, which includes the sample. The error in the air-filled volume fractions measured by this pycnometer was $0.04 \text{ m}^3 \text{ m}^{-3}$.

3.4. Results

To determine the value of E , (3.3) is written as:

$$E = \frac{\sigma}{d_s(\rho - \rho_u)} \quad (3.20)$$

Values of stress, dry matter content and bulk density were obtained from experiments 1 and 2 at the start of weeks 1, 2, 3 and 4. Organic matter decomposes during the composting process which may influence the mechanical strength of the material. The value of E was expected to be higher at the start of week 1 than at the start of week four. However, the difference between both values was not significant at a reliability level of 95%. Hence, it was decided to consider each instant the pile was (re)built as the start of a new experiment independent from the other. Figure 3.4 shows the relationship between $(\rho_s - \rho_{su})$ and σ . The intercept of the straight line was not statistically significant at 95% reliability. The value E obtained from the slope of the line was 73 J kg^{-1} with a standard error of 5 J kg^{-1} .

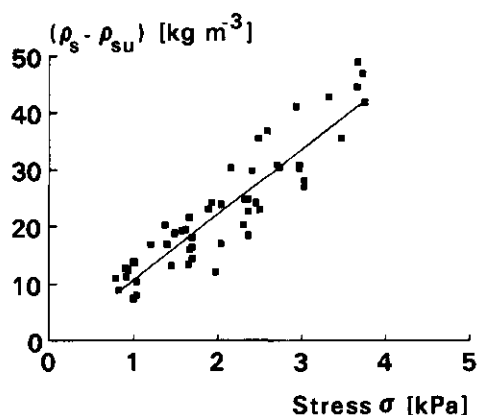


Figure 3.4 Deformation of dry material as a function of stress σ . The deformation is expressed as the difference between the dry bulk density ρ_s and the unloaded dry bulk density ρ_{su} .

The validity of (3.3) was checked by comparing values of bulk densities calculated by:

$$\rho = \rho_u + \frac{\sigma}{E d_s}, \quad (3.21)$$

with E equal to 73 J kg^{-1} and experimental values of bulk density obtained from experiment 3. Figure 3.5 shows the relationship between calculated and experimental bulk density values. Regression analysis of experimental and calculated values showed that there was no difference between the regression line through the points and the bisector at a reliability level of 95%. The error of values calculated by (3.14) was approximated from the confidence band of the regression line in figure 3.5 and was equal to an average value of 12% at the same reliability level.

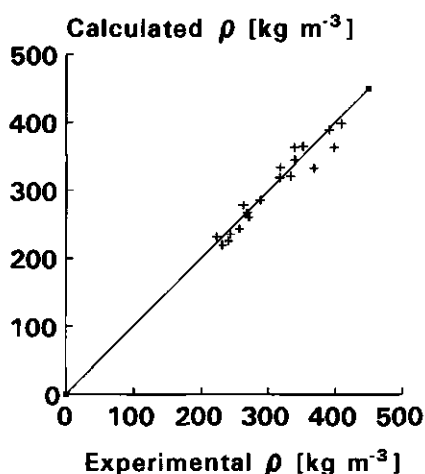


Figure 3.5 Relation between calculated and observed values of the bulk density ρ . Observed data are obtained from experiment 3. Calculated data are computed by (3.14) with $E = 73 \text{ J kg}^{-1}$, based on experiment 1 and 2.

Predicted values of total bulk density as a function of height calculated by (3.7) are depicted by the line in figure 3.6. These calculated values can only be compared with observed data at the start of the process when the amount of displaced water is regarded as negligible. This follows from the assumption that the gravimetric dry matter content is independent of position. In the same figure observed data from the start of experiment 3 are indicated by asterisks. The observed values and the curve of calculated data are almost parallel, which

indicates that the gravimetric water content was independent of height at the start of the process. Of course, the calculated values slightly underestimate the observed data because the weight of the grids is not accounted for in (3.7).

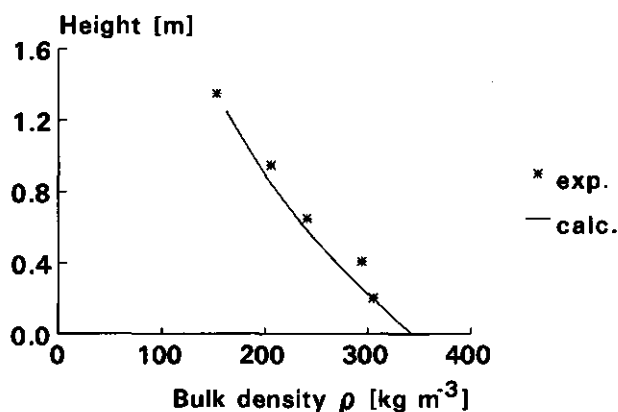


Figure 3.6 Relation between total bulk density ρ and height. The line indicates values calculated by (3.7) and the points indicate data observed at the start of experiment 3.

The true density of the dry matter of composting material was computed by means of (3.15) with measured values of bulk density ρ , dry matter content d_s and air-filled volume fraction θ_g . Usually, the value of an experimentally determined quantity is given as the average of a number of observation and its accuracy is given by the standard error on the mean. For the true densities calculated on the basis of (3.15) this leads to unrealistic values as a result of the small amounts of dry matter contained in the samples. Therefore, the sample with the largest θ_g was chosen. This sample consisted of composting material of 5 weeks old. The resulting value of γ_s was $1.9 \times 10^3 \pm 400 \text{ kg m}^{-3}$. To determine the true density of organic matter, the ash concentration c_a was calculated on the basis of 12 replicates. The resulting value was 0.44.

The ash fraction consists of minerals. The ash fraction of wheat straw contains 91% silica (Staniforth, 1979) and the ash fraction of chicken manure contains a large amount of sand and lime from the grit admixed in chicken feed as a calcium source (Hafez et al., 1974). The true density of sand and lime are given by Ulrich (1894) (cited by De Vries (1963)) and are equal to 2.65×10^3 and $2.71 \times 10^3 \text{ kg m}^{-3}$, respectively. Both values are of the same order of magnitude. No more quantitative information about the chemical composition of

ash is available yet. For calculation purposes it is therefore assumed that ash only consists of sand and the value $2.65 \times 10^3 \text{ kg m}^{-3}$ is adopted as the true density of the ash fraction. The true density of organic matter can now be computed by means of (3.19) and is found to be $1.6 \times 10^3 \pm 400 \text{ kg m}^{-3}$. The true density of cellulose is equal to $1.66 \times 10^3 \text{ kg m}^{-3}$ (Weast, 1985). Cellulose is one of the most important constituents of plant materials. This value is close to the magnitude of γ_o found in this study. Busse (1964) gives a value of $1.5 \times 10^3 \text{ kg m}^{-3}$ for compressed straw and Dexter (1964) found the same value for the true density of the dry matter of alfalfa calculated from water pycnometer measurements. These values also have the same order of magnitude. However, Lang (1878) (cited by De Vries (1963)) found a value of $1.26 \times 10^3 \text{ kg m}^{-3}$ for humus in soils. Humus can be considered as the final product of the degradation of plant materials and it is chemically different from cellulose. After only 4 weeks of thermophilic composting the state of total humification is not approached by far. It is therefore not surprising that the value of γ_o found in this study lies between that of cellulose and humus.

The analytical data obtained from literature cited above are given without estimates of errors because no information about experimental errors was included in these literature data.

The ash content in dry matter of composting material will increase during the process. To describe the time course of the ash content it appears to be most appropriate to divide the actual ash concentration c_a by its initial value. The course of this relative ash content χ_a is given in figure 3.7. The values shown in this figure are average values based on 10 replicate samples. A mathematical relationship was obtained from nonlinear regression analysis of these experimental data:

$$\chi_a = 1.0 + 0.9 \left\{ 1 - \exp(-0.02 t) \right\}, \quad (3.22)$$

in which t is the process time [day]. This regression equation accounts for 92.6% of the variance.

To calculate the time course of the true density of dry matter (3.16) is rearranged:

$$\gamma_s = \frac{1}{\frac{c_o}{\gamma_o} + \frac{c_a}{\gamma_a}}. \quad (3.23)$$

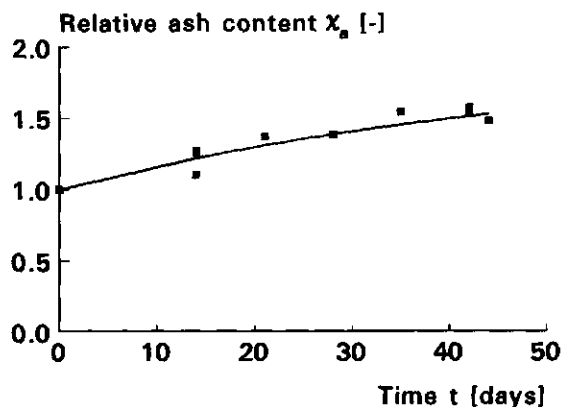


Figure 3.7 Relative ash content χ_a as a function of the process time.

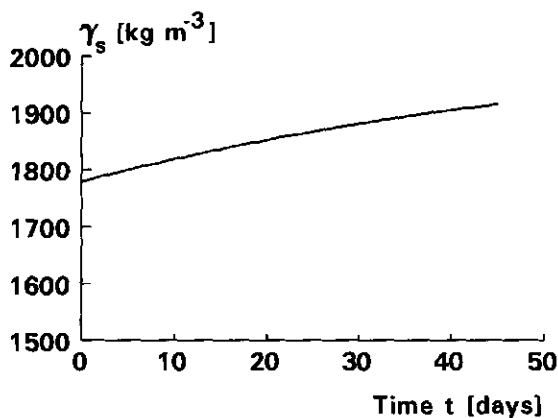


Figure 3.8 The true density of dry matter γ_s as a function of the process time.

In figure 3.8 the course of γ_s during the process is given. This time course was computed by (3.22) and (3.23) with a starting value of 0.29 for the ash content. During the thermophilic stage of the process the value of γ_s increased from 1.8×10^3 to 1.9×10^3 kg m⁻³. This increase may be regarded as insignificant compared to the value of 400 kg m⁻³ for $\Delta\gamma_s$. Therefore, an average value of 1850 kg m⁻³ for γ_s was used in computations and the dynamic changes of this value during the composting process were neglected.

The dynamic changes of ρ and θ_g are shown in the figures 3.9a and b and in table 3.1. Figure 3.9a gives the position of the top of separate layers during the first week of experiment 3 as described in section 3.2.

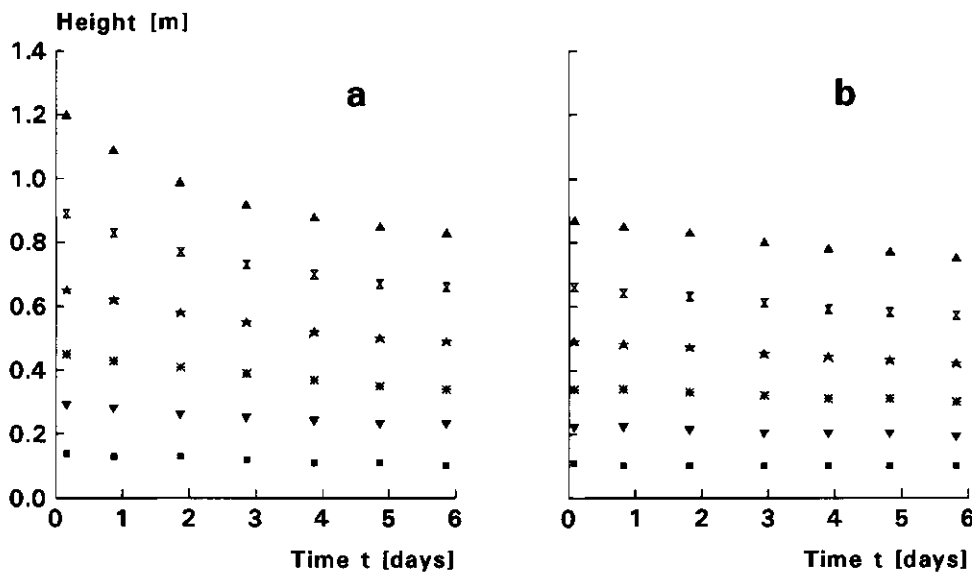


Figure 3.9 The time course of the top of separate layers during (a) the first week and (b) the last week of experiment 3.

This figure shows that the largest volume reduction occurred in the top layer during the first two days. Figure 3.9b gives analogous information for the last week (week 4) of experiment 3. In the last week the volume reduction was very small.

Table 3.1 Relative volume changes due to subsidence and material loss during the first and last week of experiment 3. V_i is the initial volume of a layer at the start of each week [m^3], ΔV is the total decrease of volume of a compost layer [m^3], $\Delta V'$ is the volume decrease resulting from loss of dry matter and water only [m^3] and l is the number of the compost layer (layer 1 is the bottom layer and layer 6 is on top of the pile).

l	week 1		week 4	
	$(\Delta V - \Delta V')/V_i$	$\Delta V'/V_i$	$(\Delta V - \Delta V')/V_i$	$\Delta V'/V_i$
6	0.50	0.02	0.09	0.03
5	0.27	0.03	0.15	0.02
4	0.24	0.04	0.16	0.02
3	0.22	0.05	0.13	0.02
2	0.17	0.04	0.11	0.03
1	0.19	0.05	0.14	0.04

Table 3.1 presents data about the relative volume changes due to subsidence and material loss only. The last parameter was calculated from measured values of dry matter and water loss divided by their respective true densities. Subsidence was computed as $(\Delta V - \Delta V')/V_i$. From the tabulated data it is possible to determine whether the volume reduction by subsidence exceeded the reduction by loss of dry matter and water. During both weeks the volume reduction due to material loss was small, about 4% in week 1 and 3% in week 4. The volume reduction due to subsidence varied, on average, from 27% during the first to 13% during the last week. During the first week subsidence tended to decrease going from the top to the bottom layer. This tendency was absent in week 4.

3.5 Discussion

In section 3.3 the validity of (3.7) was checked by comparing calculated data with experimental data described in section 3.2. In this section bulk density distributions calculated by (3.7) are compared with experimental distributions reported by other authors. Ohm (1972) described two experiments (A and C) with chopped hay, with dry matter contents of 69 and 68% respectively. Experiment B was carried out with unchopped hay with a dry matter content of 74%. In figure 3.10 the curves represent values calculated by (3.7). In these calculations the

value of the bulk modulus E was taken to be 73 J kg^{-1} . The experimental data, including values of unloaded bulk density, were obtained from Ohm (1972, p. 82, graph 3-5B). Figure 3.10 clearly shows the validity of equation (3.7) with respect to chopped hay. It is remarkable that E , obtained from experimental data of composting material with a dry matter content of approximately 25% also gives good results for chopped hay with a dry matter content of about 70%. Equation (3.7) seems not appropriate to predict the behaviour of unchopped hay.

Van Lier (1988) reported some experimental data of total bulk density as a function of height in a pile of mushroom compost. The mushroom compost mainly consisted of wheat straw and chicken manure. His data were also used to check the validity of (3.7). In his experiment the floor load amounted to 1800 kg m^{-2} , the total height Z was equal to 2.8 m and the dry matter content was 25%. In another experiment Van Lier determined the relation between water content and unloaded total bulk density. From these data a value of 222 kg m^{-3} was obtained at a dry matter content of 25%.

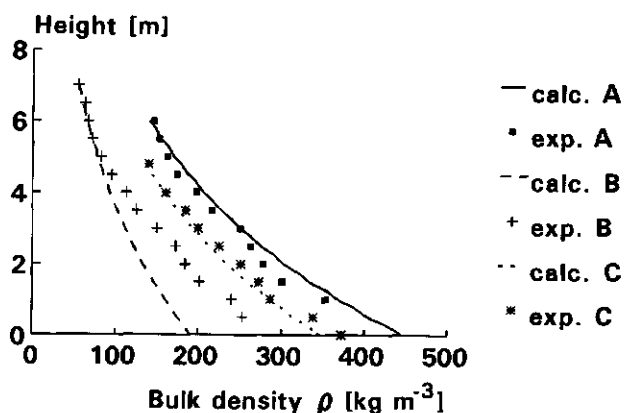


Figure 3.10 The relationship between calculated and observed total bulk densities and height. Observed data were obtained from Ohm (1972). Experiment A and C were carried out with chopped hay, whereas in experiment B unchopped hay was used. Calculated values are computed by (3.7).

12% at a reliability level of 95%;

- It seems likely that the presented equations will give reasonable results for other values of dry matter content and other kinds of chopped fibrous materials as long as the gravimetric dry matter content remains independent of height.

CHAPTER 4. PHYSICAL PROPERTIES OF COMPOSTING MATERIAL

4.1 Introduction

Knowledge of physical properties of composting material is necessary to calculate the distributions of temperature and gas concentrations in a compost pile. Only a few experimental data of these properties are known from the literature. Therefore, measurement of the air permeability κ , the oxygen diffusion coefficient D_{O_2} and the thermal conductivity coefficient λ is an important part of this study.

Many modern composting systems use forced aeration to control the process (Haug, 1993). To obtain a homogeneous product, the air flow must be evenly distributed over the cross-section of the compost pile. The flow pattern is determined by the type of aeration system, e.g. a perforated duct or a grid floor, the shape of the pile and the spatial distribution of the air permeability κ of the composting material. Section 4.2.1 describes experiments to determine the air permeability of composting material. The results are given in section 4.2.2.

The oxygen distribution in a compost pile is determined by the oxygen consumption rate (see chapters 5 and 6) and the diffusive and convective oxygen transport processes. In an aerated pile, oxygenation by long distance diffusion is obviously unimportant, although it may be important on the meso-scale of clumps. However, in a non-aerated pile the relative importance of diffusion and natural convection is still unclear because of a paucity of diffusivity and permeability data (Miller et al., 1989). Section 4.3.1 describes the experimental set-up to determine the oxygen diffusion coefficient D_{O_2} of composting material. The results are given in section 4.3.2.

The thermal conductivity coefficient λ is one of the physical properties which plays a role in the description of the temperature distribution in a compost pile. Section 4.4.1 gives a description of the experiments and in section 4.4.2 the results are discussed.

4.2 Determination of air permeability

4.2.1 Materials and methods

The air permeability is defined by Darcy's law (equation 2.21). The air permeability depends on volume fraction, size distribution, continuity and tortuosity of the air-filled pore space. For a particular composting material these factors are in turn affected by wetness (equation 2.7), age and handling

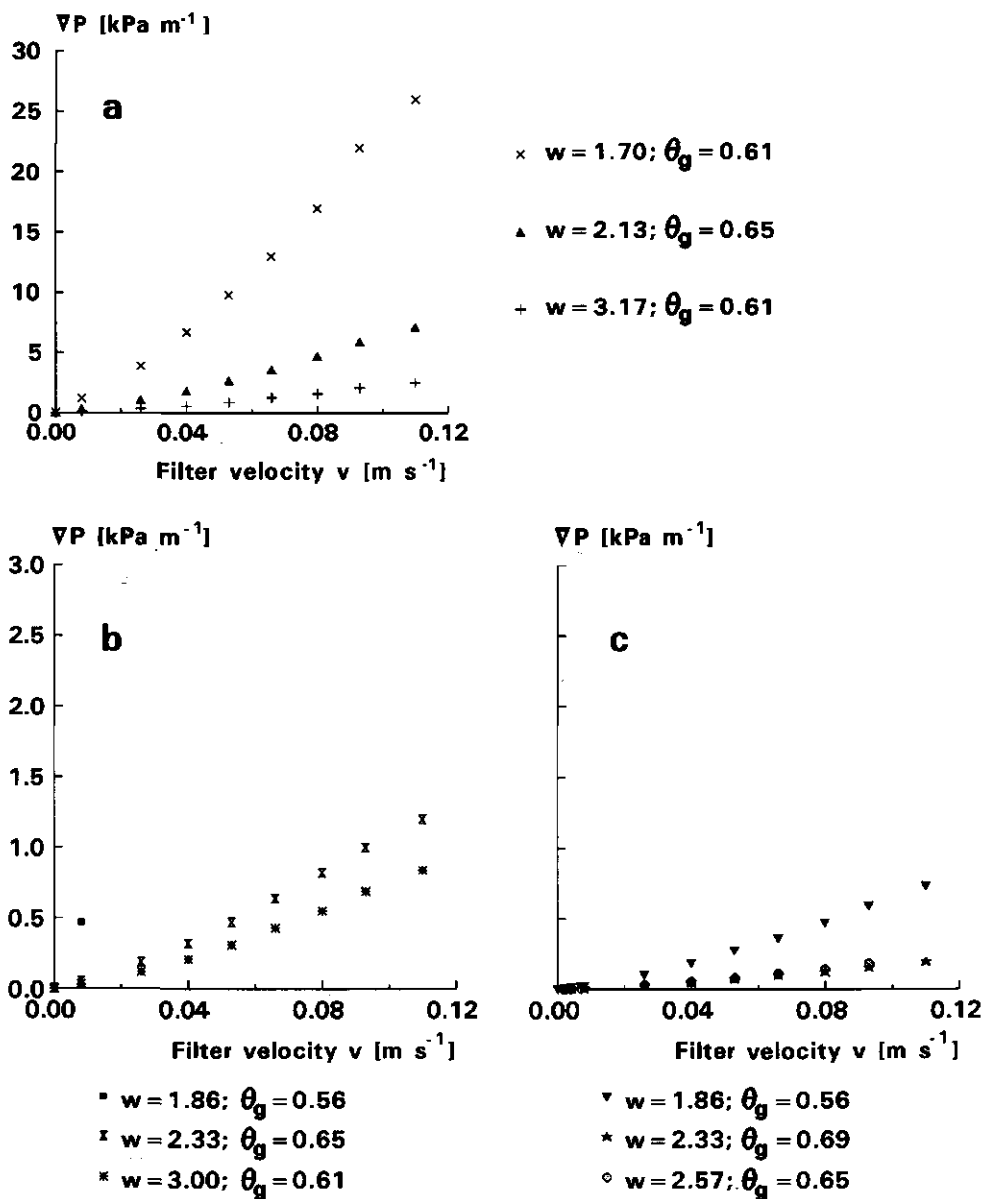


Figure 4.2 The non-linear relationship between the pressure gradient ∇P over a compost sample and the filter velocity v at three levels of wetness w . The air-filled volume fraction of the samples is designated by θ_g . Figure (a) pertains to raw material, (b) to material of 2 weeks old and (c) to material of 5 weeks old.

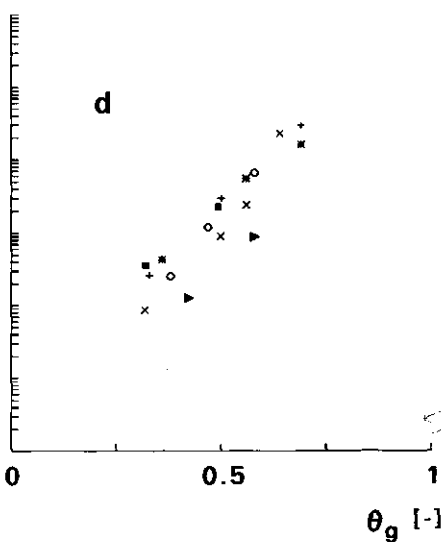
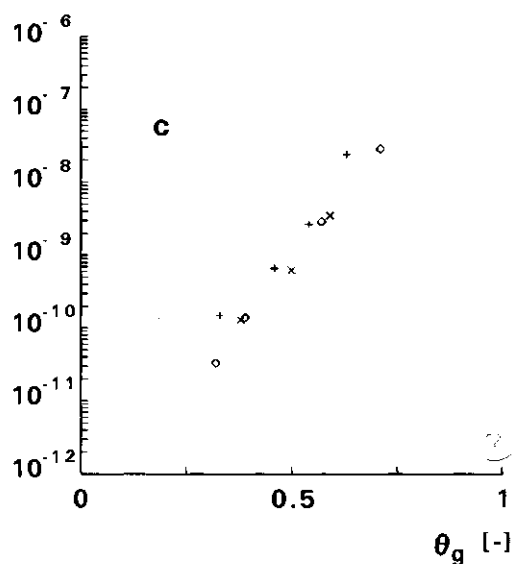
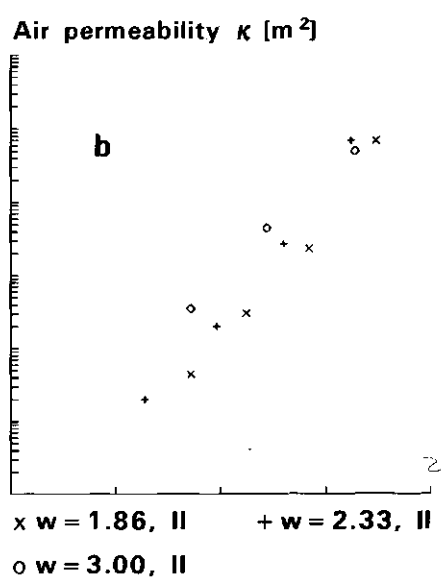
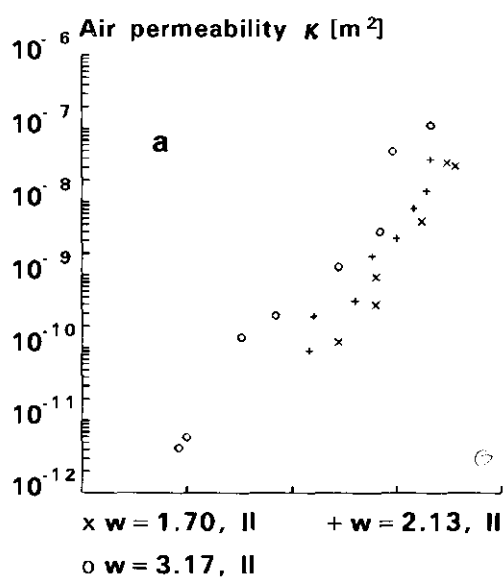


Figure 4.3 Air permeability κ as a function of the air filled volume fraction θ_g at three moisture levels w ($v = 0.008 \text{ m s}^{-1}$). Figures (a) to (d) show values of material of 0, 2, 3 and 5 weeks old, respectively.

It was observed that during the process the composting material became more sticky, probably due to the biological processes. During the thermophilic stage of the process the pile was turned at certain time intervals. Owing to these sticky properties and the mechanical forces exerted upon the material during the turning event, the compost was smeared and aggregates were formed. Within such aggregates the pore diameters will be small, but pores of large diameter will exist between these aggregates. These large inter-aggregate pores were responsible for the smaller pressure gradients of the more matured compost, in comparison with raw material.

Figure 4.3a shows the measured values of the air permeability of raw material as a function of the air-filled volume fraction. These results pertain to material of experiment II, wetnesses ranging from 1.70 to 3.17 and a filter velocity of 0.008 m s^{-1} . The permeability increased with the air-filled volume fraction and the wetness. In the figures 4.3b to 4.3d corresponding permeability values are given for 2-, 3- and 5-weeks old material. The permeability of 2-weeks old material of experiment II increased with the wetness (figure 4.3b). With 3-weeks old material of experiment I no clear relationship between permeability and wetness was found (figure 4.3c). Also, with 5-weeks old material of experiment II this relationship was not clear, but the permeability decreased with the wetness for material of experiment I.

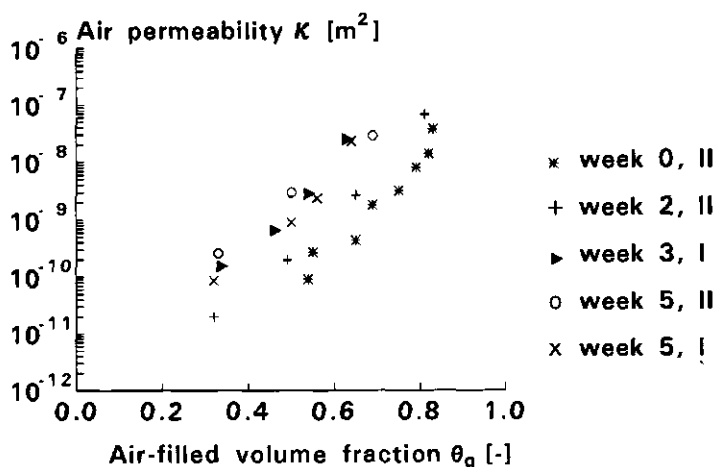


Figure 4.4 The effect of the age of the material on the air permeability κ at wetness $w = 2.33$, except week 0 which pertains to a wetness of 2.13.

Figure 4.4 shows experimental values at four ages of the material: 0, 2, 3 and 5 weeks. These values pertain to material with a wetness of 2.33, except week 0 which pertains to a wetness of 2.13. Since the permeability of raw material will be higher at 2.33 than at 2.13, it was not possible to conclude that the difference between the permeability of raw and 2-weeks old material was statistically significant. For material of experiment II the permeability increased with time going from week 2 to week 5. However, for material of experiment I the permeability decreased slightly with time going from week 3 to week 5. Since there were no permeability data of the raw material of experiment I, definitive conclusions with respect to the air permeability and materials age could not be drawn.

To asses the standard error of κ , it was assumed that the permeability did not change significantly after the first turning event. Then, samples of 2, 3 and 5 weeks old material with equal wetnesses and air-filled volume fractions were considered as replicates. In this way, four pairs of replicates with air-filled volume fractions of 0.32, 0.33, 0.50 and 0.63 were obtained. The standard errors of these replicates (with $w = 2.33$ and $v = 0.008 \text{ m s}^{-1}$) were equal to 3×10^{-11} , 6×10^{-11} , 1×10^{-9} and $5 \times 10^{-10} \text{ m}^2$, respectively. These standard errors were large. Probably, differences in pore structure between the replicates contribute very much to these large errors.

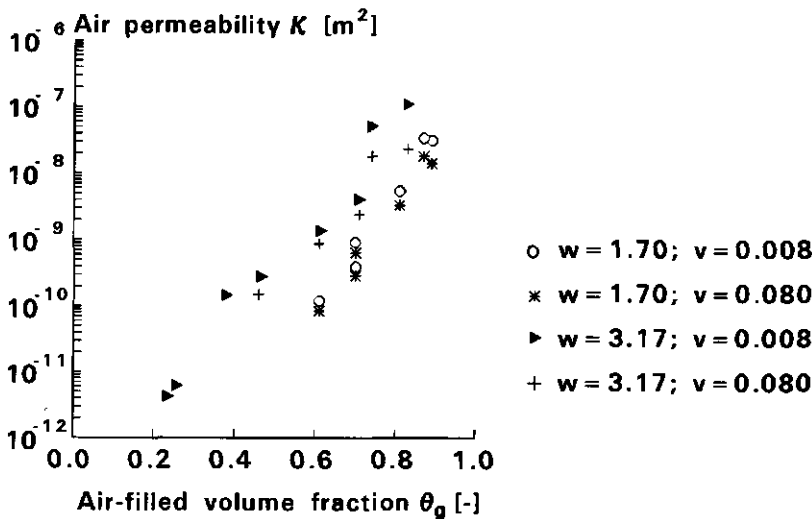


Figure 4.5 The air permeability κ of raw material as a function of the air-filled volume fraction θ_g and affected by the filter velocity v . The moisture levels were equal to $w = 3.17$ and $w = 1.70$.

Air permeabilities at high velocities were smaller than at low velocities (figure 4.5). This reflects the non-linearity of the relationship between the pressure gradient and the filter velocity.

Smith and Eilers (1980) reported some experimental values of pressure drop caused by air flow through compost. Their results were based on measurements in a 10 feet cube of composting sludge cake. They obtained permeability values of materials with 46 and 53% of dry solids. The air permeabilities were equal to 2.5×10^{-13} and $2.0 \times 10^{-13} \text{ m}^2$, respectively. To compare these permeabilities with the results given in the figures 4.3a to 4.3d it is necessary to know the air-filled volume fraction at which both permeabilities were measured. The air-filled volume fraction was calculated by equation (3.8). The total bulk densities ρ of sludge cake compost with 53 and 46% of dry solids were 885 and 862 kg m^{-3} , respectively (Smith and Eilers, 1980, p.13, figure 3). The true density γ_s of dry matter was $1.9 \times 10^3 \text{ kg m}^{-3}$ (section 3.4). Then, using (3.8), the air-filled volume fractions θ_g of both types of sludge cake were 0.33 and 0.32, respectively. The permeability values in the figures 4.3a to 4.3d at $\theta_g = 0.33$ are much larger than those given by Smith and Eiler. There appear to be two reasons for this difference. Firstly, the texture and the pore structure of sludge cake differ from that of wheat straw and chicken manure. Secondly, there will be a vertical gradient of the air-filled volume fraction because sludge cake is compressible. At the bottom of the 10 feet cube this volume fraction will be smaller than the average value of 0.33. Hence, also the permeability will be smaller.

4.3 Determination of effective oxygen diffusivity

4.3.1 Materials and methods

The diffusion coefficient was measured in the diffusion apparatus shown in figure 4.6. In the compost sample (1) microbial oxygen consumption occurred. This reduced the steady-state oxygen content in the head space (2) relative to the atmospheric content. The oxygen diffusion coefficient was calculated from this oxygen content reduction and the experimentally determined oxygen consumption rate. The oxygen content in the head space was determined by two identical O_2 -electrodes (3) with an error of $\pm 1 \text{ vol.}\%$ of oxygen. An inflated rubber tube (4) prevented air leakage along the outside of the sample cylinder into the head space. The diffusion coefficients were measured at room temperature.

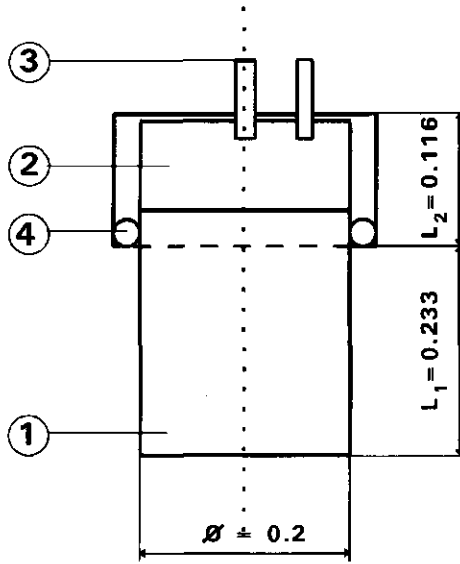


Figure 4.6 Diffusion apparatus. (1) sample cylinder filled with compost; (2) head space; (3) oxygen sensor; (4) rubber tube to prevent air leakage.

The oxygen balance of the sample in the diffusion apparatus is used as a starting point to find an expression for the diffusion coefficient. The steady state oxygen balance is given by:

$$\frac{d^2\gamma_{gO_2}}{dx^2} = \frac{r_{O_2}}{D_{O_2}}, \quad 0 < x < L_1, \text{ and } \gamma_{gO_2} > 0, \quad (4.2)$$

where L_1 is the height of the compost sample [m]. It is assumed that r_{O_2} is constant as long as $\gamma_{gO_2} > 0$. If all gases in the head space are completely mixed, the boundary conditions are given by:

$$x = 0: \gamma_{gO_2} = \gamma_{gO_2}^\circ, \quad (4.3)$$

in which $\gamma_{gO_2}^\circ$ is the atmospheric oxygen density, and

$$x = L_1: \frac{dy_{gO_2}}{dx} = 0. \quad (4.4)$$

The solution of (4.2) subjected to (4.3) and (4.4) can be written as:

$$\gamma_{gO_2} = \frac{r_{O_2}}{2 D_{O_2}} x^2 - \frac{r_{O_2}}{D_{O_2}} L_1 x + \gamma_{gO_2}^\circ. \quad (4.5)$$

For the steady-state density in the head space $\gamma_{gO_2}^\infty$ (at $x = L_1$) equation (4.5) gives:

$$\gamma_{gO_2}^\infty = - \frac{r_{O_2}}{2 D_{O_2}} L_1^2 + \gamma_{gO_2}^\circ. \quad (4.6)$$

Equation (4.6) results in an expression for the diffusion coefficient:

$$D_{O_2} = \frac{r_{O_2} L_1^2}{2(\gamma_{gO_2}^\circ - \gamma_{gO_2}^\infty)}. \quad (4.7)$$

Thus, the diffusion coefficient can be calculated from the measured oxygen consumption rate r_{O_2} and the difference between the steady-state oxygen density in the head space $\gamma_{gO_2}^\infty$ and the atmospheric density $\gamma_{gO_2}^\circ$.

Samples were obtained from two composting experiments. The samples of experiment II were taken from the raw material and after 2 and 5 weeks of composting. The samples of experiment III were taken after 0, 2, 4 and 6 weeks of composting. The dry matter content of the samples ranged from 0.17 to 0.24 and the bulk density from 2.2 to 5.7 kg m⁻³. Before the diffusion measurements took place, the air-filled volume fraction of the sample was measured in the air pycnometer. The oxygen consumption rate of the sample was determined in the experimental set-up as described in chapter 6. This measurement occurred after the completion of the diffusion experiment. The consumption rates decreased with compost age and were equal to 0.45, 0.35, 0.22 and 0.07 x 10⁻⁵ mol s⁻¹ kg⁻¹ (dm) for 0, 2, 4 and 6 weeks old compost, respectively. Unfortunately, the set-up to measure consumption rates was not available during the measurements of the samples of run II. The consumption rates of these samples were assumed to

correspond with those of the samples from experiment III. The oxygen consumption rate of 5 weeks old material was determined by interpolation between the measured values of 4 and 6 weeks old material.

For samples with high oxygen consumption rates per unit volume, the steady-state oxygen density in the head space was zero. If γ_{gO_2} became zero for x in the range $0 \leq x \leq L_1$, the assumption of a constant oxygen consumption rate was no longer valid. Otherwise γ_{gO_2} would become negative! As an example, figure 4.7 shows the distribution of the oxygen content in a sample of raw material with a bulk density of 710 kg m^{-3} .

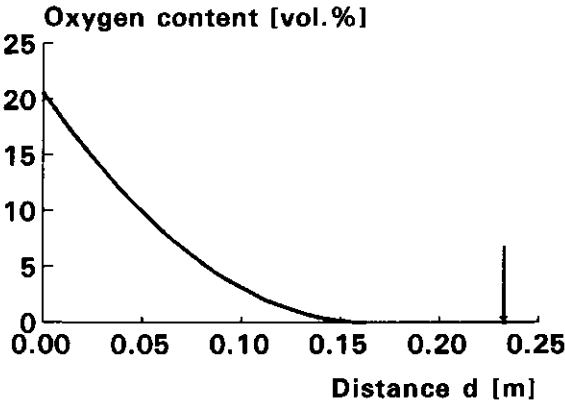


Figure 4.7 The distribution of the oxygen content in a sample with a large O_2 consumption rate. The arrow indicates the end of the sample cylinder.

This concentration distribution was calculated from equation (4.5). To avoid γ_{gO_2} becoming zero for x in the range $0 \leq x \leq L_1$, samples with large oxygen consumption rates were put in sample cylinders with $L_1 = 0.117 \text{ m}$ instead of 0.233 m .

4.3.2 Results

To get some insight in the accuracy of the measurements, the standard error of the mean of the samples was calculated. Samples were considered as replicates if they pertain to compost of the same age and if their air-filled volume fractions did not differ by more than 0.01. With these criteria five groups of 2 to 4 samples were obtained with standard errors ranging from 5×10^{-8} to $4 \times 10^{-7} \text{ m}^2 \text{ s}^{-1}$.

The oxygen diffusion coefficient increased with the air-filled volume fraction (figure 4.8). This is expected because the space available for gas diffusion increases. There was no clear relationship between the oxygen diffusion coefficient and the age of the material.

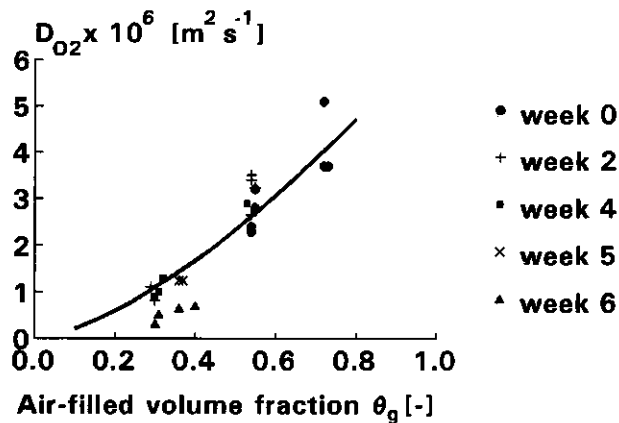


Figure 4.8 Oxygen diffusion coefficient D_{O_2} as a function of the air-filled volume fraction θ_g and depending on the age of the material. The curve was calculated by equation (4.8), with $b = 0.33$.

Nakasaka et al. (1987b) measured the oxygen diffusion through 10 mm of sterilized dehydrated sewage sludge cake. Their results obey the relationship:

$$D_e = b D_0 \theta_g^{1.5}, \quad (4.8)$$

where D_e is the effective diffusion coefficient, b a proportionality constant which depends on the pore size distribution, D_0 the diffusion coefficient in air and θ_g the air-filled volume fraction. This relationship was theoretically derived by Marshall (1959). The proportionality constant b for sewage sludge cake is equal to 0.386 (Nakasaka et al., 1987b). The curve shown in figure 4.8 pertains to the data of this study and was obtained by regression analysis using relationship (4.8). The proportionality constant b was equal to 0.33, which is reasonably close to the value for sewage sludge found by Nakasaka et al.. This conclusion and the finding that there is no effect of the materials age, give rise to the idea that the diffusion coefficient is mainly determined by the air-filled volume fraction.

4.4 Determination of thermal conductivity

4.4.1 Materials and methods

Experimental methods to determine the thermal conductivity of a medium are based on the solution of the partial differential equation (2.34) with appropriate boundary conditions. Many of these methods involve a temperature measurement of the medium at a fixed distance from a heat source dissipating a known quantity of heat. In a moist, porous medium redistribution of water will occur, due to the temperature gradient induced by the heat source. This complicates the determination of the thermal conductivity in two ways. Firstly, the heat capacity C , the bulk density ρ , and the thermal conductivity λ are functions of the water content and therefore C and ρ become time dependent and λ will depend on position. Hence, the partial differential equation and its solution become more complex. Secondly, the heat transfer is not exclusively conductive, but also convection and latent heat transfer occur. Convection is strongly reduced if the duration of the measurement is short and the temperature rise induced by the source is small. These constraints imply that a nonsteady-state method will be most favourable.

The thermal conductivity was measured with a nonsteady-state probe. The basic principle of this device was first introduced by Stålhane and Pyk (1931) and was improved and modified since then by several authors (Blackwell, 1954; Van Haneghem, 1981; Van Haneghem et al., 1983; Van Loon et al., 1989). The probe consists of a thin, stainless steel tube in which a heating wire and a temperature sensor are mounted (figure 4.9).

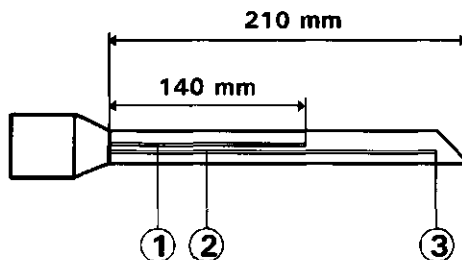


Figure 4.9 The nonsteady state probe. 1: heating wire; 2: hot junction of the thermocouple; 3: cold junction of the thermocouple.

The sensor and the heating wire are embedded in a silicon rubber compound. The length and diameter of the probe are 210 and 2 mm, respectively. The length of the double folded heating wire is 2 x 140 mm. The temperature sensor consists of a thermocouple with the cold junction near the end of the tube and the hot junction half-way the heating wire. The temperature of the cold junction is considered to stay equal to the temperature T_0 of the compost before the start of the measurement. The probe, embedded in the composting material measures the temperature response of the probe induced by an imposed constant heat supply in the probe. As a first approximation, this system can be considered as an infinitely long, infinitely thin heating wire, embedded in a homogeneous, isotropic medium (the perfect line source) and the heat balance, expressed in cylindrical coordinates, is given by:

$$\frac{\partial T}{\partial t} = a \left[\frac{\partial^2 T}{\partial r^2} + \frac{1}{r} \frac{\partial T}{\partial r} \right], \quad (4.9)$$

in which $T=T(r,t)$ is the temperature at distance r from the line source at time t and a the thermal diffusivity ($a=\lambda/(\rho C)$). With the initial and boundary conditions:

$$t = 0 \text{ and } r \geq 0: T = T_0 \quad (4.10a)$$

$$t > 0 \text{ and } r = \infty: T = T_0 \quad (4.10b)$$

$$t > 0: Q_l = \int_0^{\infty} 2\pi r C \frac{\partial T}{\partial t} dr, \quad (4.10c)$$

where Q_l is the heat production per unit length, the solution of (4.9) is:

$$T(r,t) - T_0 = \frac{Q_l}{4\pi\lambda} \left\{ - \text{Ei} \left[- \frac{r^2}{4at} \right] \right\}, \quad (4.11)$$

in which $\text{Ei}(-r^2/4at)$ is the exponential integral which can be written in a series expansion of $r^2/4at$:

$$T(r,t) - T_0 = - \frac{Q_1}{4\pi\lambda} \left\{ C_E + \ln \left(\frac{r^2}{4at} \right) + \sum_{n=1}^{\infty} \frac{(-1)^n (r^2/4at)^n}{n \cdot n!} \right\}, \quad (4.12)$$

where $C_E (= 0.5772..)$ is Euler's constant. The distance R between the hot thermocouple junction and the heating wire in the probe is less than 1 mm. It can be shown that at $r = R$ the term $r^2/4at \ll 1$ for t -values > 50 s and therefore higher order expansion terms can be neglected (Van Haneghem, 1981). Finally, equation (4.12) can be rewritten as:

$$T(R,t) - T_0 = A \ln t + B, \quad (t \gg r^2/4a) \quad (4.13)$$

with:

$$A = \frac{Q_1}{4\pi\lambda}, \quad (4.14)$$

and

$$B = \frac{Q_1}{4\pi\lambda} \ln \left(\frac{4a}{R^2 C_E^*} \right), \text{ in which } C_E^* = \exp(C_E) = 1.7811... \quad (4.15)$$

The thermal conductivity coefficient λ can be calculated from the slope A of the experimentally determined relationship (4.13) by means of:

$$\lambda = \frac{Q_1}{4\pi A}, \quad (4.16)$$

and in principle the product ρC can be found from the intercept B :

$$\rho C = \frac{4\lambda}{R^2 C_E^*} \exp(-B/A). \quad (4.17)$$

In the perfect line source approximation it is assumed that the temperature response at $r = R$ is only a function of the amount of heat dissipated by the

wire, and the thermal properties of the compost. In reality however, the temperature response is also a function of the probe thermal properties and the thermal contact resistance between the probe and the compost. Van Haneghem et al. (1983) developed a more accurate model of the probe which accounts for these additional factors. The error in measurements with this probe is $\pm 1\%$. A more detailed discussion of the probe method can be found in Bruijn et al. (1983) and Van Loon et al. (1989).

The nonsteady-state probe method avoids convective transport induced by the method itself. However, latent heat transfer due to diffusive transport of water vapour may still be induced by this method, especially in wet materials such as compost. Thus, the experimental value is composed of the genuine thermal conductivity coefficient and an apparent thermal conductivity coefficient due to latent heat transfer. In the next paragraph this apparent conductivity coefficient will be calculated.

The diffusive vapour flux can be written as:

$$\phi_v = -D_{H_2O} \frac{\partial \gamma_{gH_2O}}{\partial z} = -D_{H_2O} \left(\frac{\partial \gamma_{gH_2O}}{\partial T} \frac{\partial T}{\partial z} + \frac{\partial \gamma_{gH_2O}}{\partial \theta_l} \frac{\partial \theta_l}{\partial z} \right). \quad (4.18)$$

If the sample is well homogenized, $\partial \theta_l / \partial z$ is zero and equation (4.18) reduces to:

$$\phi_v = -D_{H_2O} \frac{\partial \gamma_{gH_2O}}{\partial T} \frac{\partial T}{\partial z}. \quad (4.19)$$

To obtain the latent heat flux (ϕ_h) due to water vapour diffusion, the vapour flux ϕ_v is multiplied by the heat of evaporation H , thus:

$$\phi_h = -H D_{H_2O} \frac{\partial \gamma_{gH_2O}}{\partial T} \frac{\partial T}{\partial z} = -\lambda_a \frac{\partial T}{\partial z}, \quad (4.20)$$

which implies an apparent conductivity coefficient λ_a [$W m^{-1} K^{-1}$] give by:

$$\lambda_a = H D_{H_2O} \frac{\partial \gamma_{gH_2O}}{\partial T}. \quad (4.21)$$

Combination of this equation with the universal gas law yields:

$$\lambda_a = H D_{H_2O} \frac{M_{H_2O}}{RT^2} \left[T \frac{\partial P_{H_2O}}{\partial T} - P_{H_2O} \right] \quad (4.22)$$

The vapour pressure P_{H_2O} is assumed to be equal to the saturated vapour pressure. This is reasonable because at a matric suction of about 1×10^6 Pa the relative humidity is still more than 99% (Koorevaar et al., 1983). The vapour diffusion coefficient D_{H_2O} is calculated from equation (4.8) with b equal to the value obtained for oxygen ($b = 0.33$). Values of the diffusion coefficient of water vapour in air are obtained from Mason and Monchick (1962) and the saturated vapour pressure is given by Goff and Gratch (1946). Figure 4.10 shows that the apparent thermal conductivity increases strongly with temperature and air-filled volume fraction. This can be expected from the nonlinear relationships between the temperature and the saturated vapour pressure and between D_{H_2O} and θ_g .

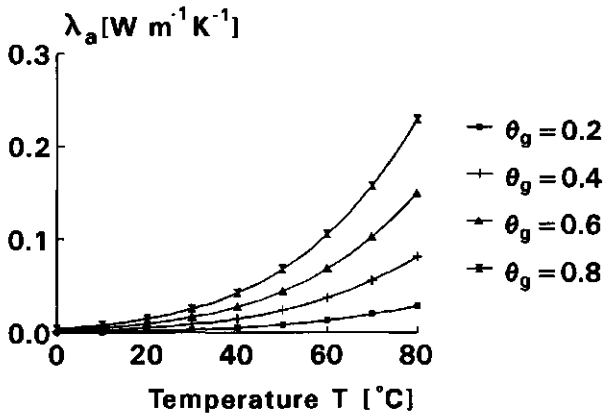


Figure 4.10 The apparent thermal conductivity coefficient λ_a due to latent heat transfer induced by the probe.

The thermal conductivity was measured both under laboratory conditions and in situ. During the laboratory experiments, the thermal conductivity probe was placed along the axis of an aluminium cylinder containing the compost sample. The internal height and diameter of the cylinder were 0.24 and 0.12 m, respectively. Four sample cylinders were located in a thermostatic bath. The measurements started after the samples had reached thermal equilibrium.

During both series the thermal conductivity was measured at different bulk densities, dry matter contents and temperatures. To obtain appropriate dry matter levels, different from the naturally occurring levels, the samples were dried at 105 °C and subsequently rewetted with tap water to the desired level.

The composting material used in the laboratory measurements was identical to the mixture described in section 3.3. This material was used to set up two static piles of about $4.35 \times 3.60 \times 1.5 = 23.5 \text{ m}^3$ each. The piles were turned, mixed and sampled at regular time intervals. Samples, taken from freshly prepared material and after 3 and 6 weeks of composting, were used to measure the thermal conductivity in the laboratory experiments.

The in situ measurements were accomplished in compost layers during experiment 1 described in section 3.2.

4.4.2 Results

The accuracy of the laboratory measurements was determined by repeatedly measuring of the thermal conductivities of two samples. The samples were well mixed before each measurement. The average standard deviation and standard error in the measurements of the two samples were 0.03 and 0.02 $\text{W m}^{-1}\text{K}^{-1}$, respectively. With an average thermal conductivity value of 0.24 $\text{W m}^{-1}\text{K}^{-1}$ this means an inaccuracy of 17% at a reliability level of 95%.

The sum of the volume fractions of the solid, liquid and gaseous phases is equal to unity. Thus, the system is determined if one fraction and the ratio between two of the fractions are given. In the figures given below the ratio between the volumetric water content θ_l and the volumetric dry matter content θ_s is used. In soil physical literature this ratio is termed the water ratio.

Figures 4.11a to d show the relationship between λ and the water ratio at 20, 35, 50 and 60 °C, respectively. The volumetric dry matter content θ_s of the samples ranged from 0.058 to 0.067. From these figures it can be concluded that λ increased with temperature. This is not surprising since the conductivity of water increases from 0.60 to 0.65 $\text{W m}^{-1}\text{K}^{-1}$ with the temperature going from 20 to 60 °C and also the apparent conductivity λ_a increases with temperature (see figure 4.10). It is not possible to discriminate upon differences in dry matter content between the samples because of the spread in the results and the narrow range of dry matter content. The conductivities increased with the water ratio. This can be expected from the lower value of the thermal conductivity of the solid phase compared to the liquid phase. The thermal conductivities of cellulose (main constituent of the dry matter of plant materials) and water at 20 °C are 0.18 and 0.60 $\text{W m}^{-1}\text{K}^{-1}$, respectively (Weast, 1985).

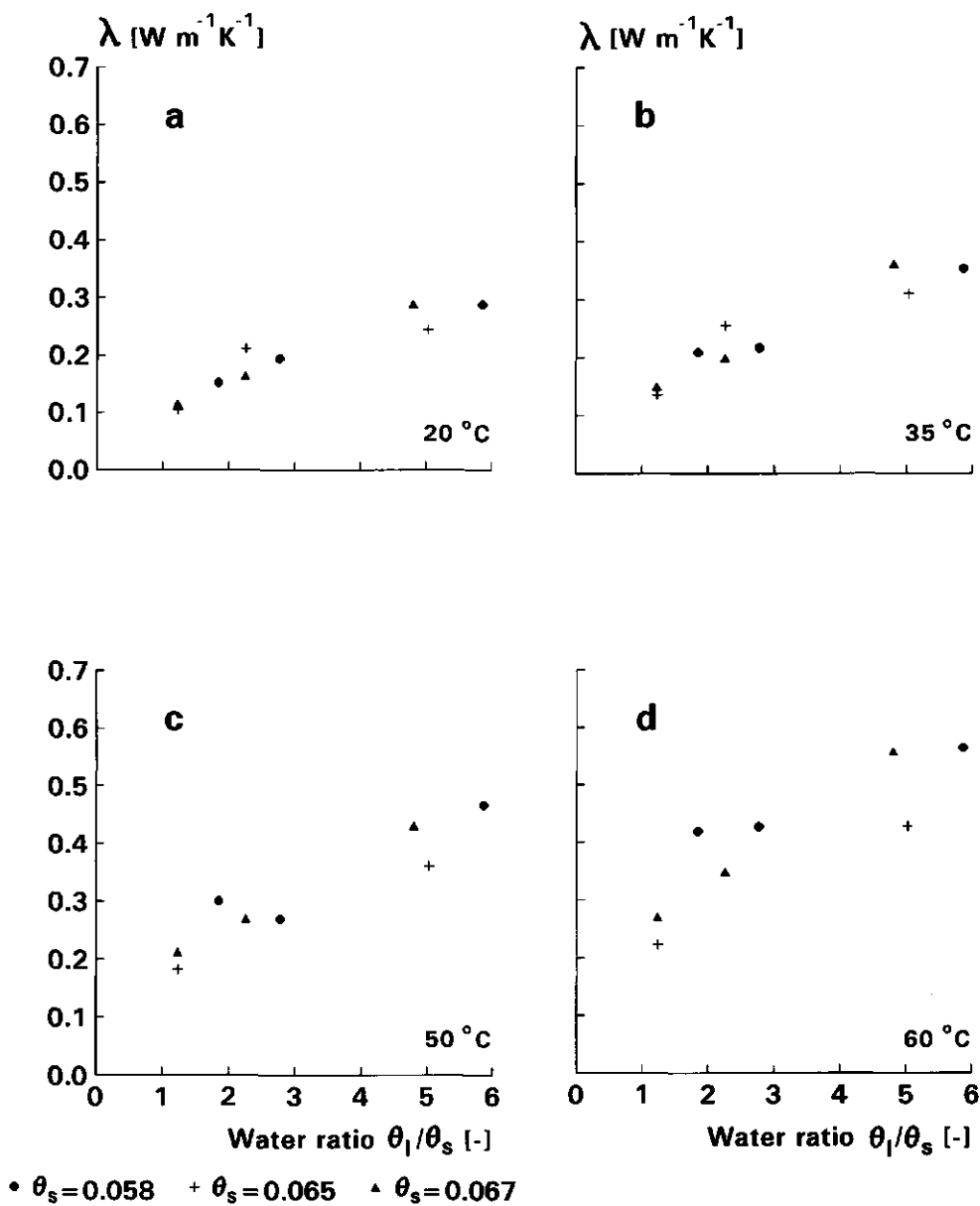


Figure 4.11 Relationship between thermal conductivity λ and the ratio between the volumetric water content θ_l and the volumetric dry matter content θ_s at (a) 20, (b) 35, (c) 50 and (d) 60 °C.

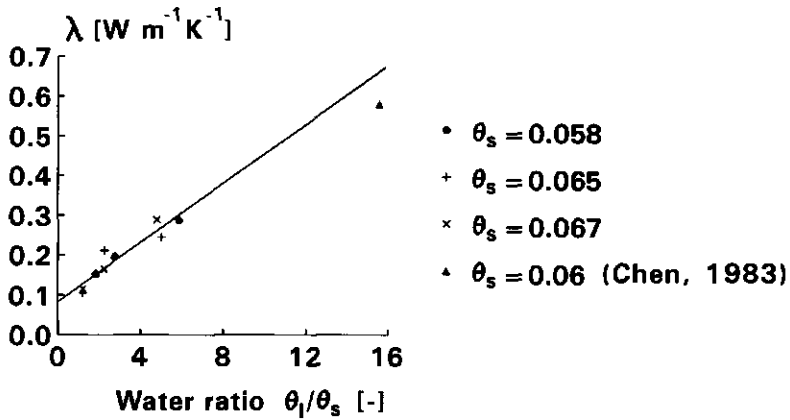


Figure 4.12 A comparison between experimental conductivities λ given by Chen (1983) and values obtained in this study.

Figure 4.12 is similar to figure 4.11a, but now the thermal conductivity of beef cattle manure given by Chen (1983) is included. Chen also used a nonsteady state probe. His value lies in the proximity of the regression line through the data obtained in this study. Chen also measured thermal conductivities at θ_s - values equal to 0.2 and 0.3 with a temperature of 20 °C. These values are shown in figure 4.13, together with conductivities at $\theta_s = 0.065$ obtained in this study.

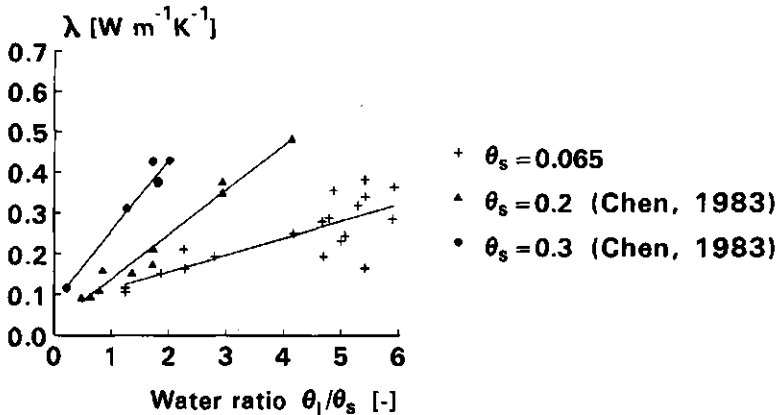


Figure 4.13 The thermal conductivity λ as a function of the water ratio at different values of the volumetric dry matter content θ_s .

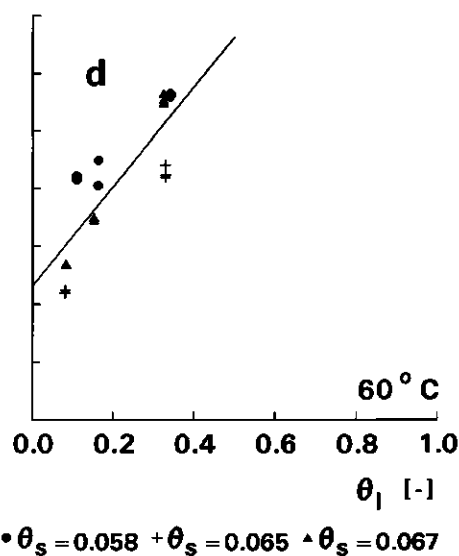
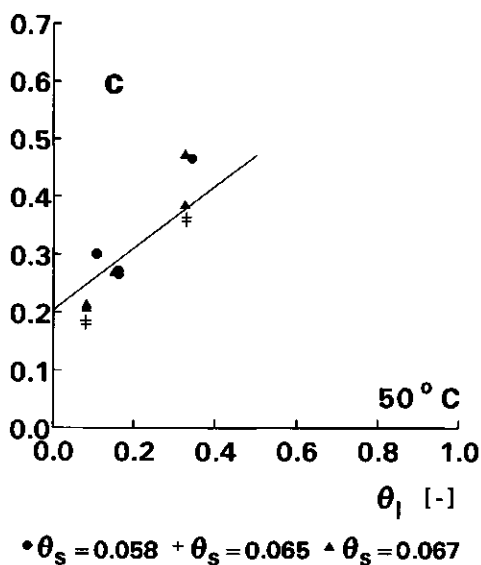
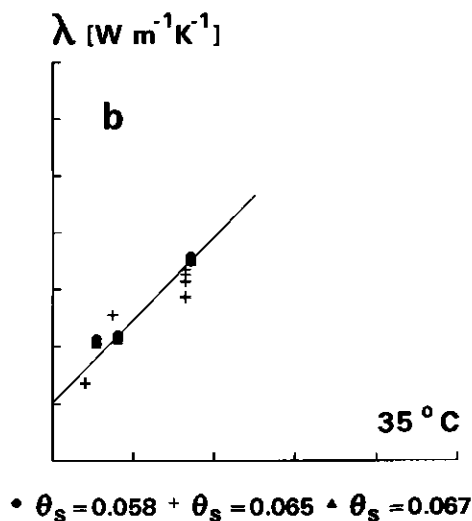
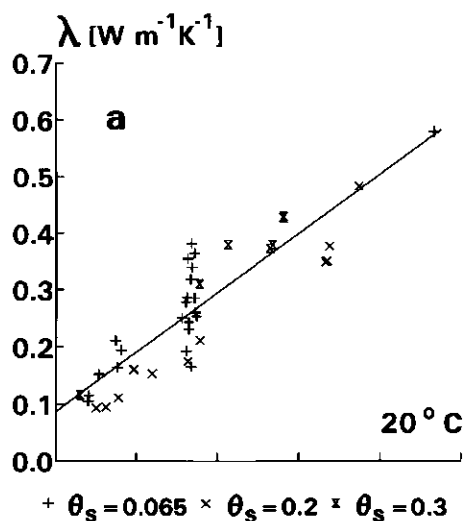


Figure 4.14 The relationship between the thermal conductivity λ and the volumetric water content θ_l at (a) 20, (b) 35, (c) 50 and (d) 60 °C.

It can be concluded that the in situ measurements of heat conduction can satisfactorily be explained by the results obtained from laboratory measurement. The results showed a linear relationship between the thermal conductivity and the temperature and between the thermal conductivity and the volumetric water content. The thermal conductivity was independent from the volumetric dry matter content θ_s for values of the dry matter content less than or equal to 0.3. The age of compost had no influence on the magnitude of λ .

4.5 Conclusions

In this chapter it was found that:

- the air permeability κ decreased as the air velocity increased;
- for raw material, the air permeability κ decreased with the wetness w , whereas for older material there was no clear relationship between κ and w ;
- The permeability of composting material which has been turned once, was larger than the permeability of raw material;
- the oxygen diffusion coefficient D_{O_2} was proportional to the air filled volume fraction to the power 1.5;
- there was no clear relationship between D_{O_2} and the age of the material;
- at a given temperature and for volume fractions of solid phase θ_s of 0.33 or less, λ increased linearly with the volume fraction of the liquid phase θ_l ;
- the age of the composting material did not influence λ ;
- the thermal conductivity coefficient λ increased with the temperature T .

CHAPTER 5. STOICHIOMETRY, ENERGETICS AND KINETICS OF THE BIOCHEMICAL DECOMPOSITION PROCESSES: THEORETICAL

5.1 Introduction

In the physical model (chapter 2), the decomposition process is represented by rates of O_2 consumption, CO_2 production and heat production. These rates depend on the chemical composition of the material, the biochemical pathways of degradation, and the kinetics of reactions and microbial growth and decay.

Wiley (1957) found that the amount of heat released during composting of municipal solid waste can be estimated from the losses of major components of the material, such as lipids, sugars and starches, and the heats of combustion of these components. The chemical composition of the raw material used in this study will be given in terms of representative compounds of major components (section 5.2.2). These compounds can decompose along various chemical pathways. The stoichiometry describes the amounts of reactants and products. Each reaction also yields a certain amount of energy, which is described in section 5.2.1. This clarifies the relationship between heat production, CO_2 production and O_2 consumption.

Substrate is used by microbes for anabolic and catabolic reactions. The main components of the substrate are polymers which are insoluble in water. These polymers are hydrolyzed by extracellular enzymes released by the microbes (Alexander, 1977). The monomers dissolve into water and enter the microbial cell where further decomposition takes place. The overall rate of the degradation is determined by the rate at which the substrate is hydrolyzed and the rates of microbial growth and decay. This is discussed in section 5.3.

5.2 Stoichiometry and energetics of aerobic and anaerobic decomposition

5.2.1 General principles

During catabolic processes energy is obtained from oxidation of the substrate. This reaction proceeds along various pathways, each of them yielding a specific amount of energy. This amount of energy can be calculated from the stoichiometry of the reaction and the Gibbs free energies of formation of reactants and products.

For the general reaction equation



the Gibbs free energy of reaction is calculated from

$$\Delta G_r = c \Delta G_{fC}^{\circ} + d \Delta G_{fD}^{\circ} - a \Delta G_{fA}^{\circ} - b \Delta G_{fB}^{\circ} + R T \ln \left[\frac{[C]^c [D]^d}{[A]^a [B]^b} \right], \quad (5.2)$$

where ΔG_r is the free energy of the reaction under prevailing conditions [kJ], ΔG_{fA}° the free energy of formation of component A and a the number of mols of substance A participating in the reaction, etc.. The superscript $^{\circ}$ indicates that these energies hold for certain standard conditions, e.g. temperature 25 °C, pressure 1 atm and concentration 1 M (Chang, 1977) or 0 °C, 1 atm and 1 M (Weast, 1985). The last term of equation (5.2) accounts for non-standard conditions.

The pathway of the catabolic reaction is mainly determined by the oxidation-reduction potential (E_h) of the substrate. If the amount of highly oxidized compounds prevails over the amount of reduced substances, E_h is positive. If more reduced forms prevail, E_h is negative. The order in which electron acceptors are used, is reflected by the decreasing oxidation-reduction potential given in table 5.1 (Scheffer and Schachtschabel, 1989). Oxygen is used as electron acceptor prior to NO_3^- and SO_4^{2-} . Finally, organic compounds will be reduced and methane will be formed.

Table 5.1 Relation between the oxidation-reduction potential and the occurrence of reduction processes (after Scheffer and Schachtschabel, 1989).

reduction status	E_h [mV] (pH = 7)
start of the NO_3^- reduction	450 - 550
O_2 below detection limit	330
NO_3^- below detection limit	220
start of SO_4^{2-} -reduction end of S^{2-} -production	- 50
methane production	-120
SO_4^{2-} below detection limit	-180

Cellulose is the most important polymer in plant materials. It is hydrolyzed to glucose prior to its uptake by microbes. Table 5.2 gives an overview of various decomposition pathways of glucose. Brock and Madigan (1988) distinguish

three catabolic pathways for the decomposition of organic substances, i.e. aerobic respiration, anaerobic respiration and fermentation. These are given by the reactions 1, 2 and 4 in table 5.2, respectively. The degradation of glucose in the presence of the sulphate ion (reaction 3) will only occur after oxygen and nitrate have been used. Reaction 3 leads to the release of H_2S , which has an offensive smell. Thus, supply of oxygen or nitrate avoids production of H_2S .

Table 5.2 Overall biochemical reactions of the microbial degradation of glucose [no = reaction number; ΔG_R° = Gibbs Free energy (kJ mol^{-1} glucose)].

no	reaction	ΔG_R°
1	$\text{C}_6\text{H}_{12}\text{O}_6 + 6\text{O}_2 \longrightarrow 6\text{CO}_2 + 6\text{H}_2\text{O}$	-2843
2	$5 \text{C}_6\text{H}_{12}\text{O}_6 + 24\text{NO}_3^- \longrightarrow 12\text{N}_2 + 18\text{H}_2\text{O} + 24\text{OH}^- + 30\text{CO}_2$	-2523
3	$\text{C}_6\text{H}_{12}\text{O}_6 + 3\text{H}_2\text{SO}_4 \longrightarrow 6\text{CO}_2 + 6\text{H}_2\text{O} + 3\text{H}_2\text{S}$	- 450
4	$\text{C}_6\text{H}_{12}\text{O}_6 \longrightarrow 3\text{CH}_4 + 3\text{CO}_2$	- 403
5	$\text{C}_6\text{H}_{12}\text{O}_6 \longrightarrow 3\text{CH}_3\text{COO}^- + 3\text{H}^+$	- 330
6	$\text{C}_6\text{H}_{12}\text{O}_6 \longrightarrow \text{CH}_3\text{CH}_2\text{COO}^- + \text{CH}_3\text{COO}^- + 2\text{H}^+ + \text{CO}_2 + \text{H}_2$	- 298
7	$\text{C}_6\text{H}_{12}\text{O}_6 \longrightarrow \text{CH}_3\text{CH}_2\text{CH}_2\text{COOH} + 2\text{CO}_2 + 2\text{H}_2$	- 259
8	$\text{C}_6\text{H}_{12}\text{O}_6 \longrightarrow 2\text{CH}_3\text{CH}_2\text{OH} + 2\text{CO}_2$	- 215
9	$\text{C}_6\text{H}_{12}\text{O}_6 \longrightarrow 2\text{CH}_3\text{CH}(\text{OH})\text{COO}^- + 2\text{H}^+$	- 208
10	$\text{C}_6\text{H}_{12}\text{O}_6 \longrightarrow 4\text{CH}_3\text{OH} + 2\text{H}_2\text{O} + 2\text{CO}_2$	- 90

If oxygen, nitrate and sulphate are absent, one or more of the reactions 4 to 10 will occur. The reactions 5 to 10, in which organic acids and alcohols are formed, can be considered as first steps of reaction 4. In the conversion of glucose to carbon dioxide and methane many different types of intermediate products are formed by a variety of organisms operating in series. The product of one organism is used as a substrate by another (Haug, 1993). If the circumstances allow the completion of the anaerobic conversion process, the final products will always be CH_4 and CO_2 . Micro-organisms performing reactions with the largest energy yield are in the most favourable position to compete with other microbes and therefore these reactions will dominate (Haug, 1993). This means that the reactions shown in table 5.2 will occur in the given order.

For microbial activity not only carbon is important but also nitrogen. Nitrogen is an important constituent of amino acids, which are building blocks

of proteins and nucleic acids. Microbial need for nitrogen is fulfilled by the incorporation of ammonia, which can be obtained from degradation of proteins from the compost. The initial step in the protein decomposition is the excretion of the protein hydrolyzing enzyme protease. By this the protein is converted to amino acids which enter the microbial cell. In the next step the nitrogen is removed from the carbon chain as ammonia, which can be lost from the system by volatilization (table 5.3, reactions 1, 2 and 3). This step proceeds under aerobic as well as anaerobic conditions. Reactions in which ammonia is formed from organic nitrogen compounds are called ammonification. The optimum temperature for ammonification lies between 40 and 60 °C. During the aerobic degradation of proteins also a moderate amount of energy is released, e.g. 682 kJ mol glycine⁻¹.

Another source of ammonia is urea, an important component of animal urine. The urease catalyzed degradation reaction finally gives ammonia and carbon dioxide (table 5.3, reaction 4).

Table 5.3 Some important biochemical reactions of nitrogen compounds.

no	reaction	
1	$\text{RCH}_2\text{CH N H}_2\text{COOH}$	$\rightarrow \text{RCH}=\text{CHCOOH} + \text{NH}_3$
2	$\text{RCH}_2\text{CH N H}_2\text{COOH} + \frac{1}{2} \text{O}_2$	$\rightarrow \text{RCOCOOH} + \text{NH}_3$
3	$\text{RCH}_2\text{CH N H}_2\text{COOH} + 2\text{H}$	$\rightarrow \text{RCH}_2\text{COOH} + \text{NH}_3$
4	$\text{CO}(\text{NH}_2)_2 + \text{H}_2\text{O}$	$\rightarrow 2 \text{NH}_3 + \text{CO}_2$
5	$\text{NH}_3 + 2 \text{O}_2$	$\rightarrow \text{HNO}_3 + \text{H}_2\text{O}$

The oxidation of ammonia to nitrate, called nitrification, is the combined action of two highly specialized chemoautotrophic bacteria, *Nitrosomonas* and *Nitrobacter* (table 5.3, reaction 5). Nitrification proceeds at a maximum rate at 37 °C, but is strongly reduced at temperatures above 38 °C (Myers, 1975).

Another reaction with important implications for the nitrogen balance is the reduction of nitrate to gaseous nitrogen which leads to nitrogen loss. This reaction is called denitrification and is given in table 5.2, number 2.

In many physiological studies the respiration quotient (RQ) is used to study biochemical processes. The respiration quotient is defined as the number of mols of carbon dioxide released, divided by the number of mols of oxygen which is consumed (Bidwell, 1979). The respiration quotient depends on the type of

substrate which reacts with oxygen, e.g. for glucose and palmitic acid the RQ's are 1 and 0.7, respectively. Carbon dioxide is not only formed during aerobic processes but also during anaerobic respiration and fermentation (table 5.2). Thus, if the composition of the substrate is known, the RQ gives insight in the relative importance of aerobic and anaerobic processes.

5.2.2 Composition of the raw material

As mentioned before the raw material used in this study consisted of a mixture of chicken manure and wheat straw in a ratio of 1 kg manure to 1 kg dry straw. The composition of the mixture was calculated on the basis of this ratio and the compositions of chicken manure and wheat straw as given in table 5.4. The dry matter contents of chicken manure and straw were 0.36 and 0.85, respectively. Sugar polymers were the main constituents of the raw material. Chicken manure was the most important source of nitrogen compounds (proteins, uric acid) and ash.

Table 5.4 Average composition of chicken manure, wheat straw and the mixture expressed as percentage of dry weight (d.w.).

constituent	representative compound	chicken manure ^a [% d.w.]	wheat straw ^b [% d.w.]	mixture [% d.w.]
lignocellulose	cellulose	47.9	88.0	76.1
N-compounds		22.8	3.4	9.2
- proteins		9.5	3.4	5.2
	glycine			
	glutamine			
-uric acid	uric acid	13.3		4.0
lipids	palmitic acid	4.5	1.5	2.4
ash		24.8	7.1	12.3

a: after Janssen (1987); b: after Staniforth (1979)

The composition given in the first column of table 5.4 is only a rough classification of substances. Every class itself (except uric acid) is a mixture of compounds, e.g. lignocellulose consists of lignin and sugar polymers whereas these sugar polymers themselves may consist of cellulose, hemicellulose, starch, or glycogen. The composition must be known more precisely to calculate the

Table 5.6 Gibbs free energies of formation obtained from Chang (1977) and Thauer et al. (1977) of some important compounds in compost.

compound	ΔG_f° [kJ mol ⁻¹]
glycine (aq)	-370.8
glutamine (aq)	-529.7
uric acid (aq)	-356.9
O ₂ (0.21 atm, g)	- 3.9
H ⁺ (pH 7, aq)	- 39.9
H ₂ O (liq)	-237.2
NH ₃ (aq)	- 26.2
NO ₃ ⁻ (aq)	-111.3
CO ₂ (g)	-386.0

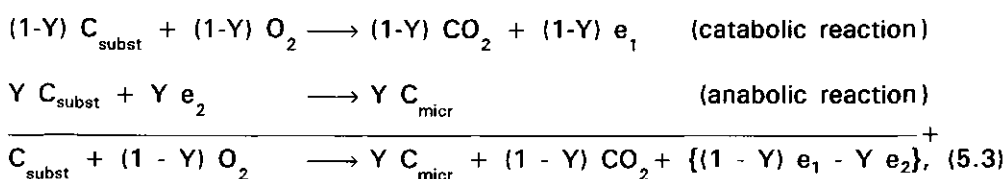
The amount of energy released during the hydrolysis of cellulose can be estimated from the difference between the heat of combustion of cellulose and glucose. During the combustion process the compounds are assumed to decompose in gaseous CO₂, gaseous N₂ and liquid water. The heat of combustion of cellulose given by Washburn (1933) is 2835 kJ mol⁻¹, whereas the heat of combustion of glucose is equal to 2817 kJ mol⁻¹. Thus, the hydrolytic energy amounts to 18 kJ mol⁻¹. However, the heat of combustion of glucose given by Haug (1993) is 2843 kJ mol⁻¹, which is 26 kJ larger than the value given by Washburn (1933). The difference in data for glucose given in the literature is larger than the hydrolytic energy and therefore this amount of energy is neglected with respect to the rough estimate of the reaction energy of raw material needed in this study. For calculation purposes the reaction energy of cellulose is set equal to the reaction energy of glucose.

The difference between reaction energies under standard and non-standard conditions (i.e. the last term of equation (5.2)) is probably small. This can be approximated for the oxidation reaction of glucose (table 5.2, reaction 1) using experimental data of Waksman et al. (1939). They found that the amount of water-soluble organic matter in the straw/manure mixture was 16 g l⁻¹. If it is assumed that this organic matter consisted entirely of glucose, its concentration in the liquid phase was 9 x 10⁻² mol l⁻¹. The concentrations of oxygen and carbon dioxide can be calculated using values of Henry's constants given by Schulze and Prausnitz (1981) and assuming that the partial pressures of

both gases in the gaseous phase are equal to 10% of the atmospheric pressure. Then, these concentrations are 1×10^{-4} and $3 \times 10^{-3} \text{ mol l}^{-1}$, respectively. Since the concentration of water in aqueous solution is arbitrarily set at 1 mol l^{-1} (Chang, 1977), it follows that the difference between ΔG_r and ΔG_r° is 63 kJ mol^{-1} glucose at a temperature of 60°C . This is about 2% of ΔG_r° , which means that the last term of equation (5.2) can be neglected.

The Gibbs free energy of reaction for the raw composting mixture can now be calculated from its chemical composition (table 5.4) and the reaction energies of the oxidation of representative compounds (table 5.5). In this calculation the energies of the first type of reaction (ammonification) and second type of reaction (nitrification) are averaged and it is assumed that one half of the weight of the proteins consists of glycine and one half of glutamine. To verify this calculation procedure, the Gibbs free energies of reaction for chicken manure and wheat straw are also computed separately and compared with data from the literature. The theoretical reaction energies of chicken manure and wheat straw are equal to 12.6 and 16.5 MJ kg^{-1} , respectively. Sobel and Muck (1983) found a value of the heat production of chicken manure equal to 12.8 MJ kg^{-1} . A gross energy production for wheat straw is 17.6 MJ kg^{-1} (Staniforth, 1979). Both values are in reasonable agreement with the theoretically calculated values. Using the same calculation scheme, the Gibbs free energy of reaction for the raw mixture was equal to 15.4 MJ per kg .

Part of the energy released during the decomposition of the substrate is used to build microbial material. The remaining part of the energy is released as heat. The catabolic and anabolic reactions can be given schematically in terms of substrate-C (C_{subst}) and microbial-C (C_{micr}) by:



in which e_1 is the energy of the catabolic reaction [kJ mol C^{-1}], e_2 is the energy needed to produce microbial bodies from the substrate [kJ mol C^{-1}], and Y is the yield expressed in mol of microbial-C per mol of substrate-C. The third term on the right hand side of equation (5.3) is the amount of heat produced during degradation. Since carbon is released as CO_2 , the energy e_1 can also be expressed in kJ mol CO_2^{-1} . This value can be calculated from the reaction energy per kg of substrate divided by the amount of CO_2 released per kg of substrate.

The latter is computed from the composition of the raw mixture (table 5.4) and the number of mols of carbon dioxide produced per mol of representative compound given in table 5.5. If the decomposition of nitrogen compounds proceeds according to the first type of reaction (ammonification), the carbon dioxide production and oxygen consumption are 32.5 and 32.1 mol kg⁻¹, respectively. If the second type of reaction (nitrification) prevails, these values are 32.5 and 35.4 mol kg⁻¹, respectively. Then, the amount of energy released per mol of carbon dioxide production e_1 is calculated as $15.4 \times 10^3 / 32.5 = 474 \text{ kJ mol}^{-1}$. For an average oxygen consumption of 33.7 mol kg⁻¹, the amount of energy released per mol of oxygen consumption is computed as $15.4 \times 10^3 / 33.7 = 457 \text{ kJ mol}^{-1}$. Both values are used in the next chapter to calculate heat production rates from measured values of the oxygen consumption rates or carbon dioxide production rates.

The energy content of microbial biomass was studied by Baas-Becking and Parks (1927). They measured the heat of combustion of autotrophic bacteria and found a value of 470 kJ per mol of microbial carbon. This value is almost equal to the amount of energy released per mol of CO₂ calculated for the oxydation of the straw/manure mixture, i.e. 474 kJ per mol CO₂. The degradation of organic material in a compost pile is brought about by heterotrophic microbes. If it is assumed that the heats of combustion of autotrophs and heterotrophs are equal, it can be concluded that the energy contents of the substrate and of the microbial biomass are approximately equal. Therefore, the amount of additional energy e_2 needed to build microbial biomass from the substrate is negligible compared to the catabolic energy e_1 in equation (5.3). Thus, for the substrate considered in this chapter e_1 is almost entirely released as heat and the amount of heat released per mol of CO₂ is approximately 470 kJ per mol. Cooney et al. (1968) measured microbial heat production and CO₂ evolution in a glucose medium and found a value of 462 kJ mol⁻¹. This value is almost equal to the expected heat production e_1 .

The amount of energy released in anaerobic processes is much more difficult to estimate than the aerobic energy production. For the class of sugar polymers three types of anaerobic reactions are considered: anaerobic respiration, reactions in which carbon dioxide is released (table 5.2, e.g. reaction 4) and reactions in which cellulose is decomposed into acetate or lactate without any release of CO₂ (table 5.2, reactions 5 and 9). To assess the importance of anaerobic respiration, the maximum amount of nitrate liberated from 1 kg of dry material is estimated from the molar composition of the raw mixture and the composition of the representative compounds. This amounts to 1.6 mol NO₃⁻ per kg.

From Table 5.2 it is deduced that 4 mols of nitrate are necessary to produce 5 mols of carbon dioxide. Therefore, a maximum of only 2 mols of CO_2 can be produced by this reaction if all the nitrogen originating from organic compounds is transferred to nitrate and then further to gaseous nitrogen. Hence, anaerobic respiration seems relatively unimportant.

The relative importance of the fermentation reactions with and without CO_2 production is not known. If lactate and acetate fermentation are assumed to be unimportant, the energy release per mol of carbon dioxide production can be calculated from the reactions given in table 5.2. These values range from 45 to $298 \text{ kJ mol}^{-1} \text{ CO}_2$ with an average value of 143 kJ mol^{-1} . It has to be emphasized that the energy released per mol CO_2 will be larger if acetate and/or lactate fermentation are relatively more important.

The RQ-values of various reactions discussed in this chapter are given in table 5.5 and range from 0.5 to 3.3. If ammonification prevails, the average RQ-value for the raw material is $32.5/32.1 = 1.0$ and for nitrification RQ is $32.5/35.4 = 0.9$. The average RQ-value then becomes 1.0. As nitrification only occurs at moderate temperatures, it can be expected that RQ will increase slightly as the temperature rises strongly to values above 38°C . In most anaerobic reactions CO_2 is released. Thus, RQ-values larger than 1 are an indication of anaerobic processes.

5.3 Process dynamics

If physical and chemical conditions are favourable, microbial growth is governed by physiological properties, such as maximum growth rate, use of energy for maintenance and death rate. However, after a certain time interval the composting process will progressively become inhibited by various limitations, such as the depletion of a certain nutrient or the fact that the pH or the temperature goes out of the favourable range. The rate limitations due to nutrient depletion and microbial physiology are considered in the next sections.

The availability of energy is a prerequisite for microbial activity. An energy rich substrate and oxygen are necessary for aerobic catabolism. It is assumed that the microbes live in the liquid phase. The energy rich substrate is primarily contained in the solid phase and the gaseous phase is the primary source of oxygen, thus disregarding nitrate and sulphate. Before the substrate can be used by the microbial community, it must be hydrolyzed by extracellular enzymes and the products must subsequently diffuse to the microbial cells. Oxygen reaches the microbial cells by transfer through the gaseous phase and subsequent solution in and diffusion through the liquid phase. This means that

the composting process can be limited by the rate of oxygen transfer, the rate of substrate hydrolysis or the rates of microbial growth and decay.

5.3.1 Limitation by oxygen transfer

To get more insight in the rate limitation by oxygen transfer, the penetration depth δ of oxygen in the liquid phase of composting material will be estimated. The oxygen penetration depth is found from the mass balance of oxygen given by:

$$\frac{\partial \gamma_{\text{O}_2}}{\partial t} = \nabla \cdot (D_{\text{O}_2} \nabla \gamma_{\text{O}_2}) - r_{\text{O}_2} \quad (5.4)$$

For steady-state conditions, in one dimension, and assuming that D_{O_2} is constant, this balance is given by:

$$\frac{d^2 \gamma_{\text{O}_2}}{dz^2} = \frac{r_{\text{O}_2}}{D_{\text{O}_2}} \quad (5.5)$$

It is assumed that the reaction by which oxygen is consumed is independent of the oxygen concentration. With the boundary conditions:

$$z = 0: \gamma_{\text{O}_2}(0) = \gamma_{\text{O}_2}^0 \quad (5.6a)$$

and

$$z = \delta: \gamma_{\text{O}_2}(\delta) = 0, \text{ and } \frac{d\gamma_{\text{O}_2}}{dz} = 0, \quad (5.6b)$$

the solution of equation (5.5) is:

$$\gamma_{\text{O}_2}(z) = \frac{r_{\text{O}_2}}{2D_{\text{O}_2}} z^2 - \frac{\delta r_{\text{O}_2}}{D_{\text{O}_2}} z + \frac{\delta^2 r_{\text{O}_2}}{2D_{\text{O}_2}} \quad (5.7)$$

with

$$\delta = \sqrt{\frac{2D_{\text{IO}_2} \gamma_{\text{IO}_2}^\circ}{r_{\text{IO}_2}}}, \quad (5.8)$$

where δ is the oxygen penetration depth [m] and $\gamma_{\text{IO}_2}^\circ$ the maximum oxygen concentration in the liquid phase occurring at the gas - liquid interface. The concentration $\gamma_{\text{IO}_2}^\circ$ is proportional to the partial oxygen pressure in the gaseous phase and obeys Henry's Law:

$$\frac{P_{\text{O}_2}}{\gamma_{\text{IO}_2}^\circ} = K, \quad (5.9)$$

where K is Henry's constant [$\text{Pa m}^3 \text{mol}^{-1}$]. Values of the Henry constant are given by Schulze and Prausnitz (1981). This constant and the oxygen diffusion coefficient depend on temperature. The diffusion coefficient is calculated from Wilke's formula (Bird et al., 1960):

$$D_{\text{IO}_2} = 7.4 \times 10^{-12} \frac{(\psi_{\text{H}_2\text{O}} M_{\text{H}_2\text{O}})^{0.5} T}{\mu_{\text{H}_2\text{O}} \bar{V}_{\text{O}_2}^{0.6}}, \quad (5.10)$$

where $\psi_{\text{H}_2\text{O}}$ is the "association parameter" equal to 2.6, $\mu_{\text{H}_2\text{O}}$ the viscosity of water equal to 1 cP and \bar{V}_{O_2} the molar volume of oxygen as liquid at its normal boiling point, which is equal to $74.4 \text{ cm}^3 \text{mol}^{-1}$.

Table 5.7 Calculated oxygen diffusion coefficients D_{IO_2} and maximum oxygen density $\gamma_{\text{IO}_2}^\circ$ in water (with $P_{\text{O}_2} = 0.21 \times 10^5 \text{ Pa}$) depending on temperature.

T [°C]	D_{IO_2} [$\text{m}^2 \text{s}^{-1}$]	K [$\text{Pa m}^3 \text{kg}^{-1}$]	$\gamma_{\text{IO}_2}^\circ$ [kg m^{-3}]
10	1.1×10^{-9}	2.2×10^6	9.6×10^{-3}
20	1.1×10^{-9}	2.5×10^6	8.3×10^{-3}
50	1.2×10^{-9}	3.4×10^6	6.4×10^{-3}
75	1.3×10^{-9}	3.8×10^6	5.8×10^{-3}

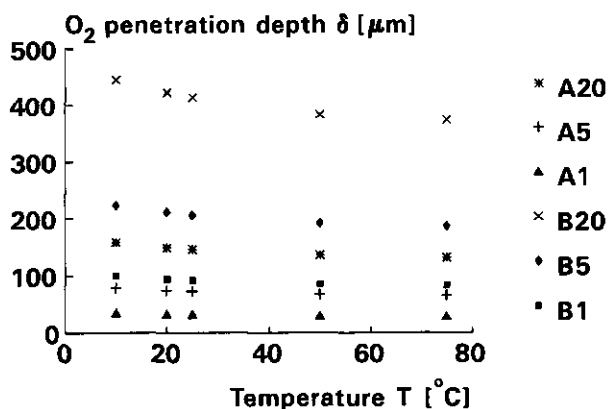


Figure 5.1 The oxygen penetration depth δ as a function of the temperature, the oxygen consumption rate in the liquid phase and the oxygen content in the gaseous phase. The symbols (A) and (B) pertain to r_{102} is equal to 1.3×10^{-2} and $1.6 \times 10^{-3} \text{ mol s}^{-1} \text{ m}^{-3}$, respectively. The O_2 -contents are equal to 20, 5 and 1 vol.%, respectively.

The oxygen diffusion coefficient and the maximum oxygen concentration at various temperatures are given in table 5.7. The diffusion coefficient increases slightly with temperature, whereas the concentration decreases with temperature. The effect of the temperature on the oxygen penetration depth is shown in figure 5.1. The δ -values are calculated with 20, 5 and 1% oxygen in the gaseous phase. The values designated with A and B pertain to an oxygen consumption of 1.3×10^{-2} and $1.6 \times 10^{-3} \text{ mol s}^{-1} \text{ m}^{-3}$, respectively. Obviously, δ decreases with increasing r_{102} and increasing temperature and δ increases with the partial oxygen pressure in the gaseous phase. Anaerobiosis will occur if the penetration depth is less than the thickness of the water layer surrounding the solid particles. This means that locally, e.g. in water filled pores, anaerobic conditions may prevail although the adjacent gaseous phase is highly aerobic. This conclusion is supported by the results of Derikx et al. (1989). They found that anaerobic processes occurred in well aerated compost piles. Thus, a high oxygen content in the gaseous phase does not guarantee that anaerobic processes are absent.

5.3.2 Rates of hydrolysis

Since carbon and nitrogen are the most important nutrients for microbes, the rates of hydrolysis of compounds containing these nutrients will now be approximated. The ratio of both rates compared to the average C/N- quotient of microbes determines whether carbon or nitrogen limits microbial activity.

The hydrolysis consists of a chain of reactions, of which the adsorption of the enzyme to the surface of the solid phase, the reaction of water with the enzyme-solid complex and the release of the soluble products are the most important ones (Lee and Fan, 1982). Enzymes are large molecules which possess several sites on which reactions can take place (Boyd and Mortland, 1990). The number of free reaction sites largely determines the reaction rate. Various compounds, including products of hydrolysis, can compete for these free sites (Grady and Lim, 1980). This reduces the rate of hydrolysis. An example of product inhibition is the limitation of cellulase activity by the cellulose products cellobiose and glucose (Lee and Fan, 1982). The hydrolysis of proteins to amino acids by protease is inhibited by humic acids (Brons et al., 1985). Since humic acids are formed during the composting process, this type of inhibition may also occur in compost.

The kinetics of an enzymatic reaction is often described by the well-known Michaelis-Menten equation (e.g. McLaren, 1978):

$$\frac{dp_o}{dt} = -k_o E \frac{p_o}{K_s + p_o}, \quad (5.11)$$

where k_o is the rate constant expressed as kg of hydrolyzed substrate per second and per kg of enzymes [s^{-1}], E the enzyme density [$kg\ m^{-3}$] and K_s the substrate affinity constant [$kg\ m^{-3}$]. Since hydrolyzing enzymes are produced by the microbial community, it is expected that the enzyme density will depend on the microbial density. In a study on cellulase activity, Lee and Blackburn (1975) found that the enzyme activity was proportional to the cell density. In composting material containing cellulose fibers, such as straw, there is only a limited number of sites available where enzymes can adsorb (Cowling and Kirk, 1976; Haug, 1993). The enzyme density and the rate of hydrolysis will reach a maximum when all available adsorption sites are used. If microbial nutrition only depends on the rate of hydrolysis, also the cell density will reach a maximum.

There are no data about rates of hydrolysis in composting material known from the literature. Owing to the complexity of the reactions and the interactions which may occur between the numerous compounds in composting material, one cannot rely on data given in the literature about rates of hydrolysis obtained in pure cultures with single substrates. Instead, the rate of sugar polymer hydrolysis was estimated from the decrease of these polymers during composting. Sugar polymers which have disappeared, must have been hydrolyzed. The cell walls of fungi contain sugar polymers (Alexopoulos and Mims, 1979). Thus, the polymers are not only degraded, but also synthesized. However, the amount of sugar polymers in the microbial biomass can be considered as insignificant relative to the amount that is hydrolyzed. Thus, the decrease of sugar polymers is regarded as a good approximation of the rate of hydrolysis. Relevant data were obtained from Waksman et al. (1939), who measured the changes in chemical composition of a mixture of straw and horse manure during incubation experiments at 28, 50, 65 and 75 °C, respectively (see figure 5.2). The substrate used by Waksman et al. and that used in this study were both mixtures of wheat straw and animal manure with C/N- ratios of about 20 and 17 and dry matter contents of 0.25 and 0.20, respectively. Therefore, these substrates are considered as comparable. The small number of data of Waksman et al. does not allow the separate determination of the Michaelis-Menten parameters k_E and K_S . As a first approximation, the rate of hydrolysis can be regarded as a first order function of p_o (Eastman and Ferguson, 1981) given by equation:

$$\frac{dp_o}{dt} = \zeta_c^* p_o \quad (2.9)$$

Comparison of equations (2.9) and (5.11) shows that (5.11) reduces to (2.9) with $\zeta_c^* = k_E E / K_S$ if E is considered to be constant and K_S is much larger than p_o . The rate constant ζ_c^* in equation (2.9) can be expressed in kmols of C per second per kg of substrate. This is achieved by assuming that cellulose and hemicellulose are converted to glucose.

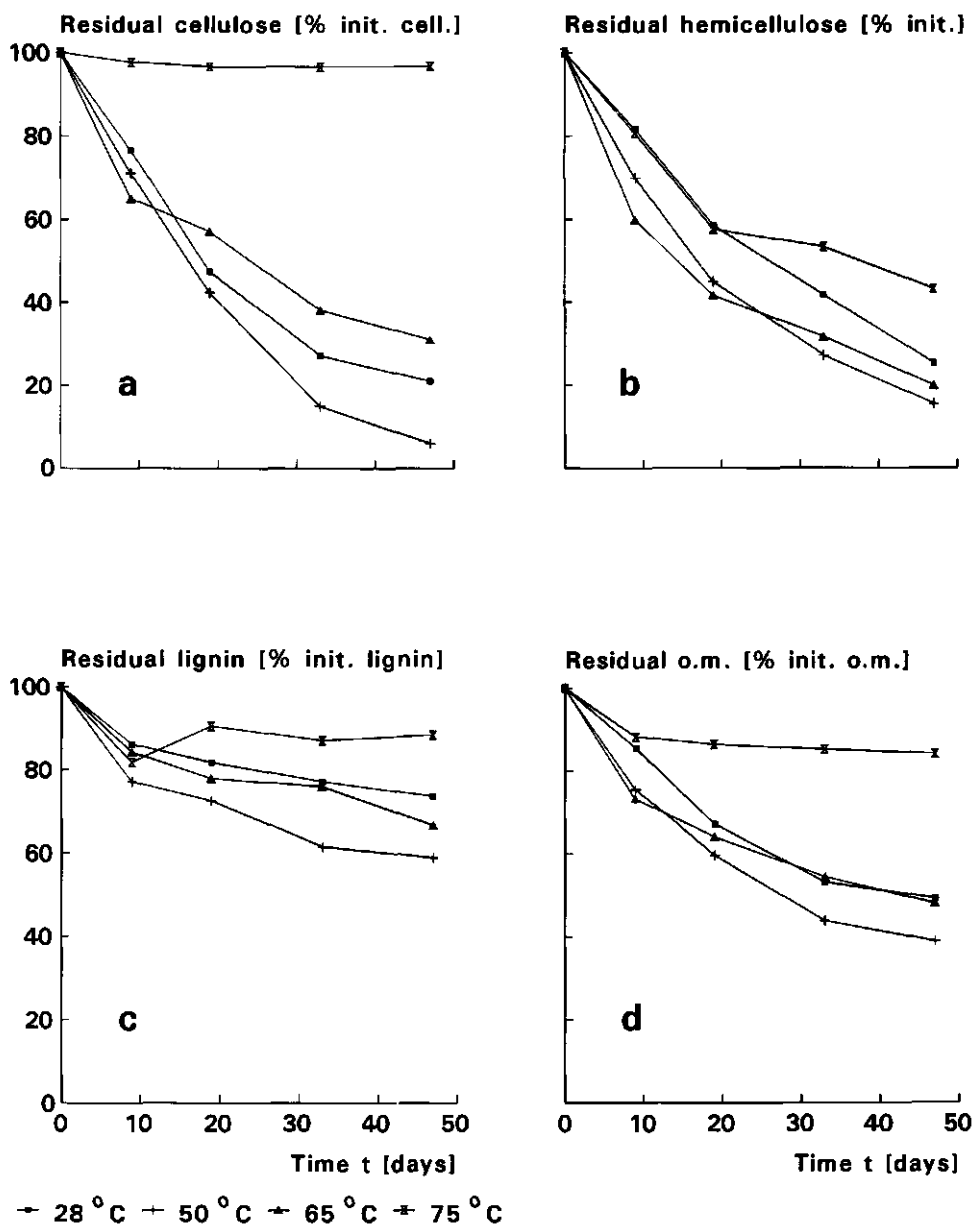


Figure 5.2 Degradation of (a) cellulose, (b) hemicellulose, (c) lignin and (d) organic matter in horse manure, incubated at various temperatures (28, 50, 65 and 75 °C). The residual amount of each component is expressed as a percentage of its initial amount (after Waksman et al., 1939).

Since 1 mol of glucose contains 6 mols of carbon, the rate constant ζ_c is given by:

$$\zeta_c = \zeta_c^* \frac{6}{M_{\text{cel}}}, \quad (5.12)$$

where ζ_c is the rate constant [$\text{kmol s}^{-1} \text{ kg}(\text{dm})^{-1}$] and M_{cel} the molecular mass of cellulose [kg kmol^{-1}]. Waksman et al. (1939) gave data of the substrate composition at days 0, 9, 19, 33 and 47. Using their data, the rate constant of hydrolysis ζ_c was approximated from the decreasing densities of cellulose and hemicellulose during the process and was calculated as:

$$\zeta_c = \left[\frac{\rho_{\text{cel}}(t_{i+1}) - \rho_{\text{cel}}(t_i)}{\rho_{\text{cel}}(t_i)} + \frac{\rho_{\text{hcl}}(t_{i+1}) - \rho_{\text{hcl}}(t_i)}{\rho_{\text{hcl}}(t_i)} \right] \frac{6}{M_{\text{cel}}(t_{i+1} - t_i)}, \quad (5.13)$$

where ρ is the density of the constituent [kg m^{-3}], the subscripts 'cel' and 'hcl' stand for cellulose and hemicellulose, respectively, t_i for days 0, 9, 19 and 33, and t_{i+1} for the sampling day following after t_i . Table 5.8 gives values of ζ_c at various temperatures. These values are assumed to pertain to the condition of maximum enzyme adsorption, because usually the microbial density reaches a maximum in 1 to 2 days (Chang and Hudson, 1967, Nakasaki et al., 1985a) which is rapid compared to the time intervals used by Waksman et al.. Thus, with ζ_c based on the data of Waksman et al., equation (2.9) describes the maximum rate of hydrolysis.

Table 5.8 Rate constant of hydrolysis [$\text{kmol C s}^{-1} \text{ kg}^{-1}$] of sugar polymers obtained from the disappearance of cellulose and hemicellulose in a straw-horse manure mixture (Waksman et al., 1939).

day	T [$^{\circ}\text{C}$]			
	28	50	65	75
0	1.0×10^{-8}	1.4×10^{-8}	1.8×10^{-8}	4.3×10^{-9}
9	1.5×10^{-8}	1.7×10^{-8}	8.2×10^{-9}	4.6×10^{-9}
19	1.1×10^{-8}	1.7×10^{-8}	9.3×10^{-9}	6.6×10^{-10}
33	8.9×10^{-9}	1.6×10^{-8}	7.7×10^{-9}	1.6×10^{-9}

The rate constant ζ_c varied only slightly with age. The highest values were found at 50 °C and the lowest at 75 °C. McClaugherty and Linkins (1990) found that rates of hydrolysis of various enzyme systems in forest soils doubled every 10 degrees of temperature increase, with the temperature in the range $2 \leq T \leq 30$ °C. For temperatures in the range 0 to 28 °C, the rate constant ζ_c was calculated on the basis of this temperature dependence, using the value of ζ_c at 28 °C as a starting point. The final results pertaining to raw material are shown in figure 5.3.

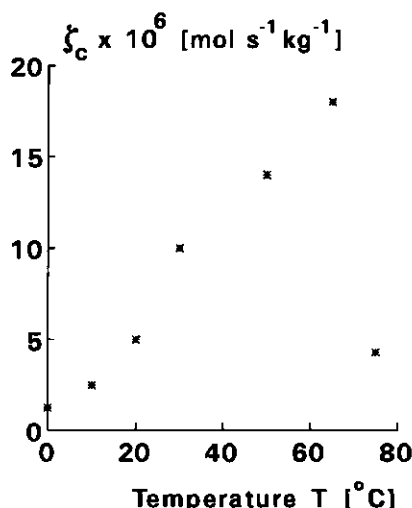


Figure 5.3 Rate constants of carbon hydrolysis ζ_c pertaining to raw material as a function of temperature T.

For sugar polymers, the rate of hydrolysis was estimated from the decrease of these compounds. To determine rates of hydrolysis of nitrogenous compounds, it is not possible to follow the same procedure because these substances are synthesized by microbes in amounts which cannot be neglected relative to the amounts hydrolyzed, e.g. in soil science the phenomenon of N-immobilization by microbes has been commonly observed. Another method is to measure the increase of products of hydrolysis. This is frequently employed in soil research to determine rates of hydrolysis of proteins and urea. However, these data should be used prudently because of interactions which may occur between enzymes and the clay-organic matter complex in the soil (Boyd and Mortland, 1990; Burns, 1982). Therefore, it is assumed that the most reliable estimate of the initial

rate of hydrolysis of proteins in raw material is given by data pertaining to soils with low contents of clay and organic matter.

The tables 5.9 and 5.10 give an overview of approximated rates of hydrolysis of proteins and uric acid in a sandy soil. The rates reported in the literature were recalculated on the basis of the initial contents of protein-N and uric acid-N in the composting material used in this study. This material contained 5.2% of proteins and 4.1% uric acid (table 5.4). The N-content (on mass basis) of proteins was computed using the data given in table 5.5 and was equal to 0.19 kg kg^{-1} . Thus, 1 kg of dry material contained $52 \times 0.19 = 10 \text{ g}$ of protein-N. The N-content of uric acid was 0.33 kg kg^{-1} . Therefore, this raw material contained 14 g of uric acid-N per kg of dry matter.

Table 5.9 Approximated rates of hydrolysis of proteins expressed as $\text{kmol NH}_4^+ \text{-N s}^{-1} \text{ kg(dm)}^{-1}$, assuming that 1 kg(dm) contains 10 g of protein-N.

substrate	sand fraction in the soil	incubation temperature	rate of hydrolysis	references
Gelatine *	85 - 95 %	37 °C	1.3×10^{-9}	Hoffmann, 1957
Casein *	60 %	50 °C	2.5×10^{-9}	Kandeler, 1988
Casein *	52 %	51 °C	2.9×10^{-9}	Nannipieri, 1982

* The composition of proteins are given by Frear (1950)

Table 5.10 Rates of uric acid-N hydrolysis expressed as $\text{kmol NH}_4^+ \text{-N s}^{-1} \text{ kg(dm)}^{-1}$ assuming that 1 kg(dm) contains 14 g of uric acid-N.

sand fraction in the soil	incubation temperature	rate of hydrolysis	reference
93 %	37 °C	2.2×10^{-10}	Tabatabai, 1973
52 %	37 °C	8.6×10^{-11}	Nannipieri, 1982

Hoffmann and Teicher (1957) measured colorimetrically the total amount of amino acids hydrolyzed after 20 hours, whereas Kandeler (1988) and Nannipieri et al. (1982) supplied casein to the soil and measured the increase in tyrosine concentration. Tyrosine is one of the amino acids of casein. Kandeler and Nannipieri et al. expressed their results in terms of k_E and K_S in the Michaelis-Menten equation (5.11). A material with a bulk density of 500 kg m^{-3}

and a dry matter content of 0.2 was used to convert their data from volumetric basis to mass basis. The rates of hydrolysis at 50 and 51 °C compare fairly well (table 5.9). The rates increase with temperature as can be expected from the literature (Moyo et al., 1989; McClaugherty and Linkins, 1990). Table 5.10 gives rates of hydrolysis of uric acid-N. This N-compound is converted to urea prior to its hydrolysis to ammonia.

For the calculation of the ratio between the rates of hydrolysis of C and N, the values obtained from soils with the highest sand fraction were assumed to pertain to the substrate used in this study. For protein-N and uric acid N the rates were equal to 1.3×10^{-9} and 2.2×10^{-10} kmol N s⁻¹ kg(dm)⁻¹ at 37 °C, respectively. On mass basis these rates were 1.8×10^{-5} and 3.1×10^{-6} g N s⁻¹ kg(dm)⁻¹, respectively. The rate of hydrolysis of sugar polymers was approximately 1.1×10^{-8} kmol C s⁻¹ kg(dm)⁻¹ (fig. 5.3), which is equivalent with 1.3×10^{-4} g C s⁻¹ kg(dm)⁻¹. The C/N hydrolysis ratio now becomes equal to $1.3 \times 10^{-4} / (1.8 \times 10^{-5} + 3.1 \times 10^{-6}) = 6.2$. The C/N ratio of microbes ranges from about 5 to 10 (Haug, 1993). As stated previously, microbes use carbon to gain energy and to synthesize new microbial material. The amount of microbial biomass obtained from the amount of degraded substrate is called the yield. This value ranges between 5 to 80% (Van Veen, 1977), but is commonly about 30%. Thus, approximately 3 units of C are needed to incorporate 1 unit of C. This means that the turning point of the C/N- ratio lies in the range 15 to 30. Therefore, microbial growth in composting material with a C/N hydrolysis ratio of 6 is carbon limited.

5.3.3 Microbial carbon consumption rate

In the previous section it was found that carbon was the rate limiting substrate for the mixture used in this study. Therefore, this section starts with a description of the carbon balance in the liquid phase:

$$\frac{dy_{ic}}{dt} = -e X - \gamma_{MU,C} \frac{dX}{dt} - \frac{dp_o}{dt} \frac{M_c}{M_{cel}} \frac{6}{\theta_1} \quad (5.14)$$

in which y_{ic} is the carbon density in the liquid phase [kg m⁻³], X the number of microbial units in the liquid phase [m⁻³], e the carbon consumption rate per microbial unit [kg s⁻¹], M_c the molecular mass of carbon [kg mol⁻¹], and $\gamma_{MU,C}$ the carbon content of a microbial unit [kg C]. The first and the second term at the right hand side of equation (5.14) are the carbon consumption rates due to

catabolic and anabolic processes, respectively. The third term is the influx of carbon into the liquid phase due to hydrolysis. Net microbial growth is equal to the difference between microbial growth and decay (Van Veen, 1977):

$$\frac{dX}{dt} = \mu_g X - k_d X, \quad (5.15)$$

where μ_g is the specific growth rate [s^{-1}] and k_d the specific decay rate [s^{-1}]. The specific growth rate depends on the density of the rate limiting substrate, i.e. carbon. Then, μ_g is given by (Monod, 1949):

$$\mu_g = \mu_{gmax} \frac{\gamma_{ic}}{K_s + \gamma_{ic}}, \quad (5.16)$$

where μ_{gmax} is the maximum specific growth rate [s^{-1}] and K_s the substrate affinity constant [$kg\ m^{-3}$]. Substitution of equation (5.16) into (5.15) gives:

$$\frac{dX}{dt} = \mu_{gmax} X \frac{\gamma_{ic}}{K_s + \gamma_{ic}} - k_d X. \quad (5.17)$$

The results of Waksman et al. (1939) show that a fresh straw/manure mixture contains a certain amount of water soluble organic matter. The bioavailability of dissolved substances might be better than the bioavailability of solid materials. These dissolved substances may serve as a readily available carbon source for the microbial population. If the initial density of carbon in the liquid phase is large enough, it allows the microbial population to grow. Under this condition the microbial activity may be limited by rates of microbial growth and decay. The carbon density γ_{ic} will decrease if the carbon consumption of the microbial population is greater than the rate of hydrolysis. Somewhere, between the start of the process and the moment that γ_{ic} becomes rate limiting, the microbes will produce extracellular enzymes and the process of hydrolysis begins. Unfortunately, the initial density of carbon in the liquid phase as well as an exact description of hydrolysis at the initial stage of the process is unknown. Therefore, equations (5.14) and (5.17) cannot be solved. However, it is expected that after a certain time interval the rate of hydrolysis will reach its maximum level (maximum enzyme density E), i.e.

$$-\frac{dp_o}{dt} \frac{M_c}{M_{col}} \frac{6}{\theta_i} = \zeta_c \frac{\rho_o}{\theta_i} M_c. \quad (5.18)$$

If the initial amount of dissolved carbon is depleted, the microbial carbon consumption rate may become equal to this maximum rate of hydrolysis. Under these conditions dy_{ic}/dt is zero and with the assumption that dX/dt is zero, equation (5.14) can be written as:

$$eX = \zeta_c \frac{\rho_o}{\theta_i} M_c. \quad (5.19)$$

It should be emphasized that equation (5.19) only holds if the density of readily available carbon in the liquid phase is small compared to the influx by hydrolysis.

5.4 Conclusions

Based on considerations of this chapter it can be expected that:

- the heat released per mol of CO_2 production is equal to the energy released per mol of CO_2 (i.e. 474 kJ mol^{-1});
- the ratio RQ between the amount of CO_2 released and the amount of O_2 consumed is approximately 1 for aerobic processes;
- RQ-values larger than 1 are an indication of anaerobic processes;
- a high oxygen content in the gaseous phase does not guarantee that anaerobic processes will not occur;
- if there is a surplus of dissolved carbon during the initial stage of the process, microbial activity is governed by rates of microbial growth and decay;
- following this initial stage, microbial activity is mainly determined by the rate of hydrolysis.

The theoretical model of microbial and biochemical processes presented in this chapter will be compared in the next chapter with experimental values of oxygen consumption, heat production and carbon dioxide production.

CHAPTER 6. DETERMINATION OF OXYGEN CONSUMPTION AND PRODUCTION OF CARBON DIOXIDE AND HEAT WITH AN ISOTHERMAL CALORIMETRIC REACTOR

6.1 Introduction

Microbial consumption of carbon influences the mass balance of the solid phase, carbon dioxide production and oxygen consumption are important factors in the mass balance of the gaseous phase and heat production affects the thermal balance. Therefore, the biochemical degradation reactions, discussed in the previous chapter, play a pivotal role in the description of the temperature and the oxygen and carbon dioxide distributions in a compost pile. Otherwise, the degradation process is largely determined by the physical environment. Thus, on the one hand the physical conditions determine the production rates, while on the other hand the production rates strongly affect the environmental conditions.

In this study production rates were measured in an isothermal calorimeter at various oxygen levels and temperatures. The experimental set-up is described in section 6.2. The results are given in section 6.3.

6.2 Design, calibration and performance of the calorimetric reactor

Microbial heat production rates are commonly measured in either adiabatic (Mote and Griffis, 1982) or isothermal (Rothbaum, 1961) calorimeters. In this study the isothermal calorimeter is chosen because it enables the control of the sample temperature and the composition of the gaseous phase during the experiments. In an isothermal calorimeter, the sample is kept at a constant temperature and the heat production is calculated from measured heat fluxes between the sample and the environment. The temperature control is achieved by putting the calorimeter vessel in a thermostatic bath. The composition of the gaseous phase is controlled by leading a gas stream of known composition through the calorimeter vessel. Rates of oxygen consumption and carbon dioxide production are determined from measured differences between the gas concentrations in the inlet and outlet gas streams.

The isothermal calorimeter used in this research project was based on the calorimeter described by Rothbaum (1961). Figure 6.1 gives a schematic representation of the experimental set-up. It was built in a thermostatic chamber kept at 20 °C. The set-up will be explained by following the route of the gas flow. The gas mixture was obtained from three containers filled with N₂, O₂ and CO₂, respectively.

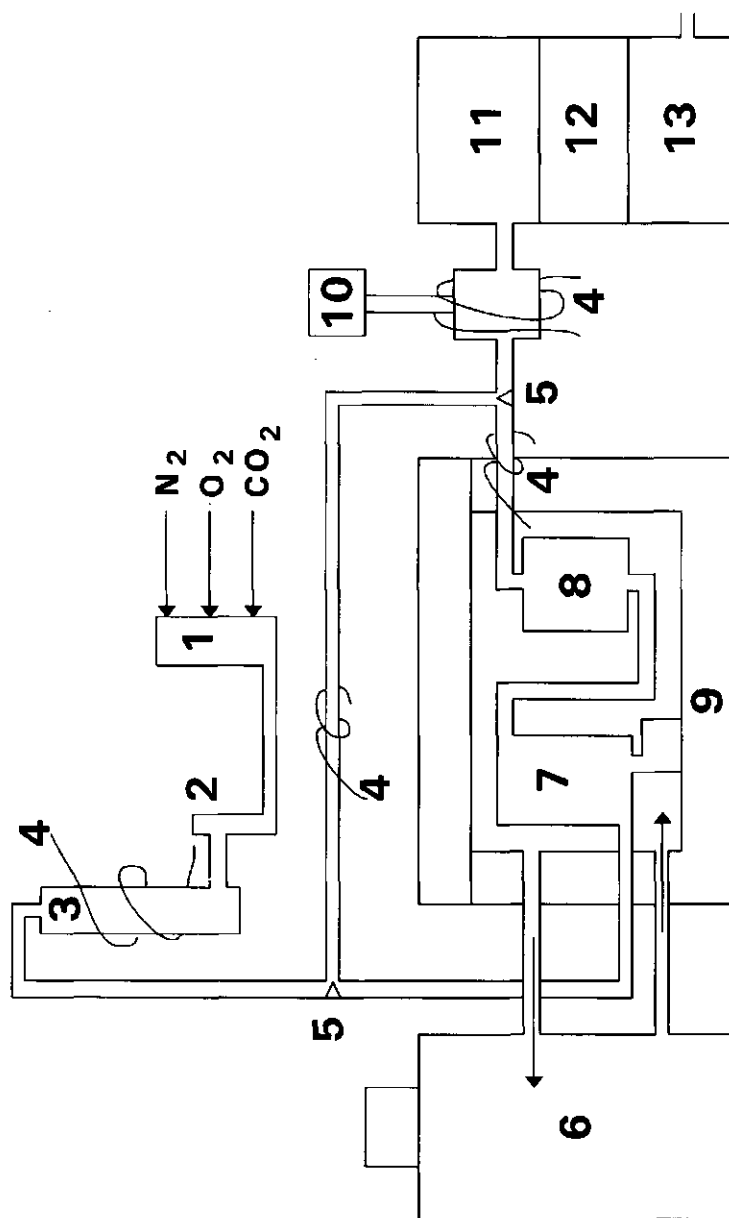


Figure 6.1 Experimental set-up to determine the biochemical production rates. (1) mass flow transducers and mass flow control box, (2) flow meter, (3) vaporizer, (4) heating wire, (5) three-way valve, (6) external thermostat bath, (7) heat exchanger, (8) calorimeter vessel, (9) thermostat bath, (10) humidity meter, (11) electric cooler, (12) oxygen analyser, (13) carbon dioxide analyser.

These three gases were mixed to obtain the desired composition, using three mass flow transducers connected with a mass flow control box (1). From (1) the gas mixture passed through a flow meter (2). The gas flow ranged from 195 to 250 ml/min depending on the composition of the mixture. Next, the gas mixture was guided through a vaporizer (3) filled with hot water to add water vapour to the mixture. This vaporizer was heated by an electric heating wire (4). Before the gas flow entered the calorimeter vessel (8), it was passed through a heat exchanger (7) fitted in the thermostatic bath (9). This bath was controlled by an external bath (6). After the gas flow left the calorimeter vessel, its temperature and relative humidity (RH) were measured by device (10) with an accuracy of 0.1% RH. Next, the gas flow was cooled by an electric cooler (11) to 5 degrees below room temperature to avoid condensation problems in the paramagnetic oxygen analyzer (12) and infra-red carbon dioxide analyzer (13). The accuracy of the oxygen analyzer was 0.2% of O_2 and the accuracy of the carbon dioxide analyzer was 0.1% of CO_2 . With these analyzers the composition of the output as well as the input gas flow could be measured. To measure the composition of the input, it was led via a by-pass between two three-way valves (5). These valves were computer controlled. After every switch of the valves, the gas flow was allowed to flow for 15 minutes to achieve that the entire system was filled with the new mixture before the composition was measured. To avoid condensation problems in the gas tubes, all tubes between (3) and (10) were heated. The data of the analyzers and the temperature sensors were read by a data logger controlled by a personal computer. Not only the distribution of the temperature in the calorimeter vessel (see fig 6.2b), but also the temperatures of the vaporizer (3) and the thermostatic bath (9) were measured. Each temperature sensor consisted of a thermistor mounted in a cone at the end of a stainless steel tube with a diameter of 4 mm and a length of 70 mm. The accuracy of the temperature sensors was 0.2 K.

During the experiments it appeared that in the vaporizer (3) saturation was never attained. To improve this, the temperature of the vaporizer was maintained at least 15 °C above the temperature of the thermostatic bath (9) and the flowing gas was subsequently cooled to the bath temperature. However, evaporation in the reactor could not be avoided by this procedure, due to the existence of a small temperature difference between the thermostatic bath and the sample as a result of the microbial heat production.

The heat production of the sample was calculated from measured heat fluxes between the sample and the environment. Three different heat fluxes can be distinguished: heat transfer through the vessel wall and transfer of both

sensible and latent heat due to the gas flow through the calorimeter vessel. The heat balance of the sample is given by:

$$\int_V Q \, dv = \int_A \alpha_w (T - T_{\text{bath}}) \, da + \phi \gamma_g C_{gp} (T_{\text{out}} - T_{\text{bath}}) + \quad (6.1)$$

$$+ \phi H (\gamma_{\text{gH}_2\text{O},\text{out}} - \gamma_{\text{gH}_2\text{O},\text{in}}).$$

In this equation Q is the heat production rate [W m^{-3}], V the volume of the vessel [m^3], α_w the heat transfer coefficient of the vessel wall [$\text{W m}^{-2} \text{K}^{-1}$], T the temperature of the sample close to the vessel wall [K], T_{bath} the thermostatic bath temperature [K], A the area of the vessel through which the heat transfer occurs [m^2], ϕ the gas flow [$\text{m}^3 \text{s}^{-1}$], γ_g the density of the gaseous phase [kg m^{-3}], C_{gp} the specific heat capacity of the gas [$\text{J kg}^{-1} \text{K}^{-1}$], T_{out} the temperature of the outlet gas stream [K], T_{bath} the temperature of the inlet gas streams [K], H the heat of vaporization [J kg^{-1}], $\gamma_{\text{gH}_2\text{O},\text{in}}$ the water vapour concentration in the inlet gas stream [kg m^{-3}] and $\gamma_{\text{gH}_2\text{O},\text{out}}$ the water vapour concentration in the outlet gas stream [kg m^{-3}].

A steady state heat balance is used because the time constant of the thermal system is much smaller than the bacterial generation time which governs the kinetics of the microbial system. The time constant of the thermal system is calculated as the quotient of the heat capacity and the rate of heat production. As the specific heat capacity of dry organic matter can be neglected compared to the specific heat capacity of water, the heat capacity of raw material is calculated as the specific heat capacity of water times the water content of the raw material. The heat production during composting of organic matter, given by Mote and Griffis (1982), is equal to about 25 W per kg of dry matter. For a compost sample with a dry matter content of 0.22, the thermal time constant then becomes: $(0.78 \times 4200)/(0.22 \times 25) = 600 \text{ s per K}$. The generation time can be used as an approximation of the characteristic time of the microbial system. This generation time is the time interval between two cell divisions and ranges from 1 to 3 hours for most bacteria (Brock and Madigan, 1988). Thus, the thermal system is, on average, 12 times faster than the microbial system.

A description of the calorimeter vessel is given in figure 6.2a. Each number in the figure indicates the position of a temperature sensor. The gas inlet, the gas outlet and the entrance for the sensor wires are designated by A, B and C, respectively.

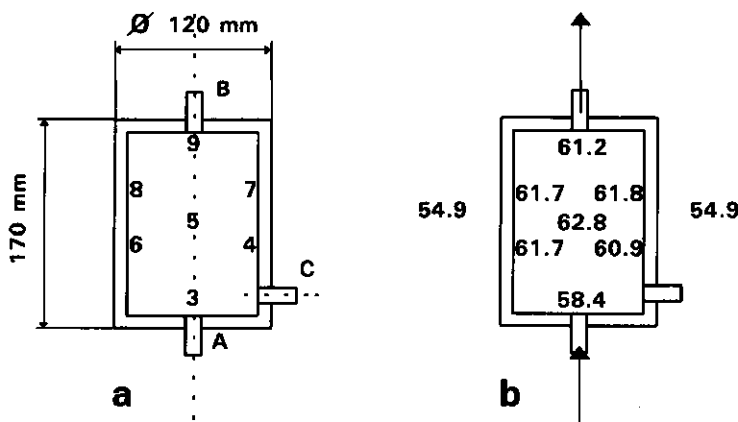


Figure 6.2 (a) Schematic representation of the calorimeter vessel. (A) gas inlet, (B) gas outlet, (C) sensor wire entrance. The numbers indicate the positions of the temperature sensors. (b) Typical temperature distribution in the calorimeter vessel. The arrows indicate the main flow direction.

The reactor was made of glass and consisted of a double walled cylinder with internal diameter and height of 120 and 170 mm, respectively. The space between the two walls was evacuated (10^{-2} Pa) to reduce convective heat transfer and the walls adjacent to the space were coated with silver to suppress radiative heat transfer. To reduce the latent heat flux, the flowing gas was moistened with water vapour before it entered the reactor. Figure 6.2a shows that the sample temperature close to the vessel wall is only known at 6 points. The surface integral in equation (6.1) is therefore written as the summation of the heat fluxes through 6 half cylindrical wall sections and through the top and bottom discs of the vessel. If the temperature of each cylindrical section is assumed to be the average of the temperatures of two subsequent sensors, equation (6.1) becomes:

$$Q^* = \alpha_w [(T_3 + T_4 + T_6 + T_7 + T_8 + T_9 - 6T_{\text{bath}}) \pi r l / 3 + (T_3 + T_9 - 2T_{\text{bath}}) \pi r^2] + \phi \{ \gamma C_{9p} (T_9 - T_{\text{bath}}) + H(\gamma_{\text{gH}_2\text{O},\text{out}} - \gamma_{\text{gH}_2\text{O},\text{in}}) \}, \quad (6.2)$$

where Q^* is the heat production rate in the calorimeter vessel [W], T_3 to T_9 the temperatures close to the vessel wall (the subscripts refer to the sensor numbers in figure 6.2a), l the internal height [m] of the vessel and r the internal vessel radius [m].

The heat transfer coefficient α_w of the calorimeter wall can be calculated from the heat balance of the sample if the magnitude of the heat production rate, the temperature difference over the vessel wall and the sensible and latent heat fluxes are known. This was achieved during the calibration experiments. A known rate of heat production was obtained from an electric heating wire, whereas the unknown microbial heat production was reduced to zero by sterilization of the raw material before the calibration. The material was sterilized in an autoclave. As there was always some risk of recontamination of the sterilized raw material during filling of the calorimeter vessel, in addition, pure nitrogen gas was led through the sample during the calibration. Therefore, only anaerobic processes may occur which, in general, release a much smaller amount of heat than aerobic processes. So, if any microbial heat production occurred, it was negligible compared to the electric heat production of about 7 W. The heating wire was enveloped by a glass tube of 150 mm length and 12 mm diameter. This heater was inserted in the middle and parallel to the axis of the vessel.

The latent, conductive and sensible heat flows in the isothermal calorimeter during the runs 1 and 2 are given in the figures 6.3a and b, respectively.

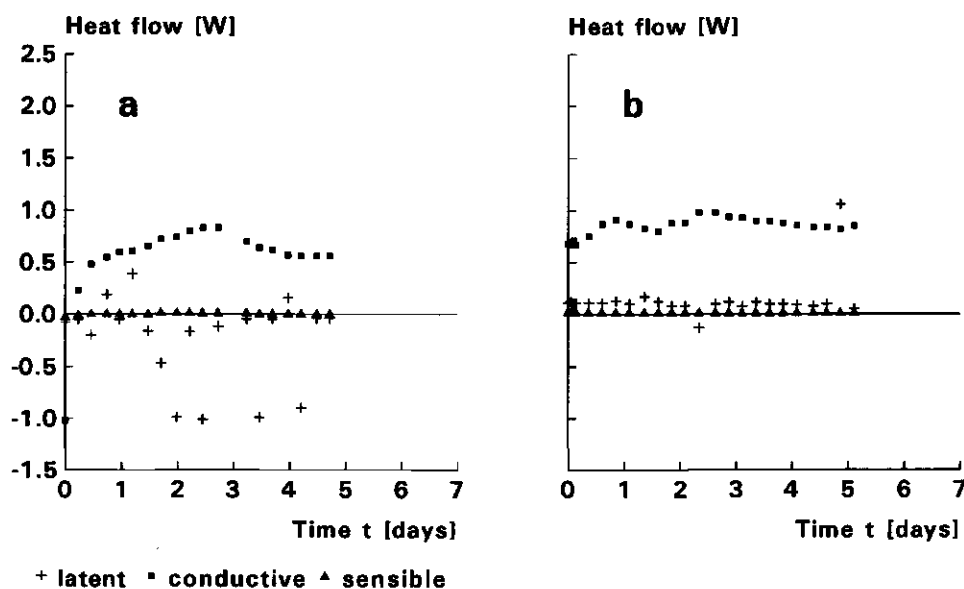


Figure 6.3 Heat flows in the calorimeter during (a) run 1 and (b) run 2.

The latent heat flow in run 1 (figure 6.3a) fluctuated strongly. This influenced significantly the experimental values of the heat production (figure 6.4a). It is not well understood why these variations in the latent heat flow occurred in run 1. In the other experiments this heat flow was almost constant. This is illustrated for run 2 in figure 6.3b, which is representative for the other runs. Table 6.1 gives an overview of the physical conditions prevailing during 19 experimental runs discussed in the next sections.

Table 6.1 Physical conditions prevailing during the experiments.

run	conditions	
1	$T = 22\text{ }^{\circ}\text{C};$	aerobic/ 2 days elevated P_{CO_2}
2	$T = 37\text{ }^{\circ}\text{C};$	aerobic/ 2 days anaerobic
3	$T = 53\text{ }^{\circ}\text{C};$	aerobic
4	$T = 57\text{ }^{\circ}\text{C};$	aerobic
5	$T = 32, 55\text{ }^{\circ}\text{C};$	aerobic
6	$20 \leq T \leq 50\text{ }^{\circ}\text{C};$	aerobic
7	$20 \leq T \leq 60\text{ }^{\circ}\text{C};$	aerobic
8	$20 \leq T \leq 55\text{ }^{\circ}\text{C};$	anaerobic
9	$20 \leq T \leq 55\text{ }^{\circ}\text{C};$	anaerobic
10	$T = 20\text{ }^{\circ}\text{C};$	$8 \leq P_{\text{O}_2} \leq 20\%;$ 0 weeks
11	$T = 20\text{ }^{\circ}\text{C};$	$8 \leq P_{\text{O}_2} \leq 20\%;$ 0 weeks
12	$T = 20\text{ }^{\circ}\text{C};$	$8 \leq P_{\text{O}_2} \leq 20\%;$ 2 weeks
13	$T = 20\text{ }^{\circ}\text{C};$	$8 \leq P_{\text{O}_2} \leq 20\%;$ 2 weeks
14	$T = 20\text{ }^{\circ}\text{C};$	$8 \leq P_{\text{O}_2} \leq 20\%;$ 4 weeks
15	$T = 20\text{ }^{\circ}\text{C};$	$8 \leq P_{\text{O}_2} \leq 20\%;$ 4 weeks
16	$T = 20\text{ }^{\circ}\text{C};$	$8 \leq P_{\text{O}_2} \leq 20\%;$ 6 weeks
17	$T = 20\text{ }^{\circ}\text{C};$	$8 \leq P_{\text{O}_2} \leq 20\%;$ 6 weeks
18	$T = 20\text{ }^{\circ}\text{C};$	$8 \leq P_{\text{O}_2} \leq 20\%;$ 6 weeks
19		$8 \leq P_{\text{O}_2} \leq 20\%;$ 6 weeks

The heat production rate (Q_g) on the basis of oxygen consumption and carbon dioxide production was calculated as the oxygen consumption rate times 457 kJ plus the difference between the carbon dioxide production rate and the oxygen consumption rate times 143 kJ (see section 5.2.3, p. 78 and 79). If no experimental data of the carbon dioxide production rate were available, Q_g was

calculated as the oxygen consumption rate times 457 kJ. If no oxygen consumption data were available, Q_g was calculated as the carbon dioxide production rate times 474 kJ. These theoretical Q_g -values were then compared with the experimental values of the heat production rate Q_t obtained directly from the heat balance of the isothermal calorimeter.

During the measurements as well as the calibration, the 1.9 l calorimeter vessel was filled with approximately 0.8 kg of raw material. The raw material consisted of a mixture of chopped and wetted wheat straw and chicken manure as used before.

If during the experiments the rate of carbon dioxide production exceeds the rate of oxygen consumption, the surplus of carbon dioxide is assumed to be of anaerobic origin (chapter 5). It has to be noticed that carbon dioxide may also originate from carbonate ions in the liquid phase (Ponnamperuma, 1967). However, in experiments with sterilized raw material no carbon dioxide production could be detected and therefore the carbon dioxide production is most probably of biological origin.

To calculate the heat transfer coefficient α_w of the calorimeter vessel wall, equation (6.2) was written as:

$$\alpha_w = \frac{UI - \phi[\gamma_g C_{gp} (T_g - T_{bath}) + H(c_{H_2O,out} - c_{H_2O,in})]}{(T_3 + T_4 + T_6 + T_7 + T_8 + T_9 - 6T_{bath}) \pi r l / 3 + (T_3 + T_9 - 2T_{bath}) \pi r^2}, \quad (6.3)$$

where U is the electrical potential [V] and I the electrical current [A]. Using the data from the calibration experiment, α_w was found to be equal to $4.0 \pm 0.6 \text{ W m}^{-2} \text{ K}^{-1}$. The error in the heat production calculated by equation (6.2) was $2 \text{ W kg}^{-1}(\text{dm})$.

The temperature of the sample in the calorimeter vessel will be unevenly distributed due to the air flow through the vessel. The most extreme situation can be expected if the temperature difference between the sample and the thermostatic bath is large. Figure 6.2b shows the temperature distribution of the sample under such conditions. The arrow indicates the direction of the gas flow. The temperature at the gas inlet (T_3) was significantly lower than the average of the sensors 4, 6, 7, 8 and 9 due to the local sensible and latent heat transfer. The standard deviation of the temperatures of the sensors 4, 6, 7, 8 and 9 was 0.5 K. The temperatures of the sensors 4 and 6 were not significantly lower than the temperatures of the sensors 7, 8 and 9. Thus, the effect of the gas flow was a local phenomenon close to the gas inlet.

6.3 Experimental results obtained from the isothermal calorimeter

6.3.1 Study of the rate of exchange of water vapour between the gaseous phase and the combined solid/liquid phase

In chapter 2 it was assumed that the partial pressure of water vapour in the gaseous phase is equal to the saturated vapour pressure at any time and position in the pile. In this subsection the conditions are deduced which are required for the validity of this assumption.

Air flowed through the mass of wet composting material in the calorimeter (figure 6.2b). The temperature of the composting material was always slightly higher than the temperature of the thermostatic bath. Therefore, water evaporated from the material into the air stream. During the experiments the vapour densities in the inlet and outlet air were measured. The vapour transfer coefficient can be calculated from the vapour balance of the calorimeter. The local mass balance of water vapour in the gaseous phase is given by:

$$\frac{\partial(\theta \gamma_{gH_2O})}{\partial t} = - \nabla \cdot (v \gamma_{gH_2O}) + k'_{H_2O} A (\bar{\gamma}_{gH_2O} - \gamma_{gH_2O}), \quad (6.4)$$

where k'_{H_2O} is the vapour transfer coefficient [$m \ s^{-1}$], A the specific area [$m^2 \ m^{-3}$] of the material and $\bar{\gamma}_{gH_2O}$ the saturated vapour density in the gaseous phase [$kg \ m^{-3}$]. The specific area is unknown. Therefore, A is lumped together with k'_{H_2O} which gives k_{H_2O} . For steady-state conditions and for air flow in the x -direction only, equation (6.4) becomes:

$$v \frac{d\gamma_{gH_2O}}{dx} + \gamma_{gH_2O} \frac{dv}{dx} = k_{H_2O} (\bar{\gamma}_{gH_2O} - \gamma_{gH_2O}). \quad (6.5)$$

Since v is uniform, equation (6.5) reduces to:

$$\frac{k_{H_2O}}{v} dx = - \frac{d(\bar{\gamma}_{gH_2O} - \gamma_{gH_2O})}{(\bar{\gamma}_{gH_2O} - \gamma_{gH_2O})}. \quad (6.6)$$

Integration between the boundaries $x = 0$ and $x = L$ yields:

$$k_{H_2O} = - \frac{v}{L} \ln \left(\frac{\bar{\gamma}_{gH_2O} - \gamma_{gH_2O}(L)}{\bar{\gamma}_{gH_2O} - \gamma_{gH_2O}(0)} \right). \quad (6.7)$$

The vapour transfer coefficient k_{H_2O} was calculated from equation (6.7) and experimental values of the vapour densities at the inlet and outlet of the calorimeter (table 6.2). It was independent of θ_g in the range $0.61 \leq \theta_g \leq 0.78$. There was no clear relationship between k_{H_2O} and temperature. The average value of k_{H_2O} was $2 \times 10^{-3} \text{ s}^{-1}$. Since the standard errors of k_{H_2O} were large, this average value must be considered only as a rough estimate.

Table 6.2. Values of the vapour transfer coefficient k_{H_2O} calculated on the basis of experimental results obtained in the calorimeter with $v = 3.7 \times 10^{-3} \text{ m s}^{-1}$.

exp. run	ρ [kg m ⁻³]	T [°C]	θ_g [-]	d_s [-]	k_{H_2O} [s ⁻¹]	s.e. [s ⁻¹]
1	502	22	0.54	0.19	5×10^{-3}	2×10^{-3}
2	244	37	0.78	0.18	2×10^{-3}	8×10^{-4}
3	388	53	0.65	0.19	2×10^{-3}	9×10^{-4}
4	397	57	0.64	0.22	1×10^{-3}	7×10^{-4}
5	427	32	0.61	0.21	2×10^{-3}	3×10^{-4}
5	427	55	0.61	0.21	2×10^{-3}	8×10^{-4}

s.e. means standard error

If ambient air flows into the pile its temperature will increase and so will the saturated vapour pressure. Since the exchange of water between the combined solid/liquid phase and the gaseous phase is not instantaneous, saturation will be reached at some distance from the outer edge of the pile. It is assumed that saturation is approached if the vapour density in the gaseous phase is equal to 95% of the saturated vapour density. To calculate the distance L_{95} between the outer edge of the pile and the place where the vapour density is 95%, equation (6.7) can be rewritten as:

$$L_{95} = - \frac{v}{k_{H_2O}} \ln \left(\frac{0.05 \bar{\gamma}_{gH_2O}}{\bar{\gamma}_{gH_2O} - \gamma_{gH_2O}(0)} \right). \quad (6.8)$$

Values of $\bar{\gamma}_{g,H_2O}$ and $\gamma_{g,H_2O}(0)$ can be calculated for known temperature and relative humidity of the air outside the pile and the temperature of the compost phase. Assume that the values of these variables are 10 °C, 65% and 65 °C, respectively. Figure 7.17 (chapter 7) shows that the buoyancy term $\Delta\gamma_g$ at 65 °C is equal to approximately 0.2 kg m⁻³. Then, the air velocity can be calculated using the permeability data shown in section 4.2.2. If $L_{95} = 0.05$ m is considered as threshold value, it can be concluded from table 6.3 that vapour saturation is reached in material with θ_g less than about 0.5.

Table 6.3 Calculated distances from the outer edge of the compost pile to the position in the pile where the vapour density of the gaseous phase is equal to 95% of the saturated level pertaining to the temperature of the compost phase

θ_g [-]	κ [m ²]	v [m s ⁻¹]	L_{95} [m]
0.25	1 x 10 ⁻¹¹	1 x 10 ⁻⁶	0.00
0.40	2 x 10 ⁻¹⁰	2 x 10 ⁻⁵	0.03
0.50	4 x 10 ⁻¹⁰	4 x 10 ⁻⁵	0.06
0.65	2 x 10 ⁻⁹	2 x 10 ⁻⁴	0.30
0.78	1 x 10 ⁻⁷	1 x 10 ⁻²	14.80

The air-filled volume fraction distributions given in the figures 7.4a to 7.4f and 7.5a to 7.5f show that θ_g is approximately equal to 0.6. Thus, vapour saturation is not attained in the outer zone of about 20 cm from the edge of the pile. Since L_{95} increases with v , the saturated vapour pressure will not be approached with forced convection.

6.3.2 Microbial production rates as a function of the temperature

Figures 6.4 to 6.7 show the heat production rates measured at a gas composition of 80% N₂, 20% O₂ and temperatures of 22, 37, 53 and 57 °C, respectively. These temperatures are the averages of the sensors T₃ to T₉ during the experiment. Each figure is composed of two sub figures a and b showing the

heat production rates (a) and the oxygen consumption and carbon dioxide production rates (b). In these figures the production rates are expressed per kg of dry matter (dm).

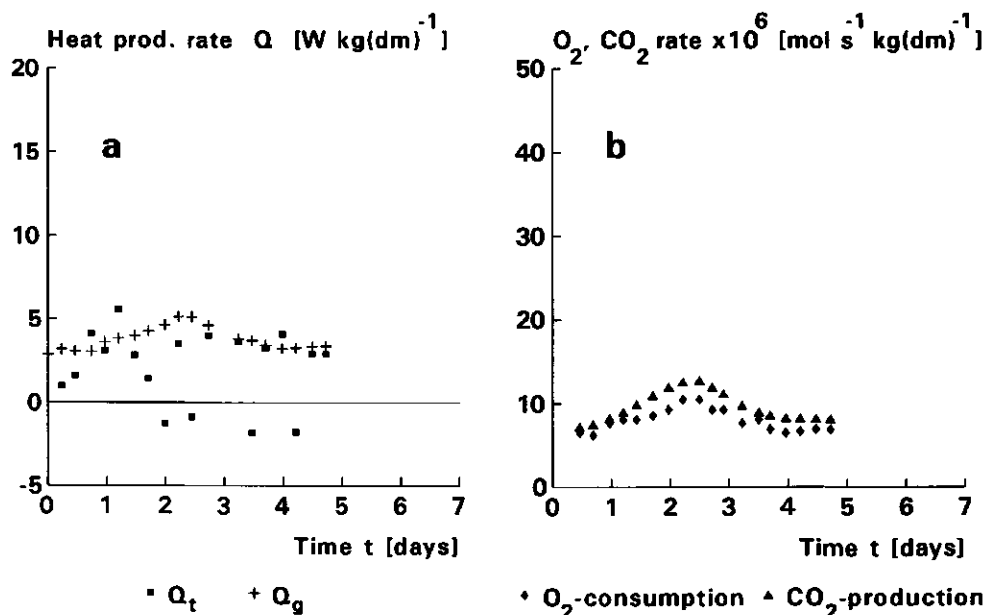


Figure 6.4 (a) The heat production rate of raw material of run 1 as a function of time. The average sample temperature was 22°C and the air flow at the inlet was composed of 80% N₂ and 20% O₂. Q_t is the heat production rate obtained from the heat balance of the sample in the calorimeter vessel, Q_g is the theoretical heat production rate calculated on the basis of O₂-consumption and CO₂-production rates and the Gibbs free energies of degradation reactions of representative constituents in the raw material.

(b) The oxygen consumption and carbon dioxide production rates as functions of the process time. The oxygen consumption rate and carbon dioxide production rate are designated by O₂ and CO₂, respectively.

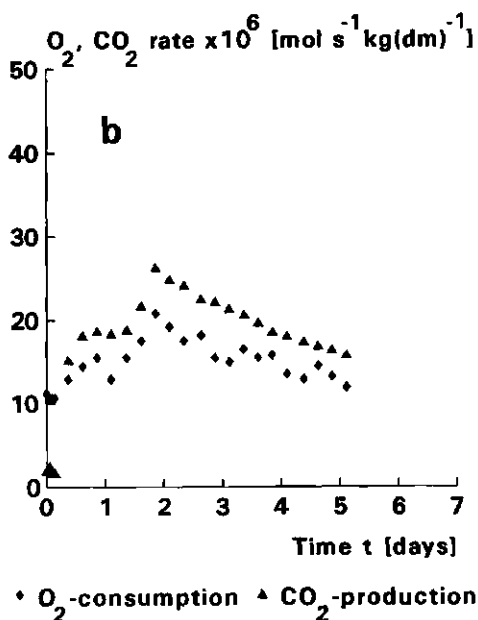
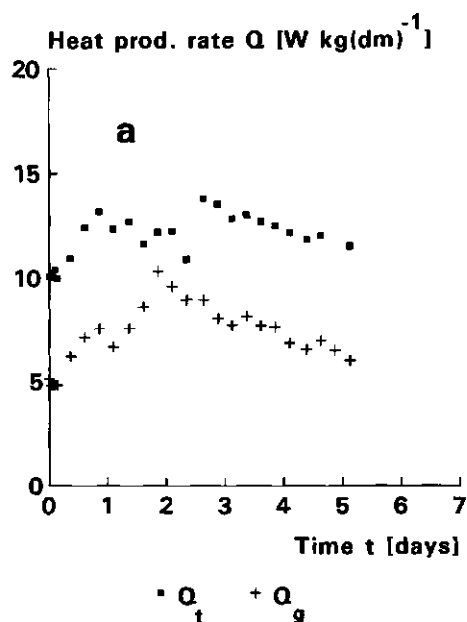


Figure 6.5 Corresponds to figure 6.4. Run 2 at 37 °C.

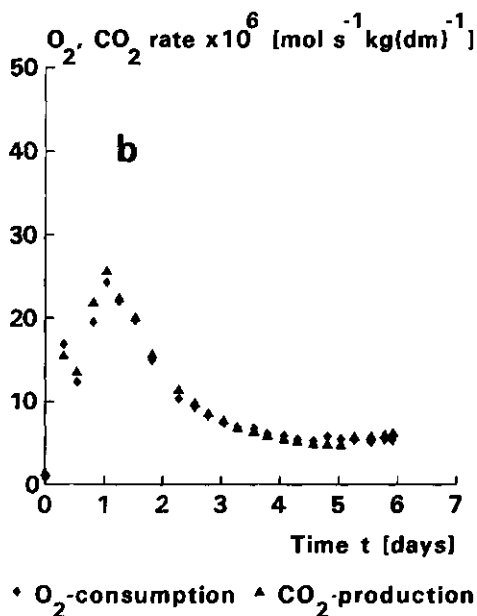
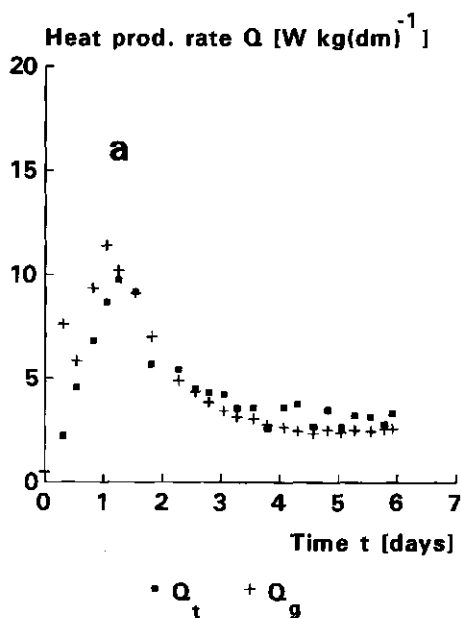


Figure 6.6 Corresponds to figure 6.4. Run 3 at 53 °C.

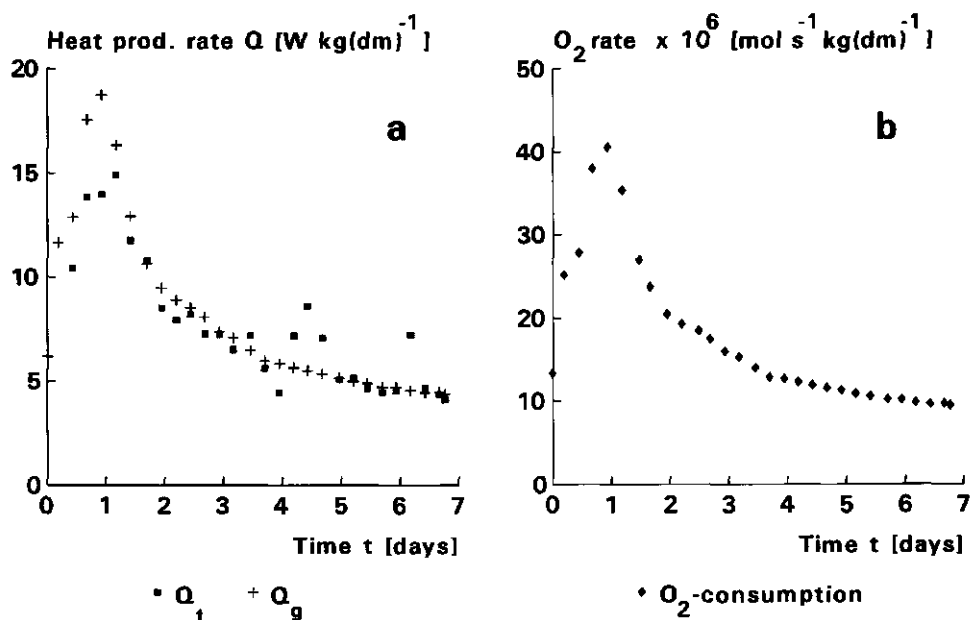


Figure 6.7 Corresponds to figure 6.4. Run 4 at 57 °C.

Figure 6.4a (run 1) shows that there is only a moderate agreement between Q_t and Q_g . This was already addressed in section 6.2. In figure 6.5a (run 2) Q_t is always larger than Q_g . During this experimental run, the calorimeter vessel was filled with 0.47 kg of raw material, instead of 0.8 kg which was normally used. The thermal resistance between the sample and the vessel wall will be larger at smaller bulk densities of the sample. Therefore, it will be clear that the heat transfer coefficient (α_w) determined during the calibration with 0.8 kg of raw material was too large for the sample used in this run and thus Q_t was overestimated. Since there is a good agreement between the heat production rates Q_t and Q_g in the figures 6.6a, 6.7a and 6.8a and a moderate agreement in figure 6.4a, it can be concluded that the theoretically determined heat production rate offers a good estimate of the heat production under aerobic conditions. The maximum production rates increase with temperature (figures 6.4 to 6.7). The same figures show that the rates of oxygen consumption and carbon dioxide production parallel the time course of the heat production rate. The Q_t values peak at the same process time as the O_2 consumption and CO_2 production rates. In figure 6.7b the carbon dioxide production rate is lacking because the CO_2 -analyzer was out of order during this run.

Most striking in the figures 6.4 to 6.7 is the fact that there always appears

a peak in the production rates at the start of the process. Possibly these peaks are caused by the effect of nutrient depletion on the population dynamics. In a continuous system, microbial growth ceases if an essential nutrient becomes depleted (Brock and Madigan, 1988). Then the stationary phase sets in, in which no net increase or decrease in cell number occurs. During this phase the microbial activity is determined by the net influx of the rate limiting nutrient. In a batch system the microbial activity stops eventually when the rate limiting nutrient is depleted. A composting mixture can be considered as a combination of a batch system and a continuous system. The similarity with a batch system is based on the initial amount of easily decomposable nutrients dissolved in the liquid phase, whereas the similarity with the continuous system is based on hydrolysis by which the liquid phase is continuously fed with nutrients.

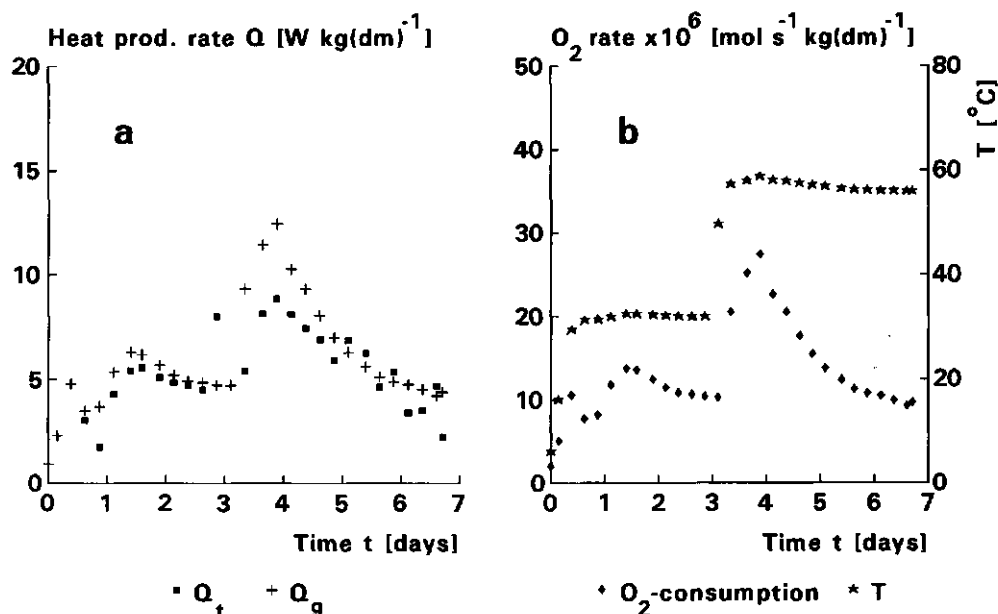


Figure 6.8 Corresponds to figure 6.4. Run 5 at 32 and 55 °C.

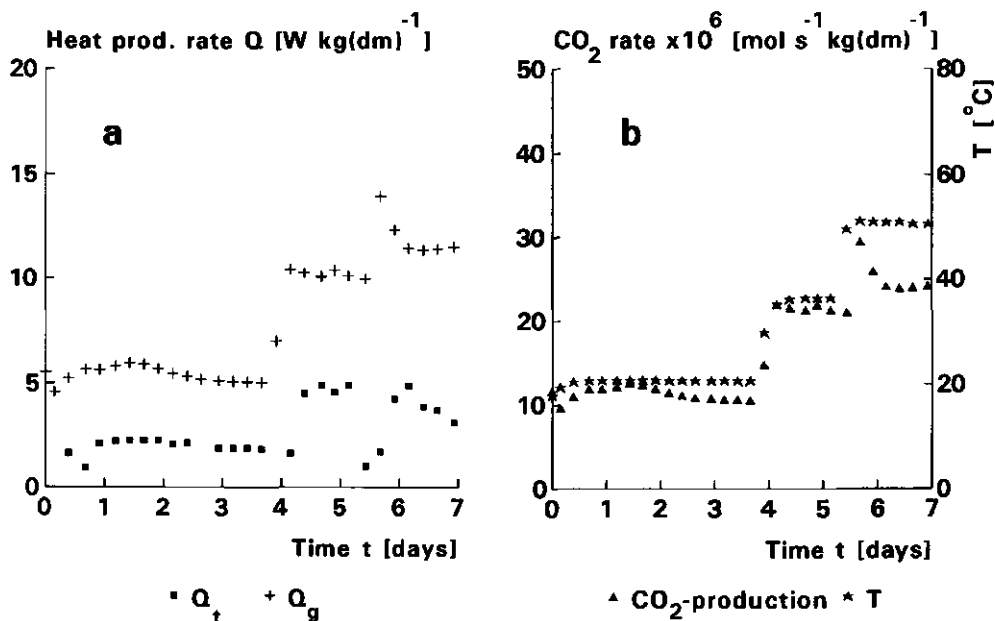


Figure 6.9 Corresponds to figure 6.4. The temperature increased step by step from 20 to 50 $^{\circ}\text{C}$ (run 6).

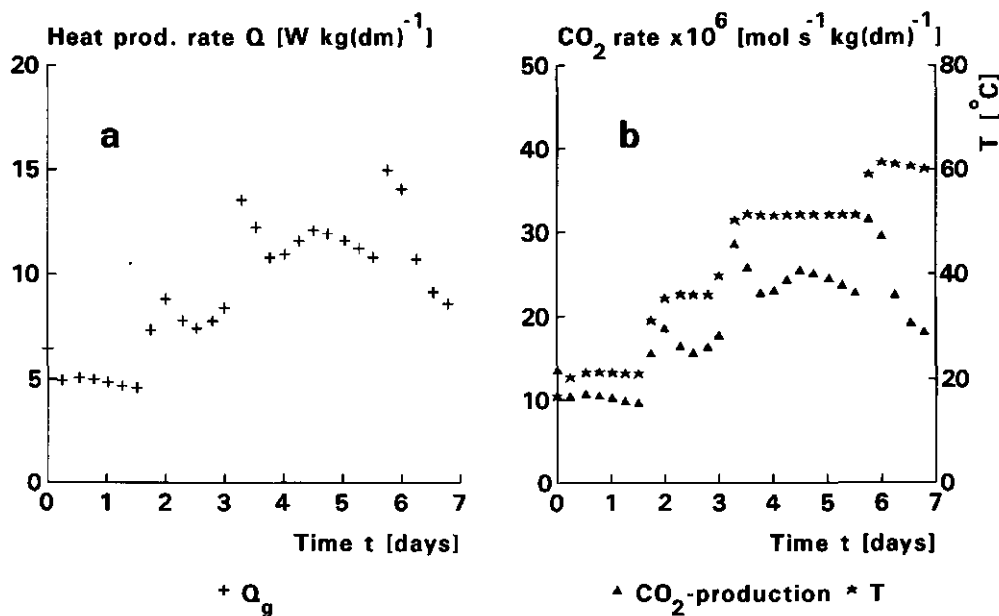


Figure 6.10 Corresponds to figure 6.4. Run 7, $20 \leq T \leq 60$ $^{\circ}\text{C}$.

In the runs described by the figures 6.8 to 6.10 the temperature was increased step by step. In run 5 (fig.6.8) the temperature rose at day 3 from 32 to 55 °C. The heat production peak at 32 °C was approximately 6 W, which lies between the peak values of 22 and 37 °C. The heat production peak at 55 °C has the same magnitude as at 53 °C (fig 6.6a). If the theory of the rate limiting nutrient is valid, the question arises why the second heat production peak appears when the temperature is increased from 32 to 55 °C. An explanation for this may be found in the fact that the solubility of organic materials, such as amino acids and starch, increases with the temperature (Tenney and Waksman, 1929; Weast, 1985). It can be expected that the bio-availability of a substance increases when it dissolves into water.

During run 5 the CO₂ analyzer did not work properly, and therefore those values were omitted. In run 6 (fig. 6.9) the temperature increased from 20 °C via 35 and 50 to 60 °C. At 60 °C the calorimeter vessel started to leak water from the thermostatic bath, so the results at this temperature were also omitted. The heat production rate Q_t was lower than Q_g during the entire run. The bulk density of the sample in this run was equal to the bulk density during the calibration. Therefore, no clear explanation could be found for the observed difference between Q_t and Q_g . There is good agreement between the magnitudes of the carbon dioxide production rates at 20, 35 and 50 °C shown in figure 6.9b and the values at corresponding temperatures in the figures 6.4b, 6.5b and 6.6b, respectively. The same holds for Q_g in figure 6.9b and the magnitudes of Q_g at the corresponding temperatures in the figures 6.4a, 6.5a and 6.6a. The heat production rates Q_g based on the carbon dioxide production rates seem therefore more reliable than the Q_t values in figure 6.9a. During run 7 (fig. 6.10) the humidity meter was out of order. Unfortunately, the measurement of the latent heat flow and the determination of Q_t were therefore no longer possible. The production rates in figure 6.10 correspond satisfactorily with the production rates in the figures 6.4 to 6.7.

In the previous chapter it was argued that following the initial stage of the process, during which the amount of readily available substrate is consumed and the rate of hydrolysis reaches its maximum level, the carbon consumption rate is equal to the rate of hydrolysis (equation 5.19). Since 1 mol of hydrolyzed carbon produces 1 mol of CO₂, this concept can be verified by comparing the values of the hydrolysis constant ζ_c [mol C s⁻¹ kg(dm)⁻¹] in figure 5.3 with the rates of CO₂ production which were measured after the activity peaks shown in the figures 6.4b to 6.8b and 6.14b (table 6.4).

Table 6.4 Comparison between CO₂ production rates, measured after the activity peak, and the CO₂ production rates predicted by the rate of hydrolysis given in figure 5.3.

run	figure	T [°C]	measured [mol s ⁻¹ kg ⁻¹]	predicted [mol s ⁻¹ kg ⁻¹]
1	6.4b	22	0.7 x 10 ⁻⁵	0.5 x 10 ⁻⁵
11	6.14b	20	0.5 x 10 ⁻⁵	0.5 x 10 ⁻⁵
5	6.8b	32	1.1 x 10 ⁻⁵	1.1 x 10 ⁻⁵
2	6.5b	37	1.4 x 10 ⁻⁵	1.2 x 10 ⁻⁵
3	6.6b	53	0.6 x 10 ⁻⁵	1.4 x 10 ⁻⁵
4	6.7b	57	1.0 x 10 ⁻⁵	1.5 x 10 ⁻⁵
5	6.8b	55	1.0 x 10 ⁻⁵	1.5 x 10 ⁻⁵

The predicted CO₂ production rates approach the measured values. Between 20 and 37 °C there is good agreement, but at about 55 °C the measured rates are smaller than the predicted rates. There reason for this difference is not clear.

The maximum heat production rates increase with temperature in the range from 20 to 60 °C. This can be explained by the fact that the rate of hydrolysis increases with temperature. Also the increased solubility of the substrate at higher temperatures can contribute to the increase of the heat production rate.

6.3.3 Microbial production rates as a function of the oxygen concentration

The first part of run 2 was already shown in figure 6.5a. On day 5 of this run the oxygen content of the gaseous phase was reduced to zero (figure 6.11a). When after 12.5 days the oxygen content was increased to 20%, the heat production rate peaked immediately and returned to approximately the same level as before the reduction of the O₂-concentration. From this it can be concluded that the reduction of the microbial heat production rate was a result of the absence of oxygen in the gaseous phase. As discussed in section 5.2.3, the theoretically determined heat production rate Q_g , calculated on the basis of anaerobic processes which release carbon dioxide, will underestimate the real heat production if acetate or lactate fermentations are important. Thus, Q_g in the anaerobic period can be regarded as a lower limit of the real heat production rate. The magnitude of Q_g under anaerobic conditions is approximately 0.27 W. The observed heat production rate Q_t in run 2 was unreliable because the

heat transfer coefficient obtained from the calibration was not applicable. Under aerobic conditions Q_g was approximately equal to Q_t . In view of this, the heat transfer coefficient (α_w) in run 2 can be adapted so that Q_t equals Q_g during the aerobic phase of this run. If this estimated value of α_w was used during the anaerobic phase, the heat production rate Q_t was equal to approximately $3 \text{ W kg}^{-1}(\text{dm})$. Just before the oxygen level was reduced to zero, the heat production rate was equal to $6 \text{ W kg}^{-1}(\text{dm})$. Using these values, the anaerobic heat production rate was about 50% of the aerobic heat production rate. The Gibbs free energy of reaction of the degradation of glucose under anaerobic conditions is, on average, 10% of the energy released per mol of glucose under aerobic conditions (table 5.2). This means that the anaerobic degradation reactions should have proceeded 5 times faster than the aerobic reaction. Walker and Harrison (1960) found that the anaerobic heat production rate in wet wool was less than 1% of the rate under aerobic conditions. If the real anaerobic production rate was close to $3 \text{ W kg}^{-1}(\text{dm})$, the acetate or lactate fermentation or anaerobic respiration with NO_3^- must have been important.

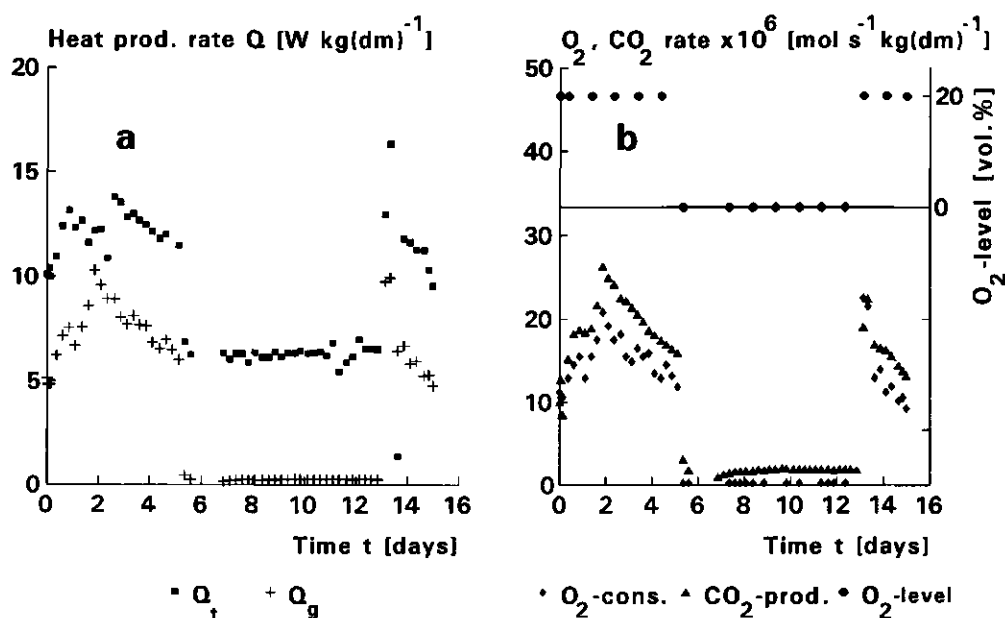


Figure 6.11 Effect of O_2 -level on (a) heat production rate and (b) on rates of oxygen consumption and carbon dioxide production in run 2.

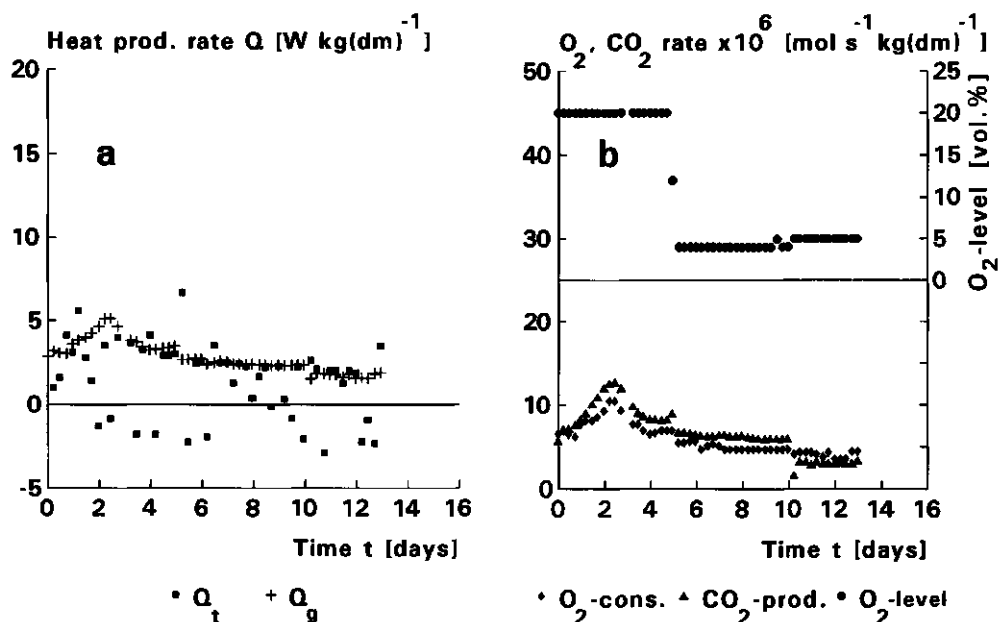


Figure 6.12 Effect of O_2 -level on (a) heat production rate and (b) on rates of oxygen consumption and carbon dioxide production in run 1.

The effect of a reduction of the oxygen content to 4% is shown in figure 6.12. The first part of this figure was already presented in figure 6.4. At 4% of oxygen the heat production rate was slightly lower than at 20%.

Figure 6.13 shows the production rates under anaerobic conditions and temperatures increasing stepwise from 20 to 55 °C. At the start of the measurements in run 9 (figure 6.13b) the CO_2 production rate was large, probably because some oxygen was left over from the moment of filling and the anaerobiosis was not complete. Although every temperature change was accompanied by a small peak in the production rate, the overall effect was a slightly decreasing rate with increasing temperature. The results of the runs 8 and 9 were equal. Figure 6.13b can be compared with the figures 6.9b and 6.10b showing the results of runs in which the temperature increased step by step under aerobic conditions. In the figures 6.9b and 6.10b the production rates increase with the temperature. Thus, the decreasing rates obtained under anaerobic conditions were not a result of the process time, but must be considered as a temperature effect.

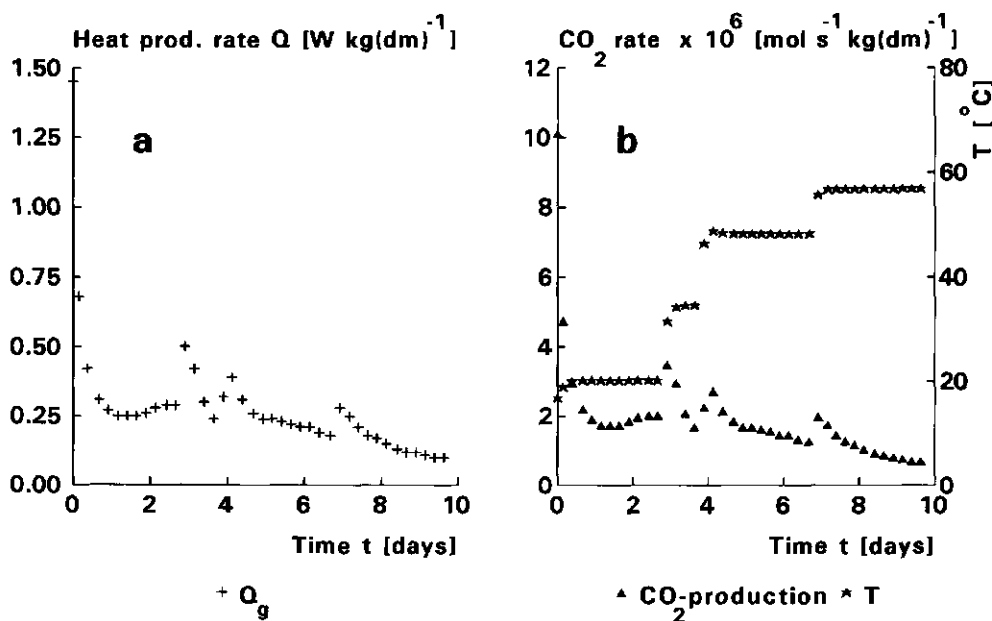


Figure 6.13 Effect of temperature on (a) the heat production and (b) the rates of O_2 -consumption and CO_2 -production under anaerobic conditions, $20 \leq T \leq 55$ $^{\circ}\text{C}$ (run 9).

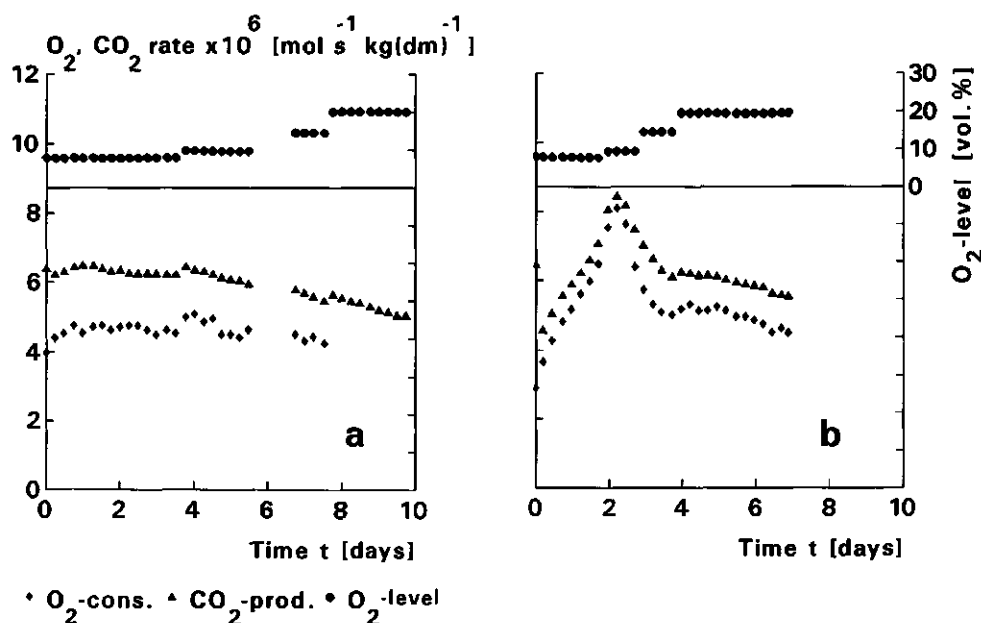


Figure 6.14 O_2 -consumption and CO_2 -production rates at O_2 -levels ranging from 8 to 20 vol.% in (a) run 10 and (b) run 11.

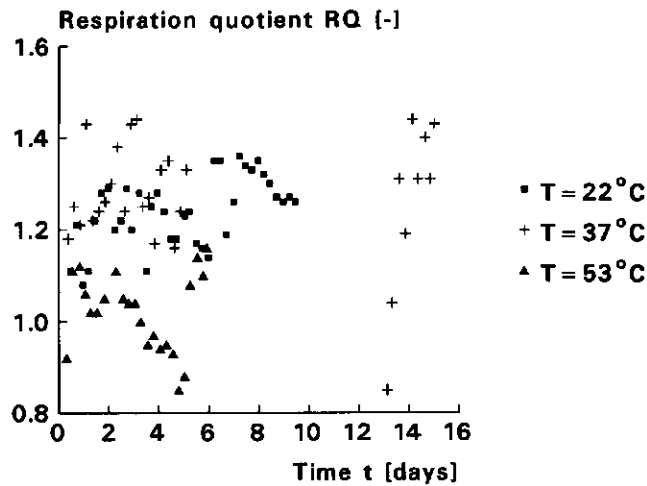


Figure 6.15 The respiration quotient RQ as a function of time influenced by temperature.

The oxygen consumption rate as a function of the oxygen content is an essential parameter in the determination of the oxygen diffusion coefficient, as discussed in chapter 4. The figures 6.14a and b show the rates of oxygen consumption and carbon dioxide production of 0 weeks old samples and at oxygen levels ranging from 8 to 20%. The determinations occurred at 20°C . There is a large difference between both figures. Figure 6.14b shows a production peak at the start of the process, whereas figure 6.14a does not. The production rates in figure 6.14a are approximately equal to the steady-state level in figure 6.14b. It is not clear why the production rates in figure 6.14a are at the steady-state level immediately from the start of the process. Probably there were not enough readily degradable compounds in this sample, so that depletion occurred almost immediately as the measurement started. In runs with 2, 4 and 6 weeks old material no activity peaks appeared. Also these runs show no clear relationship between the oxygen consumption rate and the oxygen level. For 6 weeks old material the oxygen consumption rate increased slightly with the oxygen content in the gaseous phase. The magnitude of the average oxygen consumption rate decreased with the age of the material. For 0, 2, 4 and 6 weeks old material the

average values were equal to 0.45-, 0.35-, 0.22- and 0.07 $\times 10^{-5}$ mol s⁻¹ per kg of dry matter, respectively. Samples of equal age had approximately the same oxygen consumption rate. The only exception was observed in the samples of 4 weeks old material. The oxygen consumption rate in run 14 was of the same order of magnitude (about 0.3 $\times 10^{-5}$ mol s⁻¹ kg(dm)⁻¹) as in 2 weeks old material, whereas for sample 15 the oxygen consumption rate was less than 0.1 $\times 10^{-5}$ mol s⁻¹ kg(dm)⁻¹.

In figure 6.15 the respiration quotient RQ is given as a function of the process time and the temperature. This figure is based on the runs 1, 2 and 3. It will be remembered that in run 2 the oxygen content was reduced to zero between days 5 and 13. In section 5.2.3 it was concluded that if RQ is larger than 1, anaerobic processes occur. At 22 and 37 °C RQ was about 1.25, on average. As the temperature increased to 53 °C the respiration quotient decreased to approximately 1. From figure 6.13b it is known that the CO₂ producing anaerobic processes decreased with increasing temperature. This can explain the observed lower RQ-value at 53 °C.

6.4 Conclusions

Summarizing this chapter, it was found that:

- under the condition of natural convection, the vapour pressure in the gaseous phase will be equal to the saturated vapour pressure, except in the outer zone of about 20 cm from the edge of the pile;
- the release of energy per mol of CO₂ during aerobic degradation of the straw/manure mixture is a good prediction of the microbial heat production per mol of CO₂-production;
- the rate of carbon hydrolysis is a reasonable estimate of the CO₂-production rate, measured after the initial activity peak;
- the heat production is much smaller under anaerobic conditions than under aerobic conditions; the anaerobic value amounts to 10 to 50% of the aerobic value.

CHAPTER 7. MONITORING OF PHYSICAL CONDITIONS IN A COMPOST PILE, INCLUDING THE EFFECTS OF FORCED AERATION

7.1 Introduction

In the chapters 4 and 6 physical and biochemical properties of composting material were determined as functions of prevailing physical conditions. This chapter focusses on determinations of physical conditions in three compost piles on a semi practical scale. The results were obtained from two identical non-aerated compost piles (experiments 1 and 2) and from an experiment in which an aerated and a non-aerated pile were compared (experiment 3).

In the two non-aerated piles of the experiments 1 and 2 the following process parameters were determined: the volume fractions of the solid, liquid and gaseous phases, the temperature and the oxygen and carbon dioxide concentrations in the gaseous phase. These experiments are described in section 7.2.1, while the results are given in section 7.2.2.

At modern composting plants it is common practice to use forced aeration systems to control the compost temperature. In experiment 3 the effects of forced aeration on the distributions of the temperature and the composition of the gaseous phase were studied. This experiment is described in section 7.3.1 and the results are presented in section 7.3.2.

In section 7.4, the information obtained in this chapter will be combined with data of the physical properties of composting material to determine the relative importance of the various transport processes. For moderate values of the air-filled volume fraction θ_g , the heat transfer by conduction is more important than the heat transfer by natural convection. This result will be used to find an analytical solution of the heat balance equation. Based on calculations with this solution, conclusions will be drawn regarding the degradation process and the optimal pile height. Finally, the air flow pattern during forced aeration will be studied by means of a numerical model.

7.2 Two experiments with non-aerated piles

7.2.1 Experimental set up

The composting experiments were carried out in a greenhouse, to protect the compost piles against wind and rain. During winter, whenever the outside temperature was below zero, the air in the greenhouse was heated by an air heater to maintain a temperature of 20°C .

The raw material used in these experiments consisted of a mixture of wetted

wheat straw and chicken manure. The preparation and general characteristics of this mixture were described in detail in chapter 3. About 5200 kg raw material was used to build a pile with rectangular cross-section. A top- and a side-view of the pile are shown in figures 7.1a and b, respectively. The pile was built on a wooden floor, covered with a plastic plate. Part of the raw material was used to build a stack of 8 layers at the centre of the pile. Each layer had an initial mass of 150 kg. The layers were separated from each other by a rigid iron grid mounted in a wooden frame. The height of this frame was 6 cm. The grids were used as markers to measure the deformation of the individual compost layers. The stack of 8 layers was surrounded by a 0.7 m wide buffer, initially consisting of 3000 kg of raw material. The position of the grid corners was indicated by iron bars B (fig. 7.1a) attached to each grid. The layers are indicated by the numbers 1 to 8 with layer 1 at the bottom of the pile and layer 8 at the top (see figure 7.1b).

The compost pile was turned after 2 (336 h) and 4 weeks (672 h). The experiment ended after 6 weeks (1008 h). During a turning event the compost pile was taken down and each layer was mixed separately from the other layers. Two samples of about 700 g were taken from each layer to measure the dry matter content. Next, the pile was rebuilt with the layers in the same order as at the start of the process.

The temperature distribution was measured by 40 thermistors. These semiconductor type sensors had an accuracy of about ± 0.5 K. The sensors were connected with a data logger, controlled by a personal computer in which a data acquisition program was running. The sensors were situated in the layers 2, 4, 6, and 8. Each of these layers contained two rows of 5 sensors. The two rows were considered as replicates. The positions of the sensors are indicated in figure 7.1a by x, and in figure 7.1b by S. The distances from the temperature sensors 1 to 5 to the side of the pile were 0.15, 0.45, 0.75, 1.05 and 1.40 m, respectively. The air temperature was measured with two temperature sensors shielded against direct solar radiation.

Samples of the gaseous phase were taken from 40 ceramic gas sampling cups, each of them situated in the proximity of a temperature sensor. Each cup was connected with a plastic tube leading to the outside of the pile and closed by a stopper. Gas samples were taken by means of a syringe connected to the plastic tube. Before a gas sample was taken, the tube and cup were flushed by extracting 15 cm³ of gas, which was blown off. Next, a sample of 5 cm³ was taken. The gas samples were analyzed on a gas chromatographic analyzer.

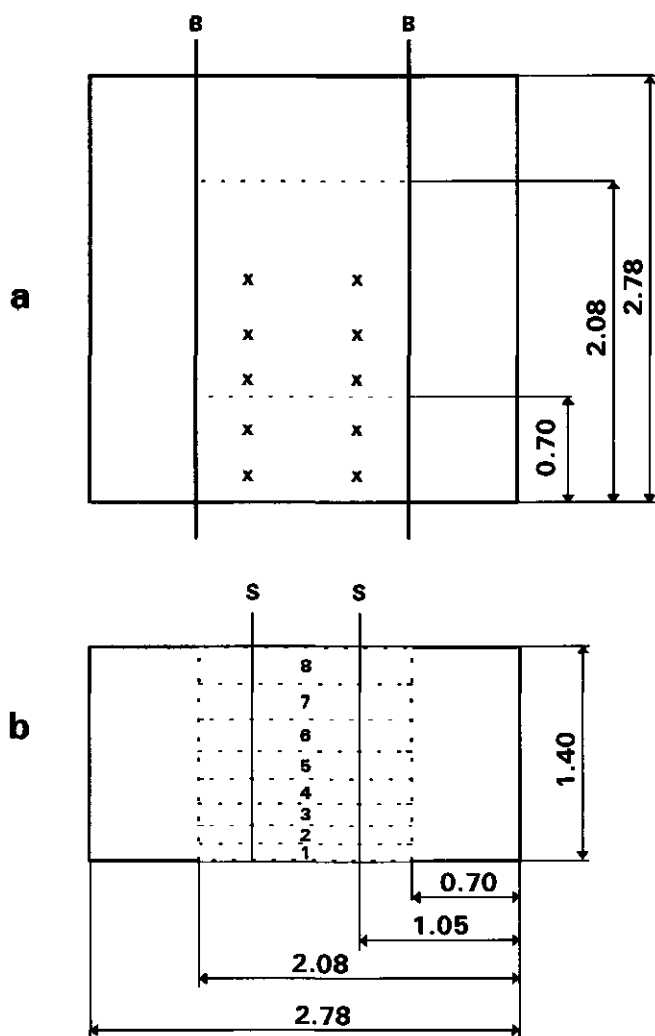


Figure 7.1 (a) Top view of the compost pile used in the experiments 1 and 2. (B) are the iron bars which indicate the positions of the grid corners, (x) are the positions of the thermistors. (b) Side view of the pile. S indicates the position of the thermistors. The numbers 1 to 8 indicate the separate layers. Distances are given in m.

The gas composition data, obtained from this analyzer, were expressed as fractions of the total amount of dry gas in the sample. However, condensation of water vapour was detected in the plastic tubes and the syringe. This was caused by the large differences in saturated vapour pressure between the inside and the outside of the pile. Therefore, the data from the gas analyzer were corrected for the saturated vapour pressure prevailing at the position of the gas cup in the pile according to:

$$P_{O_2} = \left(1 - \frac{P_{sat}}{P_{atm}}\right) P_{O_{2,anal}}, \quad (7.1)$$

where P_{O_2} is the corrected oxygen pressure in the compost pile, P_{sat} the saturated vapour pressure, P_{atm} the atmospheric pressure, and $P_{O_{2,anal}}$ the oxygen pressure obtained from the measurement in the gas chromatograph. The saturated vapour pressure was based on the observed temperature at the location of the sample cup.

7.2.2 Process parameters in two non-aerated piles

The initial dry matter contents of the raw material used in the experiments 1 and 2 were 0.18 and 0.16, respectively. Due to the microbial degradation process, the amount of dry organic matter decreased during the process. Figures 7.2a and 7.3a show the time course of the residual percentage of dry matter in the separate layers during the experiments 1 and 2, respectively. The residual percentage of dry matter is expressed relative to the initial amount of dry matter in the layer. After six weeks the dry matter reduction in experiment 1 ranged from 18 to 32%. The highest dry matter reduction occurred in layer 7, just beneath the top, and the lowest in layer 2. In experiment 2 the dry matter reduction ranged from 23 to 48% (figure 7.3a). In this experiment the highest dry matter reduction occurred in the top layer (8) and the lowest in the layers 3 and 4. The rate of dry matter degradation tended to decrease going from the top to the bottom of the pile. Since the loss of dry material under anaerobic conditions is about 50% of the loss under aerobic circumstances (Reddy and Patrick, 1975; Suler and Finstein, 1977), this was probably caused by a decreasing oxygenation going from top to bottom (e.g. figures 7.7b and 7.9b).

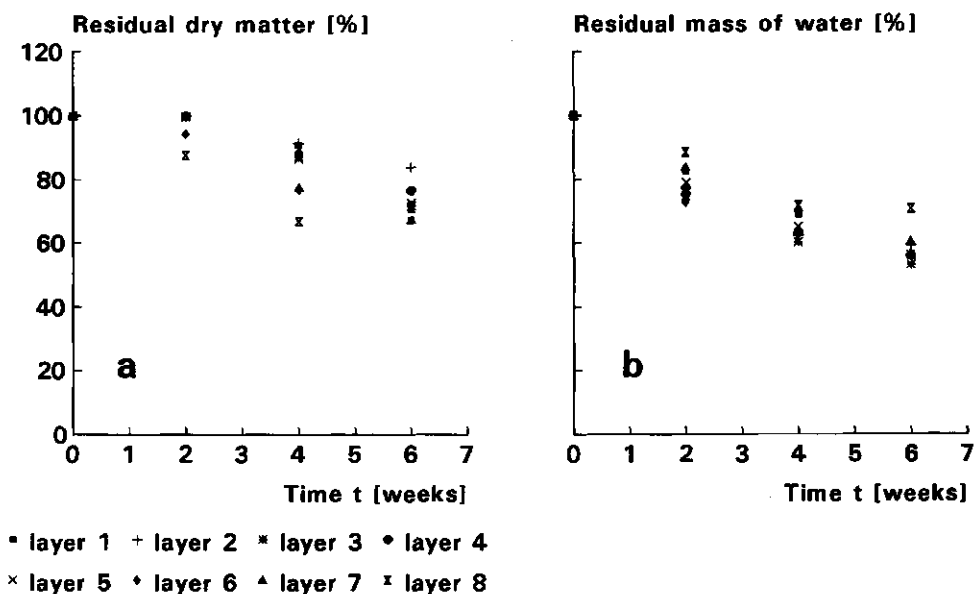


Figure 7.2 (a) The residual dry matter and (b) residual mass of water in the separate layers as a function of the process time (exp. 1).

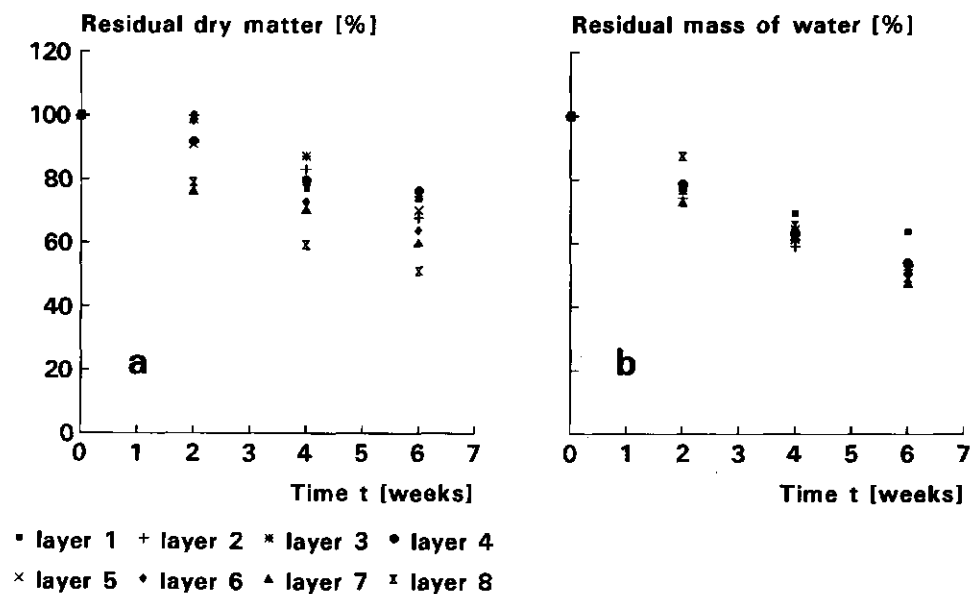


Figure 7.3 (a) The residual dry matter and (b) residual mass of water in the separate layers as a function of the process time (exp. 2).

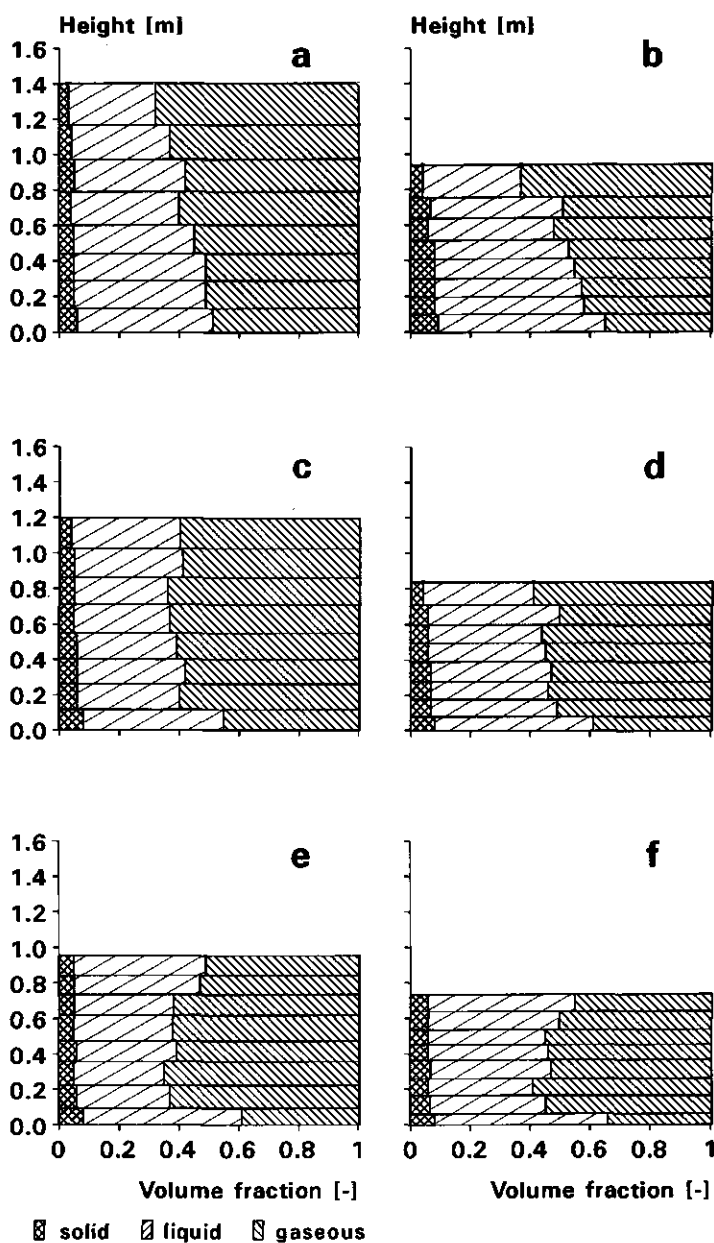


Figure 7.4 Distributions of the volume fractions of the solid, the liquid and the gaseous phases in experiment 1 (a) at the start of week 1, (b) the end of week 2, (c) the start of week 3, (d) the end of week 4, (e) the start of week 5 and (f) the end of week 6.

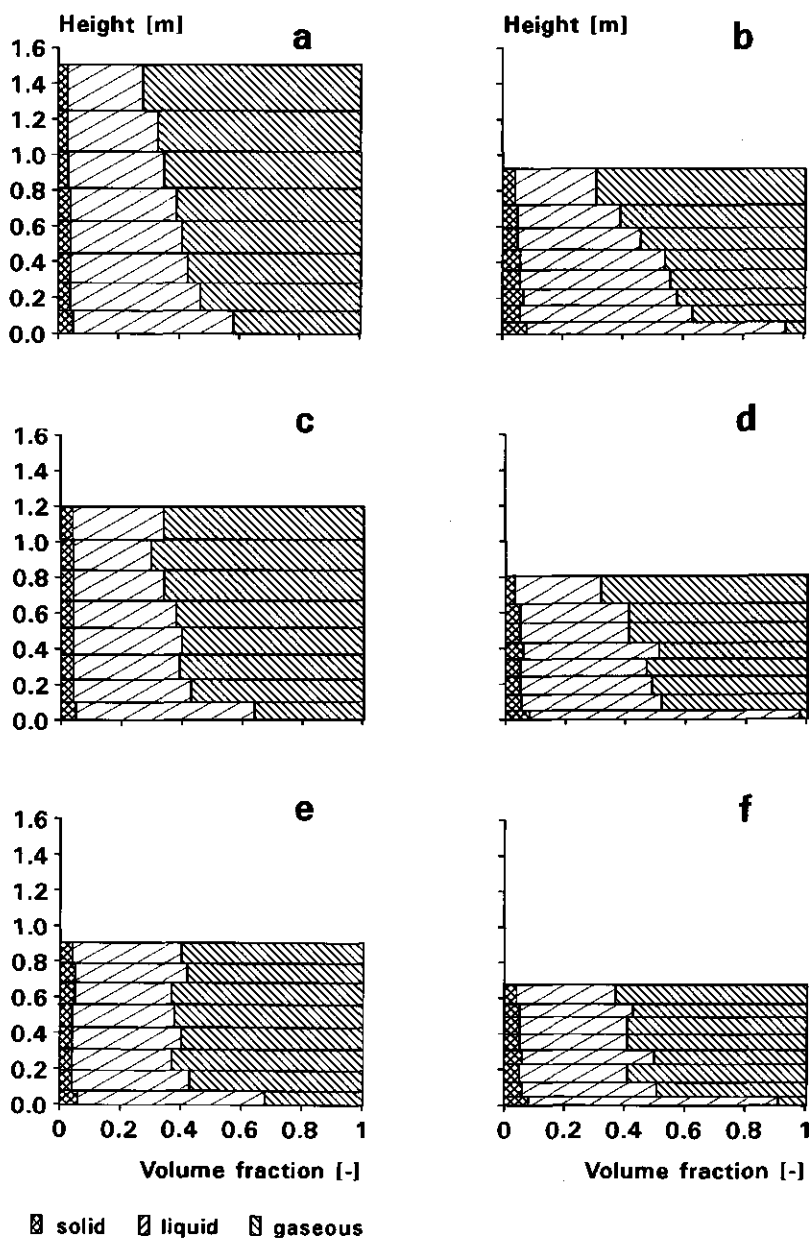


Figure 7.5 Distributions of the volume fractions of the solid, the liquid and the gaseous phases in experiment 2 (a) at the start of week 1, (b) the end of week 2, (c) the start of week 3, (d) the end of week 4, (e) the start of week 5 and (f) the end of week 6.

Although the amount of dry matter decreased, its volume fraction increased due to the simultaneous subsidence of the layers (figures 7.4a to 7.4f). For experiment 1 the volume fractions of the solid (s), liquid (l) and gaseous (g) phases at 6 instances are represented by the length of the horizontal bar pieces in the figures 7.4a to 7.4f. The bars also indicate the positions and thicknesses of the layers in the compost pile. Therefore, this set of figures also illustrates the settlement of the pile. The figures 7.4a to 7.4f pertain to the start of week 1, the end of week 2, the start of week 3, the end of week 4, the start of week 5 and the end of week 6, respectively. Figure 7.4b shows the distribution of the phases just before the first turning event and figure 7.4c gives the phase distribution just after this event. Corresponding remarks hold for figures 7.4d and 7.4e with respect to the second turning event. The subsidence was largest immediately after the start of the process. Figures 7.4a to 7.4f also show clearly that the volumetric fractions of the solid and the liquid phases increased going from the top to the bottom of the pile, whereas the air-filled volume fraction decreased. Similar results were obtained with experiment 2 (figures 7.5a to 7.5f).

Figures 7.2b and 7.3b show the time course of the residual percentage of water mass during experiments 1 and 2, respectively. The residual percentage of water mass is expressed relative to the initial amount of water in the layer. The amount of liquid water lost during the process was statistically insignificant in both experiments. The loss of water in experiment 1 ranged from 30 to 45% and in experiment 2 from 35 to 50% of the initial amount. Since in both experiments the average percentage dry matter loss was less than the average percentage loss of water, the substrate dried during the process.

The figures 7.6a to 7.6d and 7.8a to 7.8d give the temperature distributions in the right hand half of the cross-section of the pile during the experiments 1 and 2, respectively. These figures pertain to 24 h after the start of the process, the moment just before the first turning event (312 h = 13 days), just after this event (360 h = 15 days) and just before the second turning event (648 h = 27 days), respectively. The corresponding oxygen distributions are shown in the figures 7.7a to 7.7d and 7.9a to 7.9d. Based on the experimental results of Miller et al. (1989), discussed in chapter 1 (figure 1.2), one would expect the oxygen content to decrease, going from the side to the centre of the pile. It is therefore most striking that the oxygen contents in the centre of the piles were quite high (figures 7.7b, 7.7d, 7.9b and 7.9d). This can also be observed by comparing the time courses of the oxygen sensors 2 (figure 7.10a) and 4 (figure 7.10b) in layer 4 at 45 and 105 cm from the side of the pile, respectively.

Temperature 24h (exp. 1)				
10.7	10.8	10.8	11.3	11.1
12.1	12.2	12.0	12.1	12.3
11.9	11.8	14.9	14.0	11.8
11.0	10.7	11.0	11.0	10.9

a

Temperature 312h (exp. 1)				
49.3	50.5	55.1	52.8	53.0
71.3	66.9	70.4	67.6	67.8
69.2	66.9	70.7	70.1	68.5
62.8	59.4	66.1	54.0	59.1

b

Temperature 360h (exp. 1)				
18.6	19.1	21.0	23.5	25.5
27.9	29.3	29.0	29.7	28.5
26.6	27.8	28.2	28.8	28.2
29.0	29.8	29.7	28.9	28.9

c

Temperature 648h (exp. 1)				
44.1	21.8	36.6	31.5	44.8
65.4	58.0	63.3	55.6	57.5
66.0	60.3	64.3	69.4	59.8
62.4	58.1	59.5	55.1	49.7

d

Figure 7.6 Temperature distributions in the right hand half of the pile of experiment 1 at (a) 1 day after the start of the process, (b) just before the first turning event (day 13), (c) just after this event (day 15) and (d) just before the second turning event (day 27).

O_2 24h (exp. 1)				
20.7	19.4	18.7	19.0	19.2
15.9	19.2	15.1	14.1	15.4
12.7	16.3	9.7	8.9	9.5
12.4	13.5	6.3	5.9	4.3

a

O_2 312h (exp. 1)				
12.9	16.1	3.3	7.2	5.0
6.8	13.7	0.4	0.3	1.8
6.3	11.7	0.4	0.2	0.5
3.1	12.4	0.2	0.4	0.1

b

O_2 360h (exp. 1)				
19.9	20.3	18.5	17.9	20.1
18.4	19.6	10.8	8.8	14.8
17.5	19.1	1.6	1.4	6.4
10.1	18.5	1.2	1.3	10.7

c

O_2 648h (exp. 1)				
17.6	20.9	15.5	10.5	16.9
11.6	13.8	10.7	7.5	11.5
12.2	8.9	5.3	3.1	5.5
5.2	17.4	3.3	3.8	3.8

d

Figure 7.7 Oxygen distributions in the right hand half of the pile of experiment 1 at (a) 1 day after the start of the process, (b) just before the first turning event (day 13), (c) just after this event (day 15) and (d) just before the second turning event (day 27).

Temperature 24h (exp. 2)

5.9	6.5	6.8	6.6	6.6
7.0	7.2	7.2	7.1	7.2
9.1	7.1	8.5	6.7	6.6
6.8	6.8	6.9	6.7	6.3

a

Temperature 312h (exp. 2)

54.0	60.4	62.4	64.4	54.8
71.3	72.3	68.4	71.8	69.3
73.2	72.5	72.6	68.5	65.8
68.9	68.3	69.5	63.8	62.1

b

Temperature 360h (exp. 2)

8.6	16.4	11.3	18.8	14.3
10.7	19.0	15.4	14.9	13.7
15.9	24.4	21.4	20.5	19.8
16.8	21.7	20.4	23.6	20.7

c

Temperature 648h (exp. 2)

40.4	46.7	41.8	44.2	53.3
69.0	66.8	67.1	58.2	61.0
71.4	67.8	68.9	62.5	62.5
68.4	64.5	67.5	60.1	58.2

d

Figure 7.8 Temperature distributions in the right hand half of the pile of experiment 2 at (a) 1 day after the start of the process, (b) just before the first turning event (day 13), (c) just after this event (day 15) and (d) just before the second turning event (day 27).

O_2 24h (exp. 2)				
20.2	19.7	19.2	19.3	19.2
20.5	18.1	14.7	14.8	16.0
19.6	14.3	12.0	12.3	12.4
16.9	10.5	8.6	7.6	9.5

a

O_2 312h (exp. 2)				
16.0	13.4	10.7	9.5	10.9
12.3	11.1	7.2	5.6	8.6
11.4	11.4	4.3	1.7	5.8
10.3	9.6	3.4	1.5	1.5

b

O_2 360h (exp. 2)				
21.9	21.0	22.1	21.8	21.9
21.6	16.2	21.6	21.6	21.1
20.4	16.0	17.7	18.7	17.7
20.3	18.2	11.7	10.3	9.5

c

O_2 648h (exp. 2)				
17.9	16.6	15.0	10.6	15.8
14.2	13.3	7.0	2.9	11.8
12.9	11.0	6.5	2.2	9.5
12.3	12.9	2.6	1.4	6.5

d

Figure 7.9 Oxygen distributions in the right hand half of the pile of experiment 2 at (a) 1 day after the start of the process, (b) just before the first turning event (day 13), (c) just after this event (day 15) and (d) just before the second turning event (day 27).

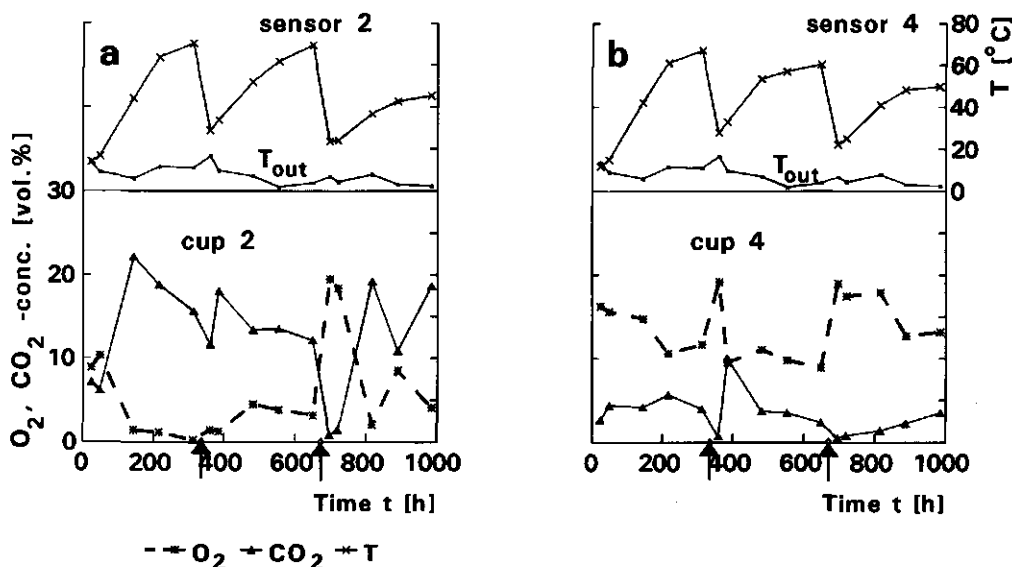


Figure 7.10 Temperature T and O_2 - and CO_2 concentrations as functions of time in layer 4 at (a) 45 cm and (b) 105 cm from the outside of the pile (exp. 1). The arrows indicate the turning events.

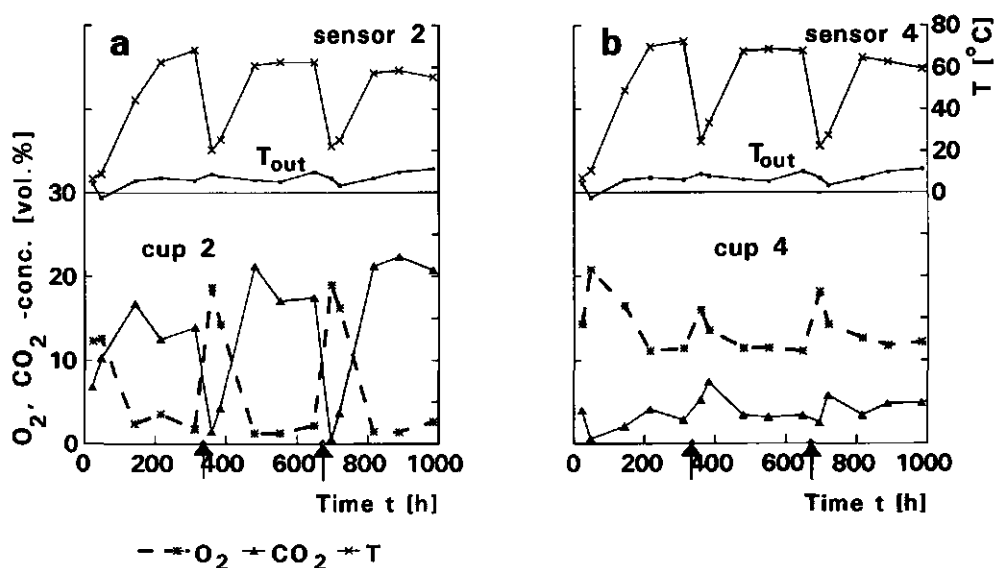


Figure 7.11 Temperature T and O_2 - and CO_2 -concentrations as functions of time in layer 4 at (a) 45 cm and (b) 105 cm from the outside of the pile (exp. 2). The arrows indicate the turning events.

Similar results are shown for pile 2 in the figures 7.11a and 7.11b. It is generally accepted that temperatures higher than 65 °C inhibit microbial activity (Miller et al., 1989). However, this cannot explain the high oxygen contents in the centre of the pile since the temperatures at this location and in the region with low oxygen contents were similar. It is therefore more likely that the explanation of this phenomenon must be found in the oxygen transfer, i.e. diffusion and convection.

Diffusion probably did not cause the differences in oxygen content because the diffusion coefficient only depends on the air-filled volume fraction θ_g (chapter 4). Due to the compressibility of the material the position relative to the top of the pile mainly determines θ_g (chapter 3). Owing to the rectangular shape of the vertical cross-section of the pile (constant height) the distance from any position, at a certain horizontal level, to the top will be constant. If redistribution of water due to drying phenomena at the outer shell of the pile is disregarded, θ_g will be constant in horizontal direction and therefore also D_{O_2} will be constant.

Most likely, the observed differences in oxygen content were caused by air circulating in the compost due to natural convection. Such circulating flow patterns were also found in other porous media with internal heat generation, such as nuclear power systems (Hardee and Nilson, 1977), or porous layers heated from below, such as geothermal fields (McKibbin, 1986). Natural convection is driven by differences in air density caused by temperature and composition gradients. At constant pressure air density decreases as the temperature increases. At the start of the process this effect can be counterbalanced by the increasing amount of carbon dioxide. The molecular mass of carbon dioxide (44 kg kmol⁻¹) is much larger than the average molecular mass of air (29 kg kmol⁻¹). Thus, an increasing carbon dioxide concentration will give an increasing density of the gaseous phase. Natural convection therefore becomes only significant after the temperature effect exceeds the effect of high carbon dioxide concentrations.

7.3 Comparison between an aerated and a non-aerated pile

7.3.1 Experimental set up

Experiment 3 was carried out in the same greenhouse and with similar raw material as the experiments 1 and 2. The experiments lasted 8 weeks (56 days = 1344 h). The compost piles were turned after 22 days (528 h) and again after 41 days (984 h). During each turning event the compost was homogenized by

passing it several times over a conveyor belt. The initial dry matter content was equal to 25% and the total mass of the mixture was 14500 kg. One half of the total amount was used to set up a normal static pile (pile 1) with dimensions 4.4 x 3.6 x 1.3 m. With the other half an aerated static pile was built (pile 2). The aeration system consisted of a centrifugal blower connected to a perforated air duct. The blower produced an air flow of $0.64 \text{ m}^3 \text{ s}^{-1}$ at 1100 Pa.

The temperature control system of the aerated pile consisted of a set of control sensors and a control module contained in the data acquisition program. This module calculated the average temperatures of the control sensors. If this average temperature was higher than 57°C , the computer switched on the blower. If the average temperature became lower than 56°C , the blower was switched off.

Figures 7.12a and 7.12b show the left hand half of the cross-section of a compost pile and the positions of the temperature sensors and gas cups, respectively. The black spot represents the air duct in the aerated pile 2. The lateral distributions of gas cups and temperature sensors are given in figure 7.12c. In each pile four cross-sectional planes can be considered: two planes in which temperature sensors are located and two planes with gas cups. Within a pile the two planes with temperature sensors can be regarded as replicates. The same holds for the two planes provided with gas cups.

Temperature sensors and gas cups were located in the cross-section of a pile in such a way that information was obtained from spots where the most extreme conditions were expected to occur. Comparison of figures 7.12a and 7.12b shows that gas cup 1 corresponds with temperature sensor 1 and cup 4 with sensor 9. Further, it is assumed that cup 2 pertains to the location of sensor 2, cup 3 pertains to sensor 7 and cup 5 to sensor 10. The plotted values always represent the average of two replicate sensors in a pile.

7.3.2 Process parameters in an aerated and a non-aerated pile.

Figure 7.13a shows the temperatures of the sensors 3, 5, 7 and 9 during the first 5 days (120 h) of the composting process of the non-aerated pile 1. It has to be emphasized that the lines shown in the figures 7.13 to 7.16 are only meant to increase the readability of the figures. They do not have any statistical meaning. Most conspicuous in figure 7.13a is that the temperature increments of the sensors 3, 5 and 9 were equal during the first 24 hours and that the temperature of sensor 7 lagged behind.

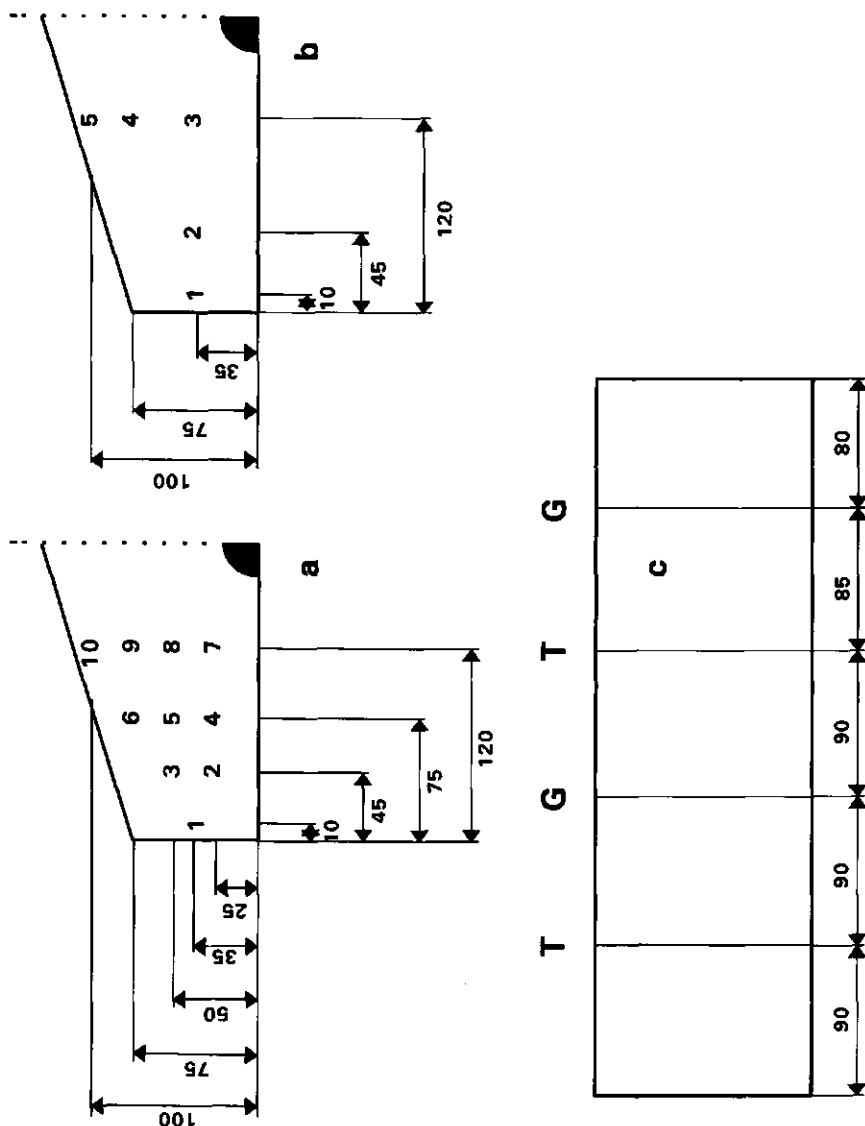


Figure 7.12 (a) The positions of the thermistors and (b) the gas cups, indicated by numbers, in the left hand half of the cross-sectional planes of the piles used in experiment 3. The black spot indicates the position of the air duct in the aerated pile. The distances are given in cm. (c) The lateral distribution of the thermistors T and the gas cups G.

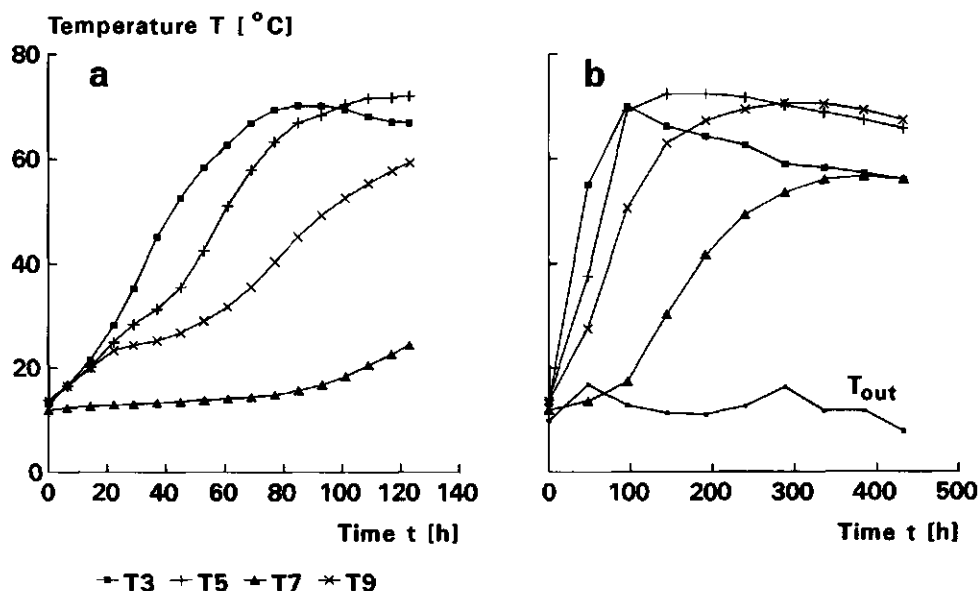


Figure 7.13 Temperature curves of the thermistors 3, 5, 7 and 9 of the non-aerated pile (1) during (a) 120 and (b) 500 hours from the start of the process. The lines do not have any statistical meaning.

During the first day of the process the oxygen content declined rapidly to 1 or 2 percent (fig. 7.14b to 7.14d), except for gas cup 1 (fig. 7.14a) for which the lowest oxygen concentration was approximately 7 percent. After 24 hours the temperature of sensor 3 still increased at the same rate, whereas the other sensors showed a temperature rise at a lower rate. This can be explained by the fact that the heat generation is lower under anaerobic conditions compared to aerobic conditions (Chapter 6). Anaerobic conditions prevailed at the locations of gas cups 2, 3 and 4 (see fig. 7.14b to 7.14d). After about two days the temperatures of the sensors 3 and 5 were 53 and 40 $^{\circ}\text{C}$ respectively. At that moment the oxygen contents of cups 1, 2 and 3 started to increase which suggests that natural convection became important. The oxygen contents started to increase when the highest temperature in the pile was 53 $^{\circ}\text{C}$. So, the effect of natural convection is a more plausible explanation than the inhibition of microbial activity as a result of high temperatures.

The oxygen content of cup 3 (fig. 7.14c) increased very slowly, presumably since the extra supply of oxygen as a result of natural convection was almost consumed before it reached cup 3.

The temperature increase of sensor 7 was very small during 80 hours from the start of the process. This is probably caused by relatively high heat losses to the environment compared with the low heat production rate under anaerobic conditions at this location. The temperature of sensor 7 started to increase as the other temperature sensors approached a maximum level (figure 7.13b). For the temperature rise in the lower central region of the pile heat transfer seems to be more important than local heat production.

After 435 hours (about 18 days) the temperature distribution varies between 58 and 68 °C (figure 7.13b), which is a relatively narrow range. This is a desirable situation from the viewpoint of sanitation.

Temperature and gas concentration curves of the entire composting process are given in the figures 7.14a to 7.14f. After 22 days (528 h) and 41 days (984 h) the pile was turned, indicated by the arrows, which caused the temperature to fall. The oxygenation was improved after the first turning event, probably because substrate depletion started to occur at that stage of the process.

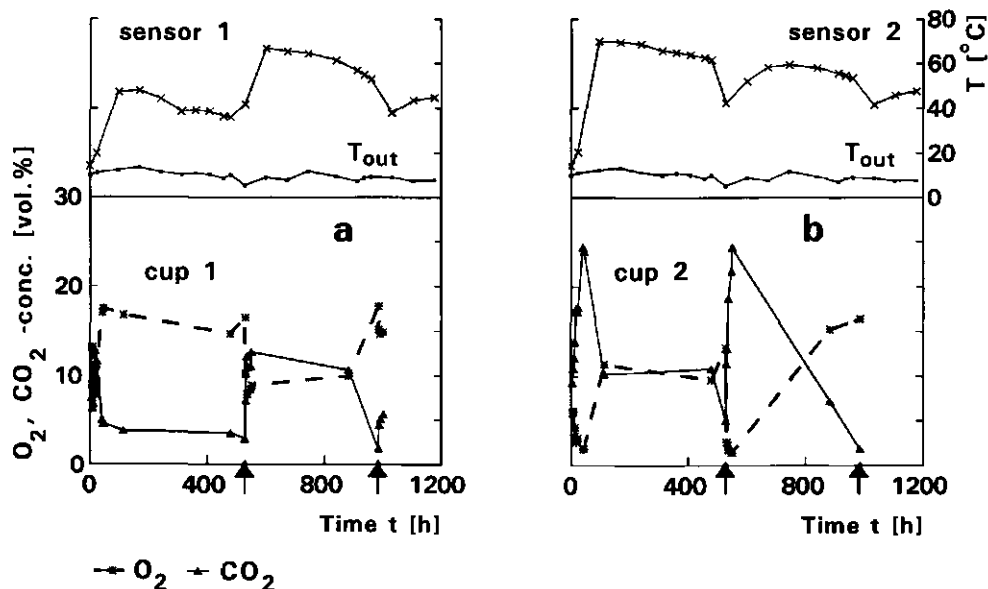


Figure 7.14 Continued on next page.

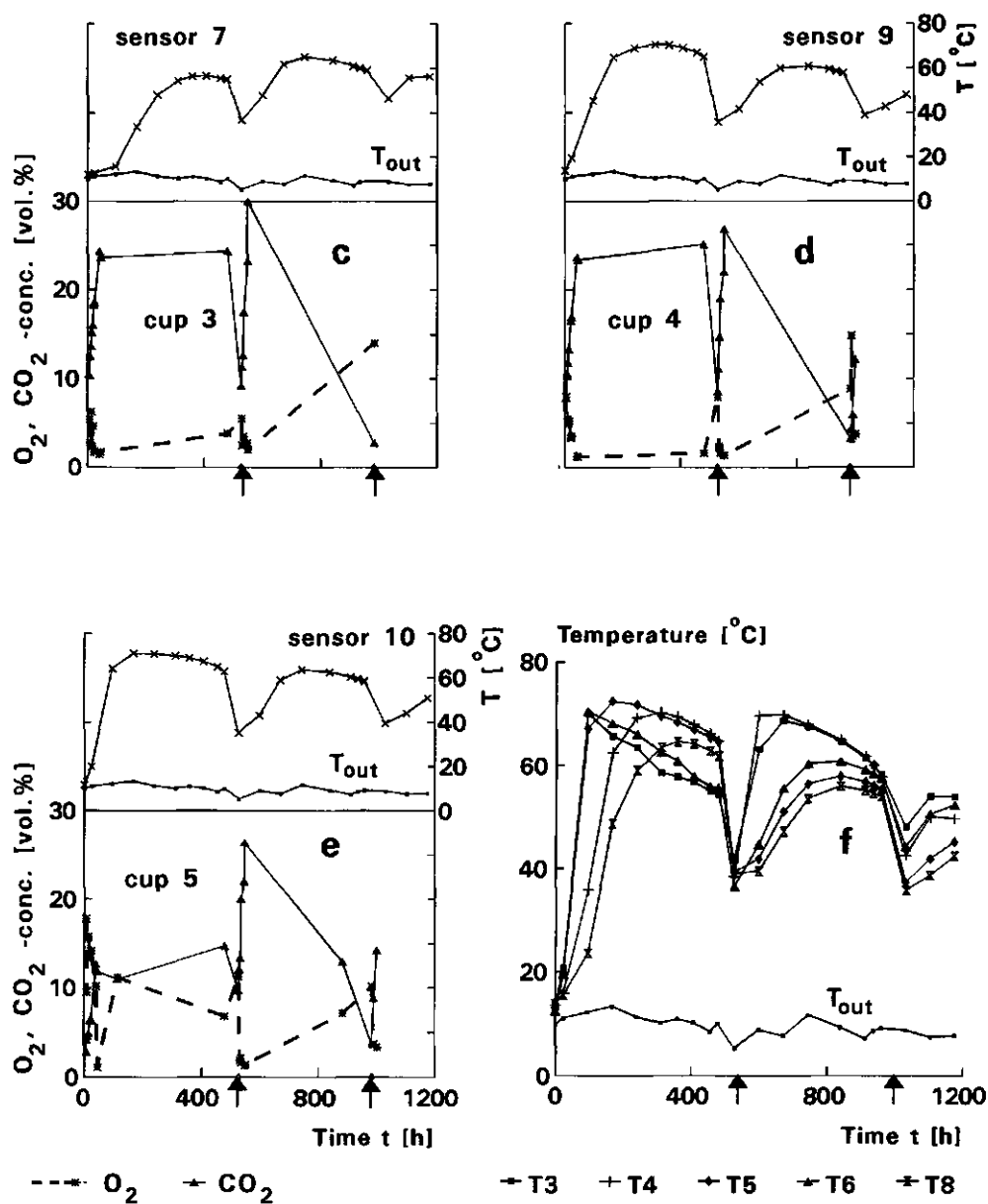


Figure 7.14 The time course of the temperature and O_2 - and CO_2 -concentrations in the non-aerated pile (1). (a) to (e) show readings of thermistors 1, 2, 7, 9 and 10, respectively. (f) gives readings of sensors 3, 4, 5, 6, and 8. The arrows indicate the time at which turning occurred.

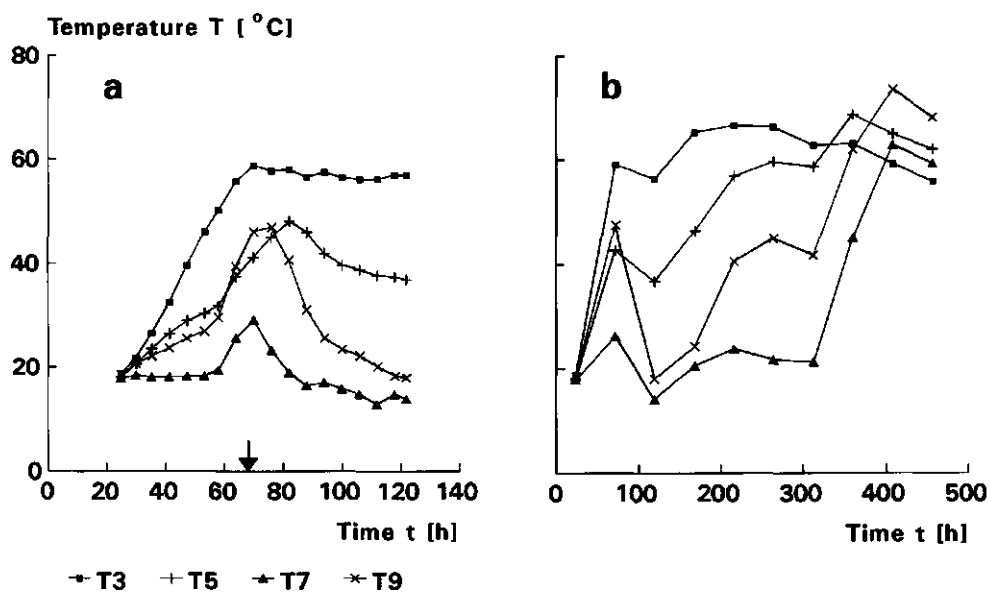


Figure 7.15 Temperature curves of the sensors 3, 5, 7 and 9 of the aerated pile (2) during (a) 120 and (b) 500 hours from the start of the process . The arrow indicates the start of forced aeration.

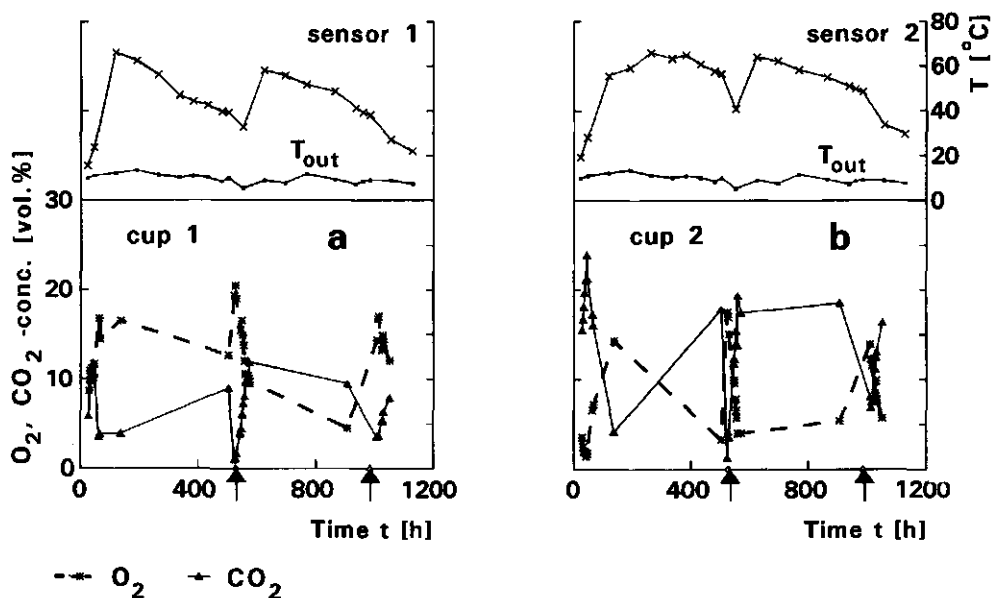


Figure 7.16 Continued on next page.

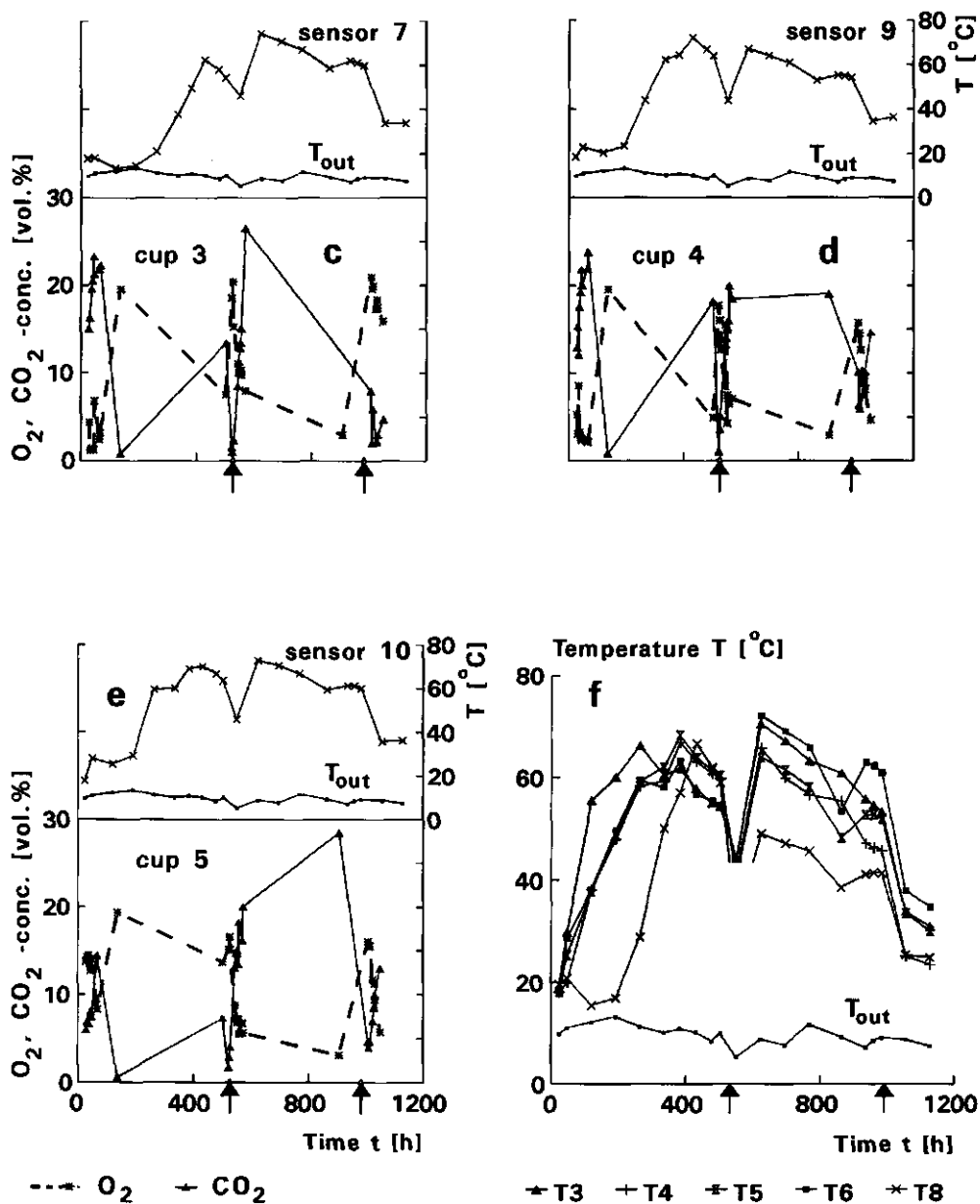


Figure 7.16 The time course of the temperature and O_2 - and CO_2 -concentrations in the aerated pile (2). (a) to (e) show readings of thermistors 1, 2, 7, 9 and 10. (f) gives readings of sensors 3, 4, 5, 6 and 8. The arrows indicate the time at which turning occurred.

The temperature curves of the first 5 days (120 h) of the aerated static pile 2 are given in figure 7.15a. Figure 7.15b shows temperature curves for a 20 days (480 h) period. In the figures 7.16a to 7.16f curves of the temperatures as well as the gas concentrations of pile 2 are presented for the entire composting process.

The temperature sensors 2 and 3 (see fig. 7.12a) were used as control sensors in the aerated pile 2. These locations were recommended by Burge (1983) from the viewpoint of sanitation.

The forced ventilation started for the first time at 68 hours from the start of the process (indicated by the arrow in fig. 7.15). From 68 to 320 hours the blower switched on and off at irregular time intervals controlled by the temperature control system. After 320 hours the set of control sensors was changed and the number of ventilation events was strongly reduced, as will be discussed later.

Until 68 hours from the start, the temperature curves of the aerated pile 2 and the non aerated pile 1 followed a similar pattern. The temperature sensors 5, 7 and 9 were strongly affected by the ventilation, as demonstrated by the decline of these temperatures (fig. 7.15a). However, three days later the temperatures started to increase again (fig. 7.15b). This might be a result of the adaptation of the microbes to the higher oxygen contents. At about 250 hours from the start of the process the temperatures reached a steady state. The temperature in the aerated pile 2 (fig. 7.15b) then varied between 21 and 67 °C, which is much more than the range of 58 to 68 °C pertaining to the non-aerated pile 1 (see fig. 7.13b). In an attempt to obtain smaller temperature variations, sensors 2 and 7 were chosen as an alternative set of control sensors 320 hours after the start of the process. These sensors were chosen because they gave the lowest temperature readings. As a result forced ventilation occurred only a few times after the set of control sensors was changed and at 450 hours the temperature curves were very similar to those of the non-aerated pile 1.

Stentiford et al. (1985) compared aerated systems with super atmospheric pressure aeration (blowing) and sub atmospheric pressure aeration (sucking). They also observed that large temperature variations occur in an aerated pile. They found the highest temperatures at the apex of the pile when super atmospheric pressure aeration was applied. In the case of sub atmospheric pressure aeration, the highest temperatures were found at the core of the pile. To ensure inactivation of pathogens they advised a hybrid system with a sub atmospheric pressure aeration at the start of the process and a super atmospheric pressure aeration when the temperatures decrease at the apex of the

pile.

In our research only super atmospheric pressure aeration was applied. The observations and conclusions of Stentiford et al. (1985) with respect to this type of ventilation system are supported by our results.

It has to be noted that the large temperature ranges obtained during forced aeration will very much depend on the type of aeration system that is used. It can be expected that a composting system consisting of a tunnel provided with a grid floor covered by a wall-to-wall compost layer will lead to a smaller temperature range than a system consisting of a single perforated air duct in the core of the pile.

7.4 Interpretation of the experimental results using data of physical and biochemical properties

7.4.1 Comparison of measured and calculated bulk densities and dry matter reduction

The bulk density distributions of the piles at the start of experiments 1 and 2 were calculated by equation (3.7). Values of the unloaded bulk density ρ_u were obtained using the data shown in figure 3.12. Table 7.1 gives the results.

Table 7.1 Comparison between measured ρ_{exp} and calculated ρ_{cal} bulk densities.

experiment 1			experiment 2		
h [m]	ρ_{exp} [kg m ⁻³]	ρ_{cal} [kg m ⁻³]	h [m]	ρ_{exp} [kg m ⁻³]	ρ_{cal} [kg m ⁻³]
1.40	345	231	1.41	308	266
1.17	407	271	1.16	365	321
0.97	462	312	0.95	402	381
0.79	437	357	0.75	453	446
0.61	489	407	0.58	473	512
0.44	534	458	0.42	492	586
0.29	539	512	0.26	533	664
0.14	561	571	0.12	678	740

The largest differences between experimental ρ_{exp} and calculated ρ_{cal} bulk densities occurred in experiment 1. These differences may be due to variations in materials handling during loading of the individual compost layers. This can be seen by comparing the experimental values at 0.97 and 0.79 m. Normally, the bulk density increases going from the top to the bottom of the pile. At the mentioned heights an inversion of this normal density distribution occurred. This suggests that some external forces acted at 0.79 m during loading. In experiment 2 the agreement between experimental and calculated values is reasonable.

The average bulk density can be computed from the floor load divided by the total height of the pile. This floor load is calculated by equation (3.11). The calculated average bulk densities are 372 and 459 kg m⁻³ for experiments 1 and 2, respectively. This can be compared with the measured value of 437 kg m⁻³ in both experiments.

The rate of organic matter degradation follows from equation (2.9):

$$\frac{d\rho_o}{dt} = -\zeta_c^* \rho_o,$$

with the rate constant ζ_c^* given by equation (5.12):

$$\zeta_c^* = \zeta_c \frac{M_{\text{cel}}}{6}.$$

Then, it follows immediately:

$$\frac{\rho_o(t)}{\rho_o(0)} = \exp\left[-\zeta_c \frac{M_{\text{cel}}}{6} t\right]. \quad (7.2)$$

An average value of ζ_c is about $1 \times 10^{-5} \text{ mol s}^{-1} \text{ kg}^{-1}$ at 65 °C (table 5.8). For experiment 1 this means that after 6 weeks the relative organic matter density is equal to 0.34. The measured value of the relative dry matter density after 6 weeks was about 0.75. Thus, the degradation rate was approximately 40 percent of the potential value. This can be caused by inhibition due to high temperatures or to anaerobiosis.

7.4.2 The relative importance of various transport processes

Magnitudes of oxygen flows by natural convection and diffusion were estimated using experimental data of the air permeability, the effective oxygen diffusion coefficient, and gradients of oxygen density and air density. These flows are given by:

$$F_{O_2,cv} = \left| \frac{\kappa}{\mu} \Delta \rho_g g \bar{\rho}_{O_2} \right|, \quad (7.3)$$

and

$$F_{O_2,dif} = \left| D_{O_2,eff} \frac{\Delta \rho_{O_2}}{\Delta x} \right|, \quad (7.4)$$

respectively. Here, the superscript - stands for the average of the densities inside and outside the pile, and Δ for the difference between these two densities. Provisionally omitting the sensible part of the heat flux, the convective heat flux is given by:

$$F_{H,cv} = \left| \frac{\kappa}{\mu} \Delta \rho_g g \bar{\rho}_{H_2O} H \right|, \quad (7.5)$$

and the conductive heat flux by:

$$F_{cond} = \left| \lambda \frac{\Delta T}{\Delta x} \right|. \quad (7.6)$$

For given values of transport properties the largest flows could be expected in the outer shell of the pile because there the largest gradients were found. Therefore, appropriate values of T and ρ_{O_2} were obtained from sensor 1, i.e 15 cm from the side of the pile (figures 7.6b and 7.7b). The ambient temperature was 10 °C, the compost temperature 60 °C, and $\bar{\rho}_{O_2}$, $\Delta \rho_{O_2}$, $\bar{\rho}_{H_2O}$ and Δx were 0.15, 0.19, 0.07 kg m⁻³ and 0.15 m, respectively. Figure 7.17 gives the distribution of the difference between the density of the ambient air and the gaseous phase in the compost pile. These values were calculated using the universal gas law and experimental values of the gas composition and the temperature. In further calculations a value of 0.2 kg m⁻³ for $\Delta \rho_g$ was used. In table 7.2 the various flows are given as functions of the air-filled volume fraction θ_g . The thermal

conductivity coefficient λ mainly depends on the volumetric water content θ_l . To estimate λ from figure 4.14, θ_l was calculated by equation (2.1) with θ_s is equal to 0.05.

$\Delta \rho_g$ 312h (exp. 1)				
0.17	0.19	0.16	0.17	0.16
0.32	0.30	0.27	0.25	0.26
0.29	0.29	0.28	0.27	0.26
0.27	0.24	0.21	0.12	0.15

Figure 7.17 Distribution of the difference between the density of the gaseous phase and the density of the ambient air $\Delta \rho_g$ [kg m⁻³] (exp. 1).

Table 7.2 The relative importance of oxygen and heat transfer by convection and diffusion depending on the air-filled volume fraction θ_g .

θ_g [-]	κ [m ²]	D_{eff} [m ² s ⁻¹]	$F_{O2,cv}$ [kg m ⁻² s ⁻¹]	$F_{O2,dif}$ [kg m ⁻² s ⁻¹]	λ [W m ⁻¹ K ⁻¹]	$F_{H,cv}$ [W m ⁻²]	F_{cond} [W m ⁻²]
0.8	3×10^{-8}	4.7×10^{-6}	5×10^{-4}	6×10^{-6}	0.18	552.1	60.0
0.7	3×10^{-9}	3.9×10^{-6}	5×10^{-5}	5×10^{-6}	0.25	55.2	83.3
0.6	1×10^{-9}	3.1×10^{-6}	2×10^{-5}	4×10^{-6}	0.30	18.4	100.0
0.5	4×10^{-10}	2.3×10^{-6}	7×10^{-6}	3×10^{-6}	0.35	7.4	116.7
0.4	2×10^{-10}	1.7×10^{-6}	3×10^{-6}	2×10^{-6}	0.45	3.7	150.0
0.3	5×10^{-11}	1.1×10^{-6}	8×10^{-7}	1×10^{-6}	0.50	0.9	166.7

From this table it can be concluded that for oxygen transfer convection is more important than diffusion with θ_g - values larger than 0.2, whereas for heat transfer the conductive flux is more important than the convective flux for θ_g -values smaller than 0.7. The average value of θ_g in the experiments was about 0.5 (figures 7.4 and 7.5). This means that for the heat balance convection is of minor importance, which is a very advantageous conclusion because it makes it easier to find an analytical solution of the heat balance equation.

Carslaw and Jaeger (1986) give an analytical solution for a steady-state two-dimensional heat transfer problem based on conduction and internal heat generation. The steady state heat balance is obtained from equation (2.34) and is given by:

$$\nabla^2 T = - \frac{Q \rho C}{\lambda} \quad (7.7)$$

For a rectangle with constant internal heat generation Q and with the surfaces $x \pm a$ and $y \pm b$ kept at zero, the solution is (Carslaw and Jaeger, 1986, p.170):

$$T = \frac{Q(a^2 - x^2)}{2\lambda} - \frac{16Qa^2}{\lambda\pi^3} \sum_{n=1}^{\infty} \frac{(-1)^n \cos\{(2n+1)\pi x/2a\} \cosh\{(2n+1)\pi y/2a\}}{(2n+1)^3 \cosh\{(2n+1)\pi b/2a\}} \quad (7.8)$$

The temperature distribution in the cross-section of any pile with rectangular shape can be calculated using this equation. As an example, the temperature distribution will be calculated for a pile similar to that shown in figure 7.6b. At 50 °C the steady state heat production is approximately 5 W kg(dm)⁻¹ (chapter 6). For an average bulk density of 437 kg m⁻³ and a dry matter content of 0.18, this means a heat production of 393 W m⁻³. For this material $\theta_1 = 0.4$ and $\lambda = 0.4$ W m⁻¹ K⁻¹. The result, given in figure 7.18a, shows that the predicted temperature in the centre of the pile is too high (> 65 °C). Thus, the heat production at this location will be inhibited by these temperatures. The same conclusion was drawn based on data of dry matter reduction in the previous section. Figure 7.18b shows predicted temperatures for $Q = 250$ W m⁻³. These temperatures are more realistic. The results do not necessarily mean that microbial heat production is inhibited by high temperatures only. It is also possible that inhibition by anaerobiosis starts before the inhibitive temperature is reached.

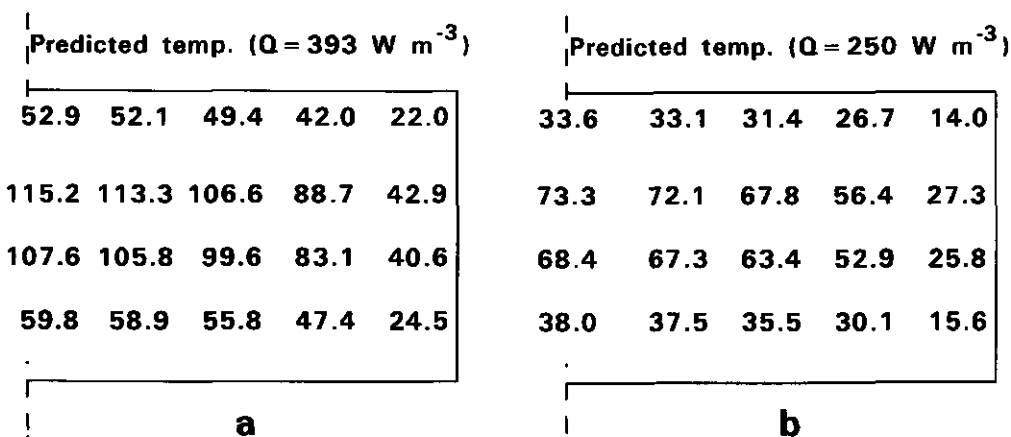


Figure 7.18 Temperature distributions calculated with equation (7.8), with a heat production of (a) 393 and (b) 250 W m^{-3} (pile height = 0.95 m).

Equation (7.8) can also be used to determine the pile height which is optimal with respect to temperatures allowing a maximum rate of decomposition (55°C) or a maximum rate of nitrification (37°C). As an example, calculations were made for material with a heat generation of 500 W m^{-3} and a thermal conductivity coefficient of $0.4 \text{ W m}^{-1}\text{K}^{-1}$. The first condition is fulfilled with a height of 0.6 m (figure 7.19a) and the second with a height of 0.5 m (figure 7.19b).

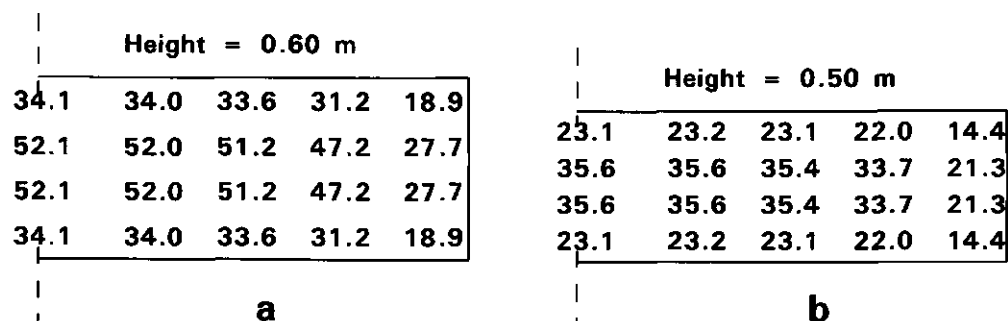


Figure 7.19 The temperature distribution in a pile with a height which is optimal (a) with respect to a maximum degradation rate and (b) with respect to a maximum nitrification rate (b).

7.4.3 A mathematical model to calculate the air flow pattern during forced aeration of a compost pile

In the previous section the calculations were restricted to natural convection and diffusion. In this section the emphasis is on forced aeration.

If a steady state is assumed, the mass balance equation of the gas phase is given by (Bird et al., 1960):

$$\nabla \cdot \gamma_g \mathbf{v} = 0. \quad (7.9)$$

The filter velocity \mathbf{v} is calculated by Darcy's law (2.21) multiplied by γ_g :

$$\gamma_g \mathbf{v} = - \frac{\kappa}{\mu} \gamma_g \nabla P. \quad (7.10)$$

If equation (7.10) is inserted in equation (7.9) and multiplied by μ , the result is:

$$\nabla \cdot (\kappa \gamma_g \nabla P) = 0. \quad (7.11)$$

An analytical solution of equation (7.11) is known only in special cases in which e.g. κ is an exponential function of P . Unfortunately, in case of air flow through compost no simple relationship between κ and P exists and therefore equation (7.10) must be solved numerically. The numerical procedure employed here was recommended by Patankar (1980) and Van Meurs (1985).

For a particular composting material, wetness and materials age, the air permeability is determined by the vertical distribution of air-filled volume fraction which can be calculated from equation (3.9). In the simulation model the vertical distribution of the air permeability is approximated from the calculated θ_g - distribution and by interpolation in the experimental results given in chapter 4.

The pressure and velocity distributions of the gas phase depend on the shape of the pile. The cross-sections of two compost piles of different shapes which will be considered in this section are illustrated in the figures 7.20a and 7.20b. The rectangular as well as the pentagonal cross-section is symmetrical with respect to the vertical z -coordinate axis. The calculation domain can therefore be restricted to one half of the cross-section.

The air flow also depends on the type of aeration system which is employed. Two types of aeration systems will be considered here: a grid floor and a

perforated duct in a central position at the bottom of the pile.

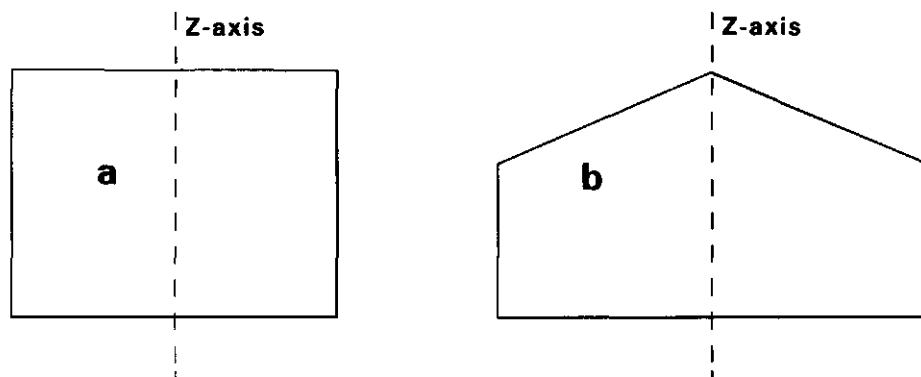


Figure 7.20 (a) Rectangular and (b) pentagonal cross-sections used to model the air flow pattern in compost piles with forced aeration.

To study the reliability of the numerical model, the result of the model has been compared with an analytical solution. The simplest way to achieve such a solution is to assume that the air permeability and the air density are constant. Then, equation (7.10) becomes equal to the well known Laplace equation:

$$\nabla^2 P = 0. \quad (7.12)$$

An analytical solution of equation (7.12) is given by Carslaw and Jaeger (1986, p. 167) for a two dimensional rectangular system with width a and height b . Here the boundary conditions are:

$$\begin{aligned} P &= C \text{ (constant),} & z &= 0, 0 < x < a, \\ P &= 0, & z &= b, 0 < x < a, \\ P &= 0, & x &= 0, 0 < z < b, \\ P &= 0, & x &= a, 0 < z < b, \end{aligned} \quad (7.13)$$

in which x is the horizontal coordinate and z the vertical coordinate. The analytical solution of equation (7.12) with boundary conditions (7.13) is:

$$P = \frac{4C}{\pi} \sum_{n=0}^{\infty} \frac{1}{(2n+1)} \sin \frac{(2n+1)\pi x}{a} \sinh \frac{(b-z)(2n+1)\pi}{a} \operatorname{cosech} \frac{(2n+1)\pi b}{a}. \quad (7.14)$$

The analytical solution (7.14) and the numerical solution of equation (7.12) are both shown in figure 7.21. The numerical solution is illustrated by the isopressure lines indicating 20, 40, 60 and 80% of the static pressure of the blower. Corresponding analytical results are depicted by points. This figure pertains to the right hand half of the rectangular cross-section of a pile provided with a grid floor through which super atmospheric pressure aeration is performed. Figure 7.21 shows that the agreement between the numerical and analytical solution is very good. Thus, the simulation model seems reliable.

In the next discussion the air flow pattern is characterized by isopressure and isovelocity lines. The numbers below the a-figures with isopressure lines indicate the percentage of the static pressure of the blower; the numbers below the b-figures with isovelocity lines are related to the air velocity [m s^{-1}].

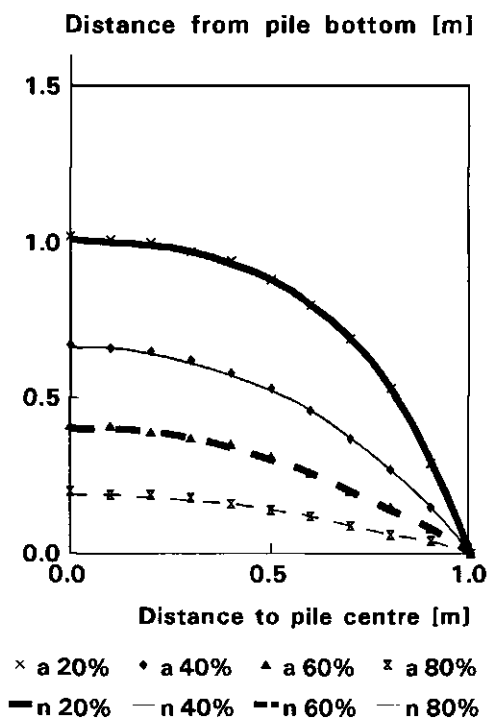


Figure 7.21 Comparison between the analytical and numerical solution of (7.12). The numbers below this figure indicate the percentage of the static pressure exerted by the blower. This figure shows the right hand half of the rectangular cross-section of a pile provided with a grid floor (a means analytical, n means numerical).

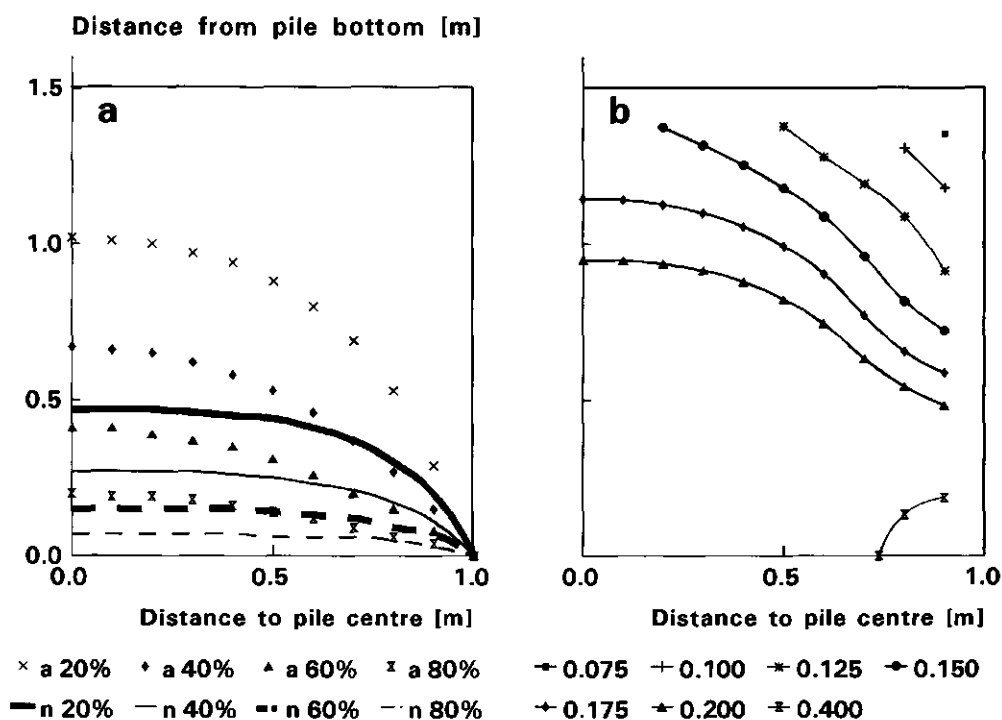


Figure 7.22 (a) The isopressure lines of a pile with variable air-filled volume fraction θ_g compared with the isopressure values of a rigid pile with a homogeneously distributed θ_g . (b) The isovelocity lines of the non-rigid pile (variable θ_g). These figures pertain to the right hand half of the rectangular cross-section of a pile with a grid floor (a means analytical, n means numerical).

In figure 7.22a isopressure values of a rigid compost pile with constant air-filled volume fraction and permeability are compared with isopressure lines of a compost pile consisting of compressible material. The values of the rigid material, indicated by points, correspond with the analytical solution shown in figure 7.21. In the lower part of the pile the pressure gradient of the compressible composting material is much steeper than that of the rigid compost. Especially at the right hand edge at the base line the pressure gradient is very large. As a result, high velocities occur at this position as indicated by the isovelocity lines in figure 7.22b.

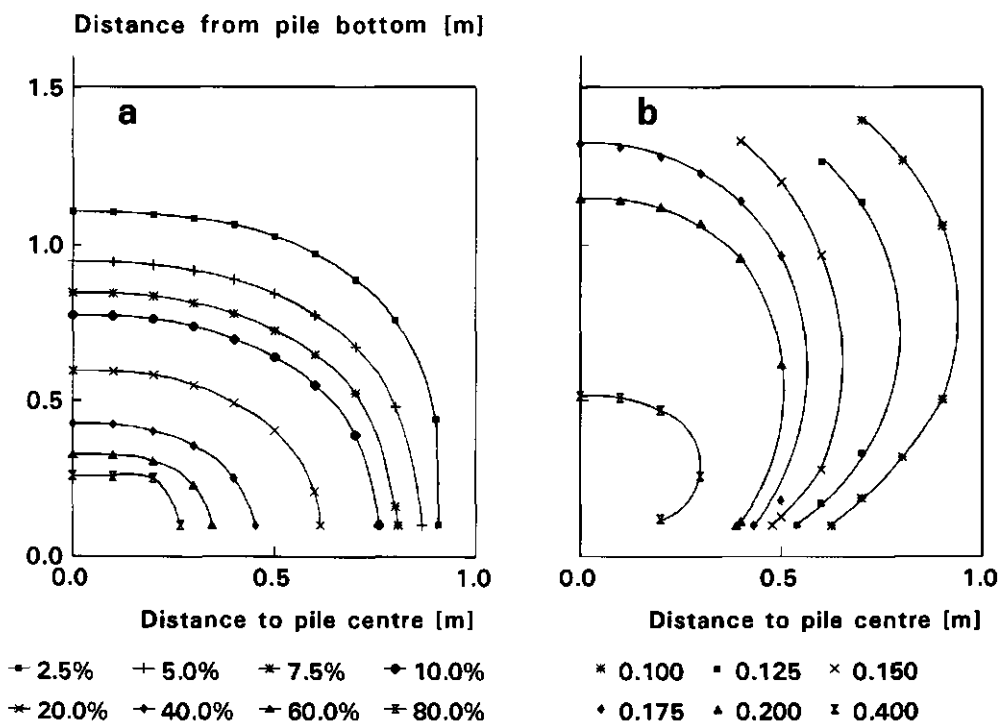


Figure 7.23 (a) The isopressure lines and (b) the isovelocity lines of a non-rigid pile with a rectangular cross-section and provided with an air duct system.

If the aeration system is changed from a grid floor to an air duct, these large pressure gradients disappear and the velocity field becomes more uniform (figures 7.23a and b). Transformation of a compost pile with a rectangular cross-section into a pile with a pentagonal cross-section provided with a grid floor, makes the pressure gradient at the edge more pronounced which leads to extreme air velocities (figure 7.24a and b). If this type of compost pile is provided with an air duct system, the air flow has a preferential direction towards the sloping line (figure 7.25a and b). This type of preferential flow can affect the temperature distribution significantly. It can explain the low temperatures of the sensors 7, 8, 9 and 10 (figure 7.12a) during forced aeration of pile 2 in experiment 3 (see the figures 7.16c to f). It can therefore be concluded that a compost pile with a rectangular cross-section and an air duct aeration system has the most uniform velocity distribution of the considered composting systems.

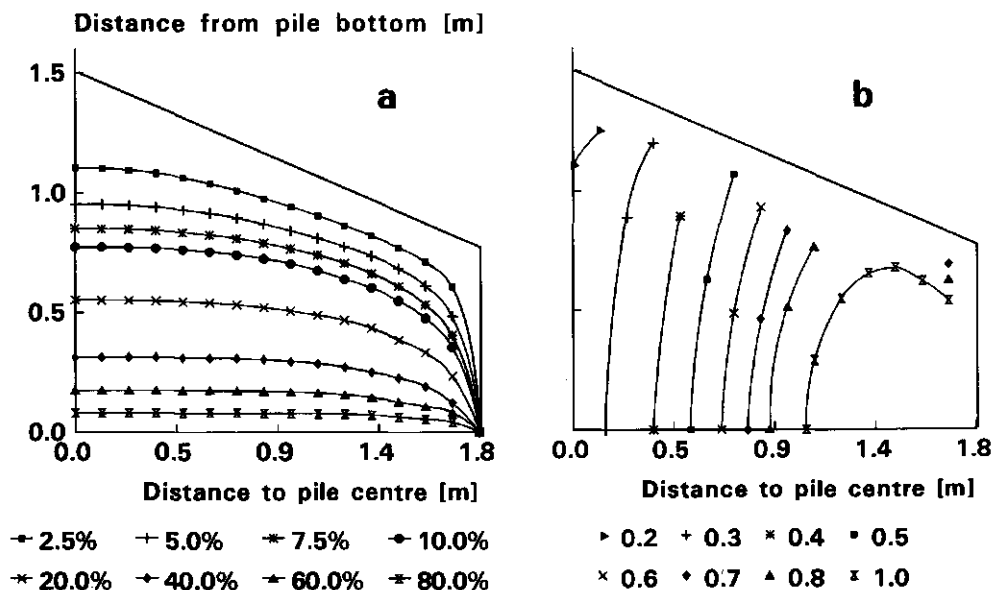


Figure 7.24 (a) Isopressure lines and (b) isovelocity lines of a non-rigid compost pile with a pentagonal cross-section and a grid floor.

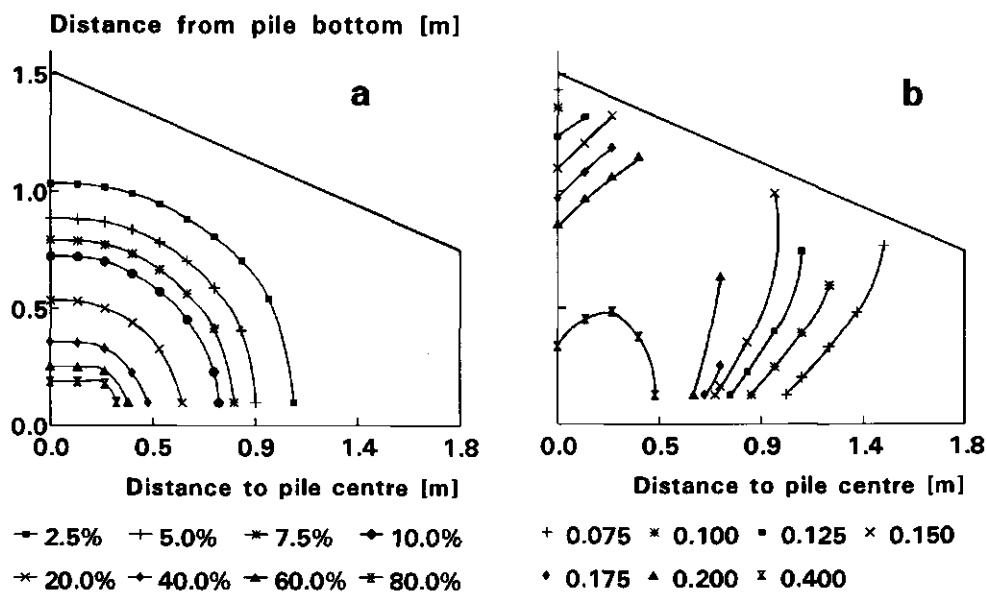


Figure 7.25 (a) Isopressure lines and (b) isovelocity lines of a non-rigid pile with pentagonal cross-section and provided with an air duct system.

7.5 Conclusions

For a pile aerated by natural convection it was found that:

- the rate of dry matter degradation tended to decrease going from the top to the bottom of the pile;
- after 6 weeks the losses of dry matter and water were, respectively, about 25 and 40% of the initial amounts;
- for air-filled volume fractions larger than 0.2, oxygen transfer by natural convection is more important than diffusion;
- for air-filled volume fractions smaller than 0.7, heat transfer by conduction is more important than convection;

For a pile aerated by forced convection it was found that:

- the most homogeneous temperature distribution can be expected in a tunnel system in which a grid floor is covered by a wall-to-wall compost layer;
- a system consisting of a single air duct in the core of the pile will lead to a larger temperature range than in a pile aerated by natural convection.

SUMMARY

In principle, organic waste can be returned to productive use when added to the soil. It can improve the physical, the chemical and the biological status of the soil (chapter 1). However, organic waste may contain weed seeds, pathogens and phytotoxins, which hinder its direct application. If properly conducted, the composting process strongly reduces these unfavourable properties of the raw material. Composting is defined as the partial decomposition of heterogeneous organic matter by a mixed microbial population in a moist, warm and aerobic environment. During the process, temperatures of more than 65 °C can be reached, which eradicate weed seeds and pathogens. The amount of phytotoxins as well as the emission of foul smelling odours is strongly reduced by oxygenation. Thus temperature and oxygen content are important parameters of the composting process.

Composting is a complex process in which physical, chemical and biological processes are mutually dependent. A proper control strategy of the composting process is necessary to obtain an end product of good quality. In principle, the process management can be improved by means of a simulation model. However, existing models do not yet predict temperature and oxygen distributions satisfactorily because of a paucity of experimental data of physical and biochemical properties of composting material. Therefore, the most important aim of this study was to determine these properties. For the experiments of this study a mixture of wheat straw and chicken manure was used.

Chapter 2 describes a mathematical model of the various processes in a compost pile. The model clarifies the mutual dependence of various processes, identifies the material properties to be determined and offers a useful tool to design appropriate experiments. In this model the composting material is considered as a porous medium consisting of a solid, a liquid and a gaseous phase. The model describes the mass balances of these three phases as well as the heat balance of the composting material. In the heat balance the coefficient of thermal conductivity and the air permeability play an important role, while the diffusion coefficient is important for the mass balance of the gaseous phase.

The transfer coefficients depend on the volume fractions of the three phases. These volume fractions vary with position because composting material is compressible. The compression depends on the force balance of the material. With this balance, an equation was deduced to describe the relationship between bulk density and position. In chapter 3 experiments are considered to measure the

bulk density distribution in a compost pile. There was a reasonable agreement between predicted and measured bulk densities. Since this agreement also held for chopped hay, it seems likely that the relationship between bulk density and position will give reasonable results for chopped fibrous materials other than the straw/manure mixture used in this study.

The relationship between bulk density and position was used to find an expression for the air-filled volume fraction as a function of position. Experiments showed that the air-filled volume fraction decreased going from the top to the bottom of the pile, whereas the volume fractions of the solid and liquid phases increased in the same direction. Local volume fractions of the solid and liquid phases increased during the first week of the process, because during this period the influence of subsidence exceeded that of the loss of dry matter and water. Chapter 3 also gives expressions for critical values of the floor load and the height of the pile. These critical values pertain to the situation that the air-filled volume fraction at the bottom of the pile is greater than a desired minimum level.

In chapter 4 experiments are described to measure the transfer coefficients. The air permeability decreased as the air velocity increased. For raw material, the air permeability decreased with the wetness at comparable air filled volume fractions, whereas for older material there was no clear relationship between permeability and wetness. The permeability of composting material which has been turned once, was larger than the permeability of raw material. This may be due to the formation of aggregates and large inter-aggregate pores during this turning event. There was no clear relationship between permeability and age for composting material which has been subjected to turning.

The oxygen diffusion coefficient was proportional to the air-filled volume fraction to the power 1.5. There was no clear relationship between the oxygen diffusion coefficient and the age of the material. The results of the straw/manure mixture were similar to those for dehydrated sewage sludge cake.

The thermal conductivity was measured according to the nonsteady state probe method. At a given temperature and for volume fractions of dry matter of 0.3 or less, the thermal conductivity coefficient increased linearly with the volume fraction of the liquid phase. The thermal conductivity increased with the temperature. The age of composting material did not influence the conductivity.

Chapter 5 gives a theoretical analysis of the rates of oxygen consumption, heat production and carbon dioxide production. These rates reflect the degradation process and depend on the chemical composition of the material, the biochemical pathways of degradation, the kinetics of reaction and microbial

growth and decay.

Microbial activity can be divided into anabolic processes, in which new microbial material is formed, and catabolic processes in which substrate is degraded to obtain energy. With respect to catabolism, distinction is made between aerobic and anaerobic degradation pathways. In both processes CO_2 is one of the final reaction products. The amount of energy produced per mol of CO_2 is calculated from the composition of the material and the stoichiometry of the degradation reactions. This energy is partly used to build new microbial material. The remaining part is released as heat. Since the substrate and the microbes contain approximately equal amounts of energy per mol of carbon, the amount of heat released during the degradation approaches the amount of energy per mol of CO_2 .

The amount of energy produced per kg of substrate under anaerobic conditions is only a small fraction of the amount released under aerobic conditions (about 10% for glucose). Therefore, the ratio between aerobic and anaerobic processes influence the amount of heat released during the process. This ratio depends on the penetration depth of oxygen in the liquid phase. Anaerobiosis will occur where the oxygen penetration depth is less than the thickness of the water layer surrounding the solid particles. Thus locally, e.g. in water filled pores, anaerobic conditions may prevail although the adjacent gaseous phase is highly aerobic.

The components of the substrate being subjected to microbial degradation mainly consist of polymers which are insoluble in water. These polymers must be hydrolyzed before they can be taken up by the microbes and therefore, the rate of hydrolysis strongly influences the overall process rate. However, initially there might be a surplus of dissolved substrate in the liquid phase. Then, in an early phase the process rates are governed by rates of microbial growth and decay. After this surplus is exhausted, the rate of hydrolysis is limiting.

In chapter 6 an isothermal calorimeter is described in which the consumption of oxygen and the productions of carbon dioxide and heat were measured. The time courses of the experimental production/consumption rates showed a characteristic pattern. This pattern consisted of a peak activity during the first 4 to 5 days, followed by a gradually decreasing pseudo steady state. The pseudo steady state CO_2 production rate was reasonably estimated by the rate of carbon hydrolysis calculated in chapter 5. The peak value of the production rates increased with the temperature. This may be due to an increase with the temperature of the amount of organic compounds dissolved into the liquid phase. The conclusion of chapter 5 that the amount of heat released per mol of CO_2 is equal to the amount

of energy produced by the degradation reactions was supported by the experimental results of chapter 6. The calorimeter experiments showed that the anaerobic heat production amounted to 10 to 50% of the aerobic value.

The experimental results were also used to study the rate of exchange of water vapour between the gaseous phase and the combined solid/liquid phase. It can be inferred that, under conditions of natural convection, the vapour pressure in the gaseous phase will be equal to the saturated vapour pressure, except in the outer zone of about 20 cm from the edge of the pile.

Chapter 7 describes experiments with compost piles on a semi practical scale. In these experiments distributions of the temperature, the oxygen and carbon dioxide contents in the gaseous phase, and volume fractions of the solid, the liquid and the gaseous phase were measured.

Going from the top to the bottom in a pile aerated by natural convection, the rate of dry matter degradation tended to decrease. The dry matter loss after 6 weeks was about 25% of the initial value which is only 40% of the theoretical value based on the rate of hydrolysis of carbonaceous compounds. The difference between the theoretical and the experimental value may be caused by inhibition due to high temperatures or anaerobiosis. The water loss in the pile aerated by natural convection, ranged from 30 to 50% of the initial amount.

The relative importance of various transport processes was studied with knowledge of the physical properties of composting material (chapter 4) and of the temperature and oxygen distributions (chapter 7). For oxygen transfer, it was concluded that convection is more important than diffusion in situations with air-filled volume fractions larger than 0.2. For heat transfer, however, the conductive flux is more important than the convective flux in situations with air-filled volume fractions smaller than 0.7. Since the average value of the air-filled volume fraction in the experimental piles was approximately 0.6, this means that conduction was the dominant mode of heat flux. Using this conclusion, an analytical solution of the differential equation describing the heat balance was derived for a compost pile with a rectangular cross-section. The analytical solution was used to estimate the height of a compost pile which is optimal with respect to the temperatures allowing a maximum process rate or a maximum rate of nitrification.

In chapter 7 a comparison is made between compost piles with and without forced aeration. In a pile with a pentagonal cross-section and aerated by a single air duct the temperature range was much larger than in a non-aerated pile. This was supported by model calculations in which the air velocity distributions were computed. The temperature distribution obtained during forced

aeration will depend very much on the type of aeration system which is used and on the shape of the pile. A composting system consisting of a tunnel provided with a grid floor covered by a wall-to-wall compost layer will lead to a smaller temperature range than a system consisting of a single perforated air duct in the core of the pile.

SAMENVATTING

Organisch afval kan worden hergebruikt door het aan de bodem toe te voegen ter verbetering van de fysische, chemische en biologische toestand van de bodem (hoofdstuk 1). Echter, organisch afval kan onkruidzaden, ziekteverwekkers en fytotoxines bevatten die een directe toepassing in de weg staan. Indien op juiste wijze uitgevoerd, kan het composteringsproces deze ongewenste eigenschappen sterk verminderen. Compostering wordt gedefinieerd als de gedeeltelijke afbraak van heterogeen organisch materiaal door een gevarieerde microbiële populatie in een vochtige, warme en aerobe omgeving. Gedurende het proces kunnen temperaturen van meer dan 65 °C worden bereikt waardoor onkruidzaden en ziekteverwekkers onschadelijk worden. De hoeveelheid fytotoxines zowel als het vrijkomen van stank worden verminderd door een goede beluchting. De temperatuur en de zuurstofconcentratie zijn belangrijke parameters bij het composteringsproces.

Compostering is een complex proces waarbij fysische, chemische en biologische processen sterk met elkaar samenhangen. Een goede besturing van het composteringsproces is noodzakelijk om een goed eindproduct te krijgen. De procesbesturing kan worden verbeterd door gebruik te maken van een simulatiemodel. De bestaande modellen zijn echter niet in staat om het verloop van de temperatuur en het zuurstofgehalte goed te voorspellen. Dit is een gevolg van het ontbreken van voldoende experimentele gegevens betreffende de fysische en biochemische eigenschappen van het composterende materiaal. Het belangrijkste doel van dit onderzoek was derhalve de genoemde materiaaleigenschappen te meten. Bij de experimenten werd een mengsel van kippemest en tarwestro gebruikt.

Hoofdstuk 2 beschrijft een wiskundig model van de processen in een composthoop. Het model verklaart de onderlinge afhankelijkheid van de processen, brengt de te meten materiaaleigenschappen in kaart en kan worden gebruikt voor het ontwerpen van meetopstellingen. In dit model wordt compostierend materiaal voorgesteld als een poreus medium bestaande uit een vaste, een vloeibare en een gasvormige fase. Het beschrijft de massabalans van deze drie fasen en de warmtebalans van het materiaal. In de warmtebalans spelen de warmtegeleidingscoëfficiënt en de luchtdoorlatendheid een sleutelrol, terwijl de diffusiecoëfficiënt van belang is voor de massabalans van de gasfase.

De transportcoëfficiënten worden beïnvloed door de volumefracties van de drie genoemde fasen. De volumefracties hangen af van de plaats in de composthoop vanwege de samendrukbaarheid van het materiaal. De mate van samendrukking wordt bepaald door de krachtenbalans van het materiaal. Uitgaande van deze

krachtenbalans werd een relatie afgeleid tussen de bulkdichtheid en de hoogte. In hoofdstuk 3 worden experimenten beschreven waarmee de verdeling van de bulkdichtheid werd gemeten. Er bestond een redelijke overeenstemming tussen gemeten en berekende waarden. Vanwege het feit dat een dergelijke overeenstemming ook gold voor gehakseld hooi, geldt deze relatie mogelijk ook voor andere vezelrijke materialen dan het kippemest/stro mengsel dat in dit onderzoek werd gebruikt.

De relatie tussen bulkdichtheid en hoogte werd gebruikt om een uitdrukking te vinden voor de relatie tussen het luchtgevulde poriënvolume en de hoogte. Experimenten lieten zien dat het luchtgevulde poriënvolume afnam in de richting van de top naar de bodem van de composthoop, terwijl de volume fracties van de vaste en de vloeibare fase juist in deze richting toenamen. Plaatselijk namen de laatstgenoemde fracties in de loop van de eerste week toe omdat in deze periode het inklinkingsproces overheerst werd door de afname ten gevolge van afbraak en verdamping.

Hoofdstuk 3 geeft ook een uitdrukking voor de kritische waarden van de vloerbelasting en de hoogte van de composthoop. Deze kritische waarden gelden voor de situatie waarin het luchtgevulde poriënvolume niet beneden een gewenste minimumwaarde komt.

In hoofdstuk 4 worden experimenten beschreven ter bepaling van de transportcoëfficiënten. De luchtdoorlatendheid neemt af bij toenemende luchtsnelheid. Voor vers uitgangsmateriaal geldt dat de luchtdoorlatendheid afneemt bij toename van het vochtgehalte, terwijl voor ouder materiaal geen duidelijke relatie kon worden vastgesteld. De luchtdoorlatendheid van materiaal dat reeds eenmaal was gekeerd, was groter dan dat van vers materiaal. Dit wordt wellicht veroorzaakt door de vorming van grote kluiten en kanalen als gevolg van de materiaalbewerkingen tijdens het keren van de composthoop. Een duidelijke relatie tussen de luchtdoorlatendheid en de leeftijd van reeds gekeerd materiaal kon niet worden vastgesteld.

De zuurstofdiffusiecoëfficiënt was evenredig met het luchtgevulde poriënvolume tot de macht 1,5. De relatie tussen de diffusiecoëfficiënt en de leeftijd van het materiaal was onduidelijk. De resultaten voor het kippemest/stro mengsel kwamen overeen met die voor ontwaterd zuiveringsslib.

De warmtegeleidingscoëfficiënt werd gemeten volgens de niet-stationaire naaldmethode. Bij constante temperatuur en voor volume fracties van de vaste fase kleiner dan 0,3 nam de warmtegeleidingscoëfficiënt lineair toe met het watergevulde poriënvolume. De warmtegeleidingscoëfficiënt nam toe met de

temperatuur en bleek onafhankelijk van de leeftijd van het materiaal te zijn.

Hoofdstuk 5 geeft een theoretische benadering van de snelheden waarmee zuurstof wordt geconsumeerd en warmte en koolzuurgas worden geproduceerd. Deze snelheden weerspiegelen het afbraakproces en worden bepaald door de chemische samenstelling van het materiaal, de biochemische afbraakroute, de kinetiek van de reacties en door microbiële groei en sterfte.

Microbiële activiteit kan worden onderverdeeld in anabolisme, waarbij nieuw celmateriaal wordt gevormd, en catabolisme waarbij het substraat wordt afgebroken voor de produktie van energie. Met betrekking tot catabolisme wordt onderscheid gemaakt tussen aerobe en anaerobe processen. In beide processen is koolzuurgas (CO_2) een van de eindproducten. De hoeveelheid energie geproduceerd per mol CO_2 wordt berekend met behulp van de stoichiometrie van de afbraakreacties, uitgaande van de samenstelling van het materiaal. De geproduceerde energie zal gedeeltelijk worden benut voor de opbouw van nieuw celmateriaal en gedeeltelijk vrijkomen in de vorm van warmte. Vanwege het feit dat het substraat en het microbiële materiaal vrijwel gelijke hoeveelheden energie per eenheid koolstof bezitten, zal de hoeveelheid warmte die vrijkomt per mol CO_2 ongeveer gelijk zijn aan de hoeveelheid energie die per mol CO_2 wordt geproduceerd door de afbraakreacties.

De hoeveelheid energie die wordt geproduceerd per kg substraat is onder anaerobe omstandigheden slechts een fractie van de hoeveelheid die vrijkomt onder aerobe omstandigheden (voor glucose is dit ongeveer 10%). Derhalve is de verhouding tussen aerobe en anaerobe processen van belang voor de hoeveelheid warmte die vrijkomt. Deze verhouding hangt vooral af van de indringdiepte van zuurstof in de vloeistoffase. Anaerobie treedt op daar waar de indringdiepte kleiner is dan de dikte van de vloeistoffilm die de vaste deeltjes omgeeft. Dus plaatselijk, bijvoorbeeld in de watergevulde poriën, kunnen anaerobe omstandigheden overheersen ondanks dat de aangrenzende gasfase rijkelijk van zuurstof is voorzien.

De componenten van het substraat die van belang zijn bij de microbiële afbraak, bestaan voornamelijk uit polymeren die onoplosbaar zijn in water. Deze polymeren moeten worden gehydrolyseerd voordat ze oplossen in water en vervolgens door de organismen kunnen worden opgenomen. Hierdoor kan worden verwacht dat de hydrolysesnelheid een sterke invloed zal hebben op de totale processnelheid. Echter, in het begin kan een overmaat aan opgelost substraat in de vloeistoffase aanwezig zijn. In dat geval worden de processnelheden bepaald door de snelheden waarmee micro-organismen groeien en afsterven. Als het substraatoverschot is uitgeput zal de hydrolysesnelheid de bepalende factor worden.

In hoofdstuk 6 wordt een isotherme calorimeter beschreven waarin de zuurstofconsumptie en de produkties van warmte en CO_2 werden gemeten. Het verloop in de tijd van de experimentele produktie-/consumptie-curven vertoonden een karakteristiek patroon. Dit patroon bestond uit een produktiepiek binnen 4 à 5 dagen gevolgd door een langzaam afnemend pseudo "steady-state" niveau. De CO_2 produktiesnelheid in deze pseudo "steady-state" fase werd redelijk benaderd door de snelheid waarmee koolstof hydrolyseert, zoals berekend in hoofdstuk 5. De piekwaarden namen toe met de temperatuur. Dit is wellicht een gevolg van de toenemende oplosbaarheid in water van organische stoffen bij stijgende temperatuur.

De conclusie uit hoofdstuk 5 dat de hoeveelheid warmte die vrijkomt per mol CO_2 gelijk is aan de hoeveelheid energie die wordt geproduceerd door de afbraakreacties, werd ondersteund door experimentele resultaten uit hoofdstuk 6. Uit calorimeterexperimenten bleek ook dat de anaerobe warmteproduktie tussen de 10 en 50% van de aerobe waarde lag.

De experimentele resultaten werden ook gebruikt ter bestudering van de uitwisseling van waterdamp tussen de gasfase en de gecombineerde vaste/vloeibare fase. De resultaten impliceren dat, onder omstandigheden van natuurlijke convectie, het redelijk is om aan te nemen dat de gasfase met waterdamp is verzadigd, behalve in een zone van ongeveer 20 cm gemeten vanaf de buitenzijde van de hoop.

Hoofdstuk 7 beschrijft experimenten met composthoopen op semi-praktijkschaal. In deze experimenten werden de ruimtelijke verdelingen gemeten van de temperatuur, het O_2 - en CO_2 -gehalte in de gasfase, en de volumefracties van de vaste, de vloeibare en de gasvormige fase.

In een composthoop belucht door natuurlijke convectie, vertoonde de afbraaksnelheid de neiging af te nemen in de richting van de top naar de bodem. Het drogestofverlies na 6 weken bedroeg ongeveer 25% van de hoeveelheid drogestof in het uitgangsmateriaal, hetgeen neerkomt op slechts 40% van de theoretische waarde gebaseerd op de hydrolysesnelheid van koolstofverbindingen. Het verschil tussen de theoretische en de experimentele waarden wordt wellicht veroorzaakt door een remming van het afbraakproces als gevolg van te hoge temperaturen dan wel zuurstofgebrek. Het vochtverlies in vergelijkbare composthoopen bedroeg 30 to 50% van de initiële hoeveelheid water in het uitgangsmateriaal.

Het relatieve belang van de verschillende transportprocessen werd onderzocht met behulp van de kennis van de fysische eigenschappen van het materiaal (hoofdstuk 4) en de gemeten temperatuur en zuurstofverdelingen (hoofdstuk 7). Voor

zuurstoftransport gold dat convectie belangrijker was dan diffusie zodra het luchtgevulde poriënvolume groter was dan 0,2. Voor het warmtetransport was geleiding belangrijker dan convectie bij een luchtgevuld poriënvolume kleiner dan 0,7. Gezien het feit dat de gemiddelde waarde van het luchtgevuld poriënvolume in de experimentele composthoven gelijk was aan 0,6, kon worden geconcludeerd dat geleiding de overheersende warmtestroom was. Uitgaande van deze conclusie werd een analytische oplossing gevonden voor de differentiaalvergelijking die de warmtebalans beschrijft voor een composthoop met een rechthoekige doorsnede. Deze oplossing werd toegepast om de hoogte van een composthoop te berekenen die optimaal is met betrekking tot de temperatuur waarbij een maximale processnelheid of nitrificatiesnelheid optreedt.

In hoofdstuk 7 werd een vergelijking gemaakt tussen composthoven met en zonder geforceerde beluchting. In een hoop met een vijfhoekige doorsnede en een beluchtingssysteem bestaande uit een enkele beluchtingsbuis was de variatie in de temperatuur veel groter dan in de niet beluchte composthoop. Deze conclusie kon ook worden getrokken uit modelberekeningen van de luchtsnelheidsverdeling bij geforceerde beluchting. De temperatuurverdeling zal sterk afhangen van het gehanteerde beluchtingssysteem en van de vorm van de composthoop. Verwacht mag worden dat in een composthoop voorzien van een tunnelsysteem met een roostervloer die volledig bedekt is met een compostlaag, de temperatuurvariatie een stuk kleiner zal zijn dan in een systeem bestaande uit een enkele beluchtingsbuis in het centrum van de composthoop.

REFERENCES

- Alexander, M., 1977. Introduction to soil microbiology, 2nd ed., 467 pp.
- Alexopoulos, C.J. and C.W. Mims, 1979. Introductory mycology. John Wiley & Sons, New York, 632 pp.
- Avnimelech, Y., 1986. Organic residues in modern agriculture. In: Y. Chen and Y. Avnimelech, The role of organic matter in modern agriculture. Martinus Nijhoff Publ. Dordrecht. pp. 1-10.
- Baas-Becking, L.G.N., and G.S. Parks, 1927. Energy relations in metabolism of autotrophic bacteria. *Physiol. Rev.* 7: 85-106.
- Baver, L.D., 1946. Soil physics. 2nd ed., Wiley, New York, 370 pp.
- Baver, L.D., W.H. Gardner and W. R. Gardner, 1972. Soil physics. 4th ed., Wiley, New York, 498 pp.
- Bernstein, R., 1912. Eine Charakteristik der Strohpresse. *Mitteilungen des Verbandes landwirtschaftlicher Maschinen-Prüfungsanstalten* 6: 161-165 (German).
- Bidwell, R.G.S., 1979. Plant physiology. Macmillan Publishing Co., New York, 726 pp.
- Bird, R.B., W.E. Stewart, and E.N. Lightfoot, 1960. Transport phenomena. John Wiley & Sons, New York, 780 pp.
- Blackwell, J.H., 1954. A transient-flow method for the determination of thermal constants of insulating materials in bulk, part 1: theory. *J. Appl. Phys.* 25: 137-144.
- Boekel, P., 1991. Betekenis van huisvuilcompost voor de bodemfysische eigenschappen van de Nederlandse gronden. Technische Commissie Bodembescherming, Leidschendam, TCB A91/08, 81 pp. (Dutch)
- Bollen, G.J., D. Volker and A.P. Wijnen, 1989. Inactivation of soil-borne plant pathogens during small scale composting of crop residues. *Neth. J. Plant Pathol.*, 95 supplement 1: 19-30.
- Bollen, G.J., 1969. The selective effect of heat treatment of the microflora of a greenhouse soil. *Neth. J. Plant Pathol.* 75: 157-163.
- Boyd, S.A., and M.M. Mortland, 1990. Enzyme interactions with clays and clay-organic matter complexes. In: Bollag, J. and G. Stotzky, *Soil biochem.* 6: 1-29.
- Brock, T.D. and M.T. Madigan, 1988. Biology of microorganisms. Prentice Hall int. ed., 5th ed., 835 pp.

- Brons, H.J., J.A. Field, W.A.C. Lexmond and G. Lettinga, 1985. Influence of humic acids on the hydrolysis of potato protein during anaerobic digestion. *Agric. Wastes* 13: 105-114.
- Bruijn, P.J., I.A. van Haneghem and J. Schenk, 1983. An improved nonsteady state probe method for measurements in granular materials, part 1: theory. *High Temp. High Press.* 15: 359-366.
- Burge, W.D., 1983. Monitoring pathogen destruction. *BioCycle* 24(2): 48-50.
- Burns, R.G., 1982. Enzyme activity in soil: location and a possible role in microbial ecology. *Soil Biol. Biochem.*, 14: 423-427.
- Busse, W., 1964. Die Theorie auf dem Gebiet des Verdichtens landwirtschaftlicher Halmgüter. Institut für Landmaschinen, TH Braunschweig, Landtechnische Forschung 14: 6-15 (German).
- Carlsaw, H.S. and J.C. Jaeger, 1986. Conduction of heat in solids. Clarendon Press, Oxford, 560 pp.
- Chang, R., 1977. Physical chemistry with applications to biological systems. Collier Macmillan int. ed., 538 pp.
- Chang, Y. and H.J. Hudson, 1967. The fungi of wheat straw compost. I Ecological studies. *Trans. Br. Mycol. Soc.* 50(4): 649-666.
- Chen, Y. R., 1983. Thermal properties of beef cattle manure. *Agric. Wastes* 6: 13-29.
- Cooper, R.C. and C.G. Golueke, 1977. Public health aspects of on-site waste treatment. *Compost Sci.* 18(3): 8-11.
- Cooney, C.L., D.I.C. Wang and R.I. Mateles, 1968. Measurement of heat evolution and correlation with oxygen consumption during microbial growth. *Biotechnol. & Bioeng.* 11: 269-281.
- Cowling, E.B., and T.K. Kirk, 1976. Properties of cellulose and lignocellulosic materials as substrates for enzymatic conversion processes. *Biotechnol. & Bioeng. Symp.* no. 6: 95-123.
- Day, C.L., 1964. A device for measuring voids in porous materials. *Agric. Eng., Januari 1964* : 36-37.
- De Bertoldi, M., F. Zucconi and M. Civilini, 1988. Temperature, pathogen control and product quality. *BioCycle* 29(2): 43-50.
- De Bertoldi, M., G. Vallini, A. Pera and F. Zucconi, 1982. Comparison of three windrow compost systems. *BioCycle* 23(2): 45-48.
- De Bertoldi, M. and F. Zucconi, 1980. Waste disposal in Italy. *Compost Sci.* 21(6): 36-37.

- De la Lande Cremer, L.C.N., 1988. Organic fertilizers for improvement and maintenance of soil fertility. In: E. Welte and I. Szabolcs (eds.), Proc. 4th intern. cie. symposium, Agricultural waste management and environmental protection, Braunschweig, 14-17 may 1987, pp. 129-140.
- Derikx, P.J.L., H.J.M. Op den Camp, W.P.G.M. Bosch, G.D. Vogels, J.P.G. Gerrits and L.J.L.D. van Griensven, 1989. Production of methane during the preparation of mushroom compost. *Mushroom Sci.* 12: 353-360.
- De Vleeschauwer, D., O. Verdonck and P. Van Assche, 1981. Phytotoxicity of refuse compost. *BioCycle* 22: 44-46.
- De Vries, D.A., 1963. Thermal properties of soils. In: W.R. van Wijk, Physics of plant environment, 382 pp.
- Domergues, Y., and F. Mangelot, 1970. *Écologie microbienne du sol*. Masson et Cie., Paris, 796 pp. (French).
- Dexter, S.T., 1964. Physical constants in Alfalfa (*Medicago Sativa* L.) silage and silage materials. *Crop Sci.* 4(6): 599-602.
- Dullien, F.A.L., 1979. Porous Media and pore structure. Academic Press, New York, 396 pp.
- Eastman, J.A. and J.F. Ferguson, 1981. Solubilization of particulate organic carbon during the acid phase of anaerobic digestion. *J. Water Poll. Control Fed.* 53(3): 352-358
- Feustel, I.C. and H.G. Byers, 1936. The comparative moisture-absorbing and moisture-retaining capacities of peat and soils mixtures. U.S. Dept. Agr. Techn. Bul. 632.
- Finger, S.M., R.T. Hatch and T.M. Regan, 1976. Aerobic microbial growth in semisolid matrices: heat and mass transfer limitation. *Biotechnol. Bioeng.* 18: 1193-1218.
- Frear, D.E.H., 1950. Agricultural chemistry; a reference text. vol. 1. D. van Nostrand Company, Inc., New York, 812 pp.
- Glenn, J., 1992. The state of garbage in America, 1992 Nationwide survey. *BioCycle* 33(4): 46-55.
- Goff, J.A. and S. Gratch, 1946. Low pressure properties of water from -160 to 212 F. *Trans. Am. Soc. Heating and Ventilating Eng.* 52: 95-122.
- Gottschall, R., 1984. Kompostierung. Alternative Konzepte no 45. C.F. Müller, Karlsruhe, 296 pp. (German).
- Grady, C.P.L. and H.C. Lim, 1980. Biological wastewater treatment, theory and applications. Marcel Dekker Inc., New York. 963 pp.
- Gray, K.R., K. Sherman and A.J. Biddlestone, 1971. A review of composting, Part 1. *Process Biochemistry* 6(6): 32-36.

- Griffis, C.L. and C.R. Mote, 1978. Weed seed viability as affected by the composting of cotton gin trash. *Arkansas Farm Research* 27(5): 8.
- Hafez, A.A.R., J. Azevedo, J. Rubin and P.R. Stout, 1974. Physical properties of farm animal manures. *California Agric. Exp. Station, bull.* 867.
- Harada, Y., A. Inoko, M. Tadaki and T. Izawa, 1981. Maturing process of city refuse compost during piling. *Soil Sci. Plant Nutr.*, 27(3): 357-364.
- Hardee, H.C. and R.H. Nilson, 1977. Natural convection in porous media with internal heat generation. *Nuclear Sci. and Eng.* 63: 119-132.
- Haug, R.T., 1993. The practical handbook of compost engineering. Boca Raton, Lewis, 717 pp.
- Hirschfelder, J.O., C.F. Curtiss and R.B. Bird, 1964. Molecular theory of gasses and liquids. Wiley, New York, 1185 pp.
- Hoffmann, G. and K. Teicher, 1957. Das Enzymsystem unserer Kulturböden VII; Proteasen II. *Zeitschrift für Pflanzenernährung, Düngung und Bodenkunde, Band 77 (3):* 243-251.
- Hoitink, H.A.J. and P.C. Fahy, 1986. Basis for the control of soilborne plant pathogens with composts. *Ann. Rev. Phytopathol.* 24: 93-114.
- Janssen, W.M.M.A., 1987. Mogelijkheden tot vermindering van de mestproblematiek door middel van voeding. *C.O.V.P., Spelderholt, Beekbergen*, 466: 5 - 33.
- Kandeler, E., 1988. Kinetische Eigenschaften von Proteasen und Phosphatasen in unterschiedliche bewirtschafteten Böden. *Die Bodenkultur* 39(3): 201-206.
- Ketterer, N. and H.C. Weltzien, 1987. Untersuchungen zur Wirkung von Kompostextrakt auf den Befall der Weinrebe durch den Roten. *Med. Fac. Landbouww. Rijksuniv. Gent*, 52(3a): 965-970. (German).
- Koorevaar, P., G. Menelik and C. Dirksen, 1983. Elements of soil physics. *Developments in soil science* 13. Elsevier, Amsterdam, 228 pp.
- Lang, C., 1878. Über die Wärmekapazität der Bodenkonstituenten. *Forschung Gebiete Agrikultur-Physik* 1: 108 (German).
- Lavake, D.E. and A.F. Wiese, 1977. Effect of composting on weed seed germination. In: *Proc. Southern Weed Sci. Soc.*, 13th. annual meeting, Dallas, Texas, p. 167.
- Lee, B.H. and T.H. Blackburn, 1975. Cellulase production by a thermophilic *Clostridium* species. *Appl. Microbiol.* 30(3): 346-353.
- Lee, Y. and L.T. Fan, 1982. Kinetic studies of enzymatic hydrolysis of insoluble cellulose: analysis of the initial rates. *Biotechnol. Bioeng.* 24: 2383-2406.
- Logsdon, G., 1990. Plant protection through compost. *BioCycle* 31(1): 52-54.

- Lopez-Real, J. and M. Foster, 1985. Plant pathogens survival during the composting of agricultural organic wastes. In: Gasser, J.K.R. (ed.), Composting of agricultural and other wastes, Elsevier Appl. Sci. Publ., p. 291-299.
- Lopez-Real, J., 1990. Agro-industrial waste composting and its agricultural significance. Proc. of the Fertiliser Soc., April: 3-26.
- Lynch, J.M., 1977. Phytotoxicity of acid production in the anaerobic decomposition of wheat straw. J. Appl. Bact. 42: 81-87.
- Lyons, L., 1991. A practical guide to data analysis for physical science students. Cambridge University Press, 95 p.
- Mason, E.A. and L. Monchick, 1962. Transport properties of polar-gas mixtures. J. Chem. Phys. 36(10): 2746-2757.
- Marshall, T.J., 1959. The diffusion of gases through porous media. J. Soil Sci. 10: 79-82.
- McClaugherty, C.A. and A.E. Linkins, 1990. Temperature responses of enzymes in two forest soils. Soil Biol. Biochem. 22(1): 29-33.
- McKibbin, R., 1986. Thermal convection in a porous layer: effects of anisotropy and surface boundary conditions. Transport in porous media 1: 271-192.
- McLaren, A.D., 1978. Kinetics and consecutive reactions of soil enzymes. In: Burns, R.G., Soil enzymes. Academic Press, London. 380 pp.
- Mesu, E.J., 1984. Het storten van afvalstoffen. In: Van den Berg, C., De Haan, F.A.M. and D.A. Zeilmaier. Handboek voor milieubeheer, Deel IV Bodembescherming, E1200-1 - E1200-12. (Dutch).
- Miller, F.C., 1989. Matric water potential as an ecological determinant in compost, a substrate dense system. Microb. Ecol. 18: 59-71.
- Miller, F.C., E.R. Harper and B.J. Macauley, 1989. Field examination of temperature and oxygen relationships in mushroom composting stacks - consideration of stack oxygenation based on utilisation and supply. Aust. J. Exp. Agric. 29: 741-750.
- Monchick, L. and E.A. Mason, 1961. Transport properties of polar gases. J. Chem. Phys. 35(5): 1676-1696.
- Monod, J., 1949. The growth of bacterial cultures. Ann. Rev. of Microbiol. 3: 371-394.
- Mote, C.R., and C.L. Griffis, 1982. Heat production by composting organic matter. Agric. Wastes 4: 65-73.
- Moyo, C.C., D.E. Kissel and M.L. Cabrera, 1989. Temperature effects on soil urease activity. Soil Biol. Biochem. 21(7): 935-938.

- Myers, R.J.K., 1975. Temperature effects on ammonification and nitrification in a tropical soil. *Soil Biol. Biochem.* 7: 83-86.
- Nakasaki, K., M. Shoda and H. Kubota, 1985. Effect of temperature on composting of sewage sludge. *Appl. and Environ. Microbiol.* 50(6): 1526-1530.
- Nakasaki, K., J. Kato, T. Akiyama and H. Kubota, 1987a. A new composting model and assessment of optimum operation for effective drying of compost material. *J. Ferment. Technol.* 65(4): 441-447.
- Nakasaki, K., Y. Nakano, T. Akiyama, M. Shoda and H. Kubota, 1987b. Oxygen diffusion and microbial activity in the composting of dehydrated sewage sludge cakes. *J. Ferment. Technol.* 65(1): 43-48.
- Nannipieri, P., B. Ceccanti, S. Cervelli and C. Conti, 1982. Hydrolases extracted from soil: kinetic parameters of several enzymes catalyzing the same reaction. *Soil Biol. Biochem.* 14: 429-432.
- Ohm, A., 1972. Broei- en droogprocessen in hooi. Ph.D. thesis of the Technical University Delft (Dutch), 183 pp.
- Patankar, S.V., 1980. Numerical heat transfer and fluid flow. Hemisphere Publ., New York, 179 pp.
- Ponnamperuma, F.N., 1967. A theoretical study of aqueous carbonate equilibria. *Soil Sci.* 103(2): 90-100.
- Press, W.H., B.P. Flannery, S.A. Teukolsky and W.T. Vetterling, 1987. Numerical recipes. Cambridge Univ. Press, Cambridge, 818 pp.
- Raats, P.A.C., 1967. Non-Darcy flow in soils. *Proc. Int. Soil Water Symp.*, vol 1. Praag, Czechoslovak Nat. Committee ICID.
- Raats, P.A.C., 1987. Applications of the theory of mixtures in soil science. *Math. Modelling* 9: 849-856.
- Randle, P.E. and P.B. Flegg, 1985. The effect of duration of composting on compost density and yield of mushrooms. *Sci. Hortic.* 27: 21-31.
- Raveh, A. and Y. Avnimelech, 1979. Leaching of pollutants from sanitary landfill models. *J. of Water Poll. Contr. Fed.* 51(11): 2705-2716.
- Raviv, M., S. Tarre, Z. Geler and G. Shelef, 1987. Changes in some physical and chemical properties of fibrous solids from cow manure and digested cow manure during composting. *Biol. Wastes* 19: 309-318.
- Reddy, K.R. and W.H. Patrick, 1975. Effect of alternate aerobic and anaerobic conditions on redox potential, organic matter decomposition and nitrogen loss in a flooded soil. *Soil Biol. Biochem.* 7: 87-94.
- Rothbaum, H.P., 1961. Heat output of thermophiles occurring on wool. *J. of Bact.* 81: 165-171.

- Rubin, B and A. Benjamin, 1984. Solar heating of the soil: Involvement of environmental factors in the weed control process. *Weed Sci.* 32: 138-142.
- Scheffer, F. and P. Schachtschabel, 1989. *Lehrbuch der Bodenkunde*. Ferdinand Enke Verlag, Stuttgart, 491 pp. (German).
- Schlegel, H.G., 1988. *General microbiology*. 6th ed., 587 pp.
- Schulze, G. and J.M. Prausnitz, 1981. Solubilities of gases in water at high temperatures. *Ind. Eng. Chem. Fundam.* 20: 175-177.
- Shuler, M.L., 1980. *Utilization and recycle of agricultural wastes and residues*. CRC Press, Boca Raton, Florida, 298 pp.
- Smith, R. and R.G. Eilers, 1980. Numerical simulation of aerated sludge composting. Wastewater Research Division, Municipal Environ. Res. Lab., Cincinnati, Ohio. EPA-600/2-80-191.
- Sobel, A.T. and R.E. Muck, 1983. Energy in animal manures. *Energy in Agric.* 2: 161-176.
- Squires, G.L., 1976. *Practical physics*. McGraw-Hill Book Company (UK), London, 224 pp.
- Staniforth, A.R., 1979. *Cereal straw*. Oxford, Clarendon, 175 pp.
- Stentiford, E.I., D.D. Mara and P.L. Taylor, 1985. Forced aeration co - composting of domestic refuse and sewage sludge in static piles. In: Gasser, J.K.R. (ed.), *Composting of agricultural and other wastes*, Elsevier Appl. Sci. Publ. pp. 42-55.
- Stålhane, B. and S. Pyk, 1931. *Teknisk tidskrift* 61: 389-393.
- Suler, D.J. and M.S. Finstein, 1977. Effect of temperature, aeration, and moisture on CO₂ formation in bench-scale, continuously thermophilic composting of solid waste. *Appl. and Environ. Microbiol.* 33(2): 345-350.
- Swift, R.S. and A.M. Posner, 1977. Humification of plant materials. In: *Soil Organic Matter Studies, Proc. of a Symp. on Soil Organic Matter Studies held in Braunschweig, 6-10 september 1976*, Intern. Atomic Agency, Vienna, 1: 171-181.
- Tabatabai, M.A., 1973. Michaelis constants of urease in soils and soil fractions. *Soil Sci. Soc. Amer. Proc.* 37: 707-710.
- Tenney, F.G. and S.A. Waksman, 1929. Composition of natural materials and their decomposition in the soil; IV. The nature and rapidity of decomposition of the various organic complexes in different plant materials, under aerobic conditions. *Soil Sci.* 28: 55-84.
- Thauer, R.K., K. Jungermann and K. Decker, 1977. Energy conservation in chemotrophic anaerobic bacteria. *Bact. Rev.* 41: 100-180.

- Tisdall, J.M. and J.M. Oades, 1982. Organic matter and water-stable aggregates in soils. *J. of Soil Sci.* 33: 141-163.
- Ulrich, R., 1894. Untersuchungen über die Wärmekapazität der Bodenkonstituenten. *Forschung Gebiete Agrikultur-Physik* 17: 1 (German).
- U.S. EPA, 1981. Technical Bulletin: Composting processes to stabilize and disinfect municipal sewage sludges. Office of water program operations. Washington D.C. EPA 430/9-81-011.
- Van Haneghem, I.A., 1981. Een niet-stationaire naaldmethode (warmtegeleiding, warmtecapaciteit, contactweerstand). PhD-thesis Agr. Un. Wageningen, the Netherlands, 187 pp. (Dutch).
- Van Haneghem, I.A., J. Schenk and H.P.A. Boshoven, 1983. An improved nonsteady- state probe method for measurements in granular materials. *High Temp. - High Press.* 15: 359-374.
- Van Lier, J.J.C., 1988. Internal report, part 2. Mushroom Experimental Station, Horst, The Netherlands, 93 pp.
- Van Loon, W.K.P., I.A. van Haneghem and J. Schenk, 1989. A new model for the nonsteady-state probe method to measure thermal properties of porous materials. *Int. J. Heat Mass Transfer* 32: 1473-1481.
- Van Meurs, G.A.M., 1985. Seasonal heat storage in the soil. PhD-thesis Technical Univ. Delft, 217 pp.
- Van Onna, M.J.G. and M.Q. van der Veen, 1990. Model voor de verwerking en het hergebruik van organische afvalstoffen vanuit nationaal- economische optiek. *Milieu*, 3: 90-93, (Dutch).
- Van Veen, J.A., 1977. The behaviour of nitrogen in the soil; a computer simulation model. PhD thesis, Vrije Universiteit Amsterdam, 164 pp.
- Waksman, S.A., T.C. Cordon and N. Hulpoi, 1939. The influence of temperature upon the microbiological population and decomposition processes in compost of stable manure. *Soil Sci.* 47: 83-113.
- Walker, I.K., and W.J. Harrison, 1960. The self-heating of wet wool. *New Zealand J. of Agric. Res.* 3(6): 861-895.
- Washburn, E.W., 1933. International critical tables of numerical data, physics, chemistry and technology, part 5: 166-167.
- Weast, R.C., 1985. CRC Handbook of chemistry and physics. CRC press, Boca Raton 2000 pp.
- Weltzien, H.C. and N. Ketterer, 1986. Control of Downy Mildew, *Plasmopara viticola* (de Bary) Berlese et de Toni, on Grapevine leaves through water extracts from composted organic wastes. *J. Phytopath.* 116: 186-188.

- Weltzien, H.C., N. Ketterer, C. Samerski, K. Budde and G. Medhin, 1987. Untersuchungen zur Wirkung von Kompostextrakten auf die Pflanzengesundheit. Nachrichtenbl. Deut. Pflanzenschutzd. 39(2): 25-28. (German).
- Wiley, J.S., 1957. II. Progress report on high-rate composting studies. Eng. Bull., Proc. of the Twelfth Industrial Waste Conference, may 13, 14 and 15, series no. 94, Purdue, 596 - 603
- Zucconi, F., M. Forte, A. Monaco and M. De Bertoldi, 1981. Biological evaluation of compost maturity. BioCycle 22(4): 27-29.

LIST OF SYMBOLS

Symbol	Description	Dimension	Chapter
A	area	[m ²]	6
c	total molar concentration	[kmol m ⁻³]	2
C	specific heat capacity	[J kg ⁻¹ K ⁻¹]	2
d _s	dry matter content	[-]	2
D _{ij}	binary diffusion coefficient	[m ² s ⁻¹]	2
e	microbial carbon consumption rate	[kg s ⁻¹]	5
E	materials resistance against deformation	[J kg ⁻¹]	3
g	gravitational acceleration	[m s ⁻²]	2
ΔG°	Gibbs free energy of reaction under standard conditions	[kJ]	5
ΔG _r	Gibbs free energy of reaction under prevailing conditions	[kJ]	5
H	heat of evaporation	[J kg ⁻¹]	2
k	Boltzmann constant	[J K ⁻¹]	2
k _{H2O}	water vapour transfer coefficient	[s ⁻¹]	6
k _d	specific microbial decay rate	[s ⁻¹]	5
K	Henry's constant	[Pa m ³ mol ⁻¹]	5
K _s	substrate affinity constant	[kg m ⁻³]	5
l	height of the calorimeter vessel	[m]	6
L	length of sample cylinder	[m]	4
M _i	molecular mass of component i	[kg kmol ⁻¹]	2
M _g	average molecular mass of gaseous phase	[kg kmol ⁻¹]	2
N _i	molar flux of component i	[kmol m ⁻² s ⁻¹]	2
N _A	Avogadro's number	[mol ⁻¹]	2
P	total pressure of the gaseous phase	[Pa]	2
P _i	partial pressure of component i	[Pa]	2
P _{sat}	saturated vapour pressure	[Pa]	7
Q	heat production	[W m ⁻³]	2
Q _g	heat production calculated on the basis of measured O ₂ -consumption and CO ₂ -production	[W m ⁻³]	6
Q _t	heat production measured in the calorimeter	[W m ⁻³]	6
r	radius of the calorimeter vessel	[m]	6
r _i	production/consumption rate of component i	[kg s ⁻¹ m ⁻³]	2
R	universal gas constant	[J kmol ⁻¹ K ⁻¹]	2
t	time	[s]	2

T	temperature	[K]	2
u	filter velocity of the liquid phase	[m s ⁻¹]	2
v	filter velocity of the gaseous phase	[m s ⁻¹]	2
v_i^D	diffusive velocity of component i	[m s ⁻¹]	2
v_i	total velocity of component i	[m s ⁻¹]	2
V	volume	[m ³]	6
w	wetness	[-]	2
X	number of microbial units	[m ⁻³]	5
x, y, z	Cartesian coordinates	[m]	2
Y	microbial yield	[-]	5
Z	pile height	[m]	3
α_w	heat transfer coefficient of the calorimeter	[W m ⁻² K ⁻¹]	6
δ	oxygen penetration depth	[m]	5
γ_{ij}	true density of component j in phase i	[kg m ⁻³]	2
κ	intrinsic air permeability	[m ²]	2
μ	dynamic viscosity	[N s m ⁻²]	2
μ_g	specific microbial growth rate	[s ⁻¹]	5
μ_{gmax}	maximum specific microbial growth rate	[s ⁻¹]	5
λ	thermal conductivity coefficient	[W m ⁻¹ K ⁻¹]	2
λ_a	apparent thermal conductivity coefficient	[W m ⁻¹ K ⁻¹]	4
χ_i	relative molar concentration of component i	[-]	2
ρ	bulk density of the composting material	[kg m ⁻³]	2
ρ_i	bulk density of phase i	[kg m ⁻³]	2
ρ_u	unloaded bulk density	[kg m ⁻³]	3
σ	mechanical stress in the composting material	[N m ⁻²]	3
θ_i	volume fraction of phase i	[-]	2
ω_{fl}	floor load	kg m ⁻²]	3
ζ_c^*	rate constant of hydrolysis	[s ⁻¹]	2
ζ_c	rate constant of hydrolysis	[kmol s ⁻¹ kg ⁻¹]	5
subscripts			
a	ash		3
atm	atmospheric		7
cel	cellulose		5
C	carbon		5
eff	effective		7
g	gaseous phase		2
hcl	hemicellulose		5
l	liquid phase		2

o	organic fraction	3
p	constant pressure	2
s	solid phase	2

CURRICULUM VITAE

Johannes Theodorus van Ginkel werd geboren op 24 februari 1956 te Vlissingen. In 1974 behaalde hij het Atheneum-B diploma. Daarna werd begonnen met de studie Industriële Vormgeving aan de TU-Delft. Na twee jaar stapte hij over naar de Landbouwniversiteit in Wageningen om aan de studie Landbouwtechniek te beginnen. De doctoraalfase bestond uit een verzwaard hoofdvak natuurkunde, een hoofdvak werktuigkunde en een extra vak alternatieve landbouw. De praktijktijd werd doorgebracht bij het Office du Niger in Mali.

In januari 1985 werd het ingenieursdiploma behaald waarna een baan volgde bij het IMAG-DLO van november 1985 tot juni 1986. Daar werd onderzoek gedaan naar de bladtemperatuur van tomaat. Aansluitend volgde een aanstelling als wetenschappelijk onderzoeker bij het Instituut voor Bodemvruchtbaarheid, thans AB-DLO. De tijdelijke aanstelling eindigde op 1 juni 1991, waarna dit proefschrift werd geschreven.